e-Zine for meteor observers meteornews.net

MeteorNews

ISSN 2570-4745 VOL 9 / ISSUE 1 / JANUARY 2024

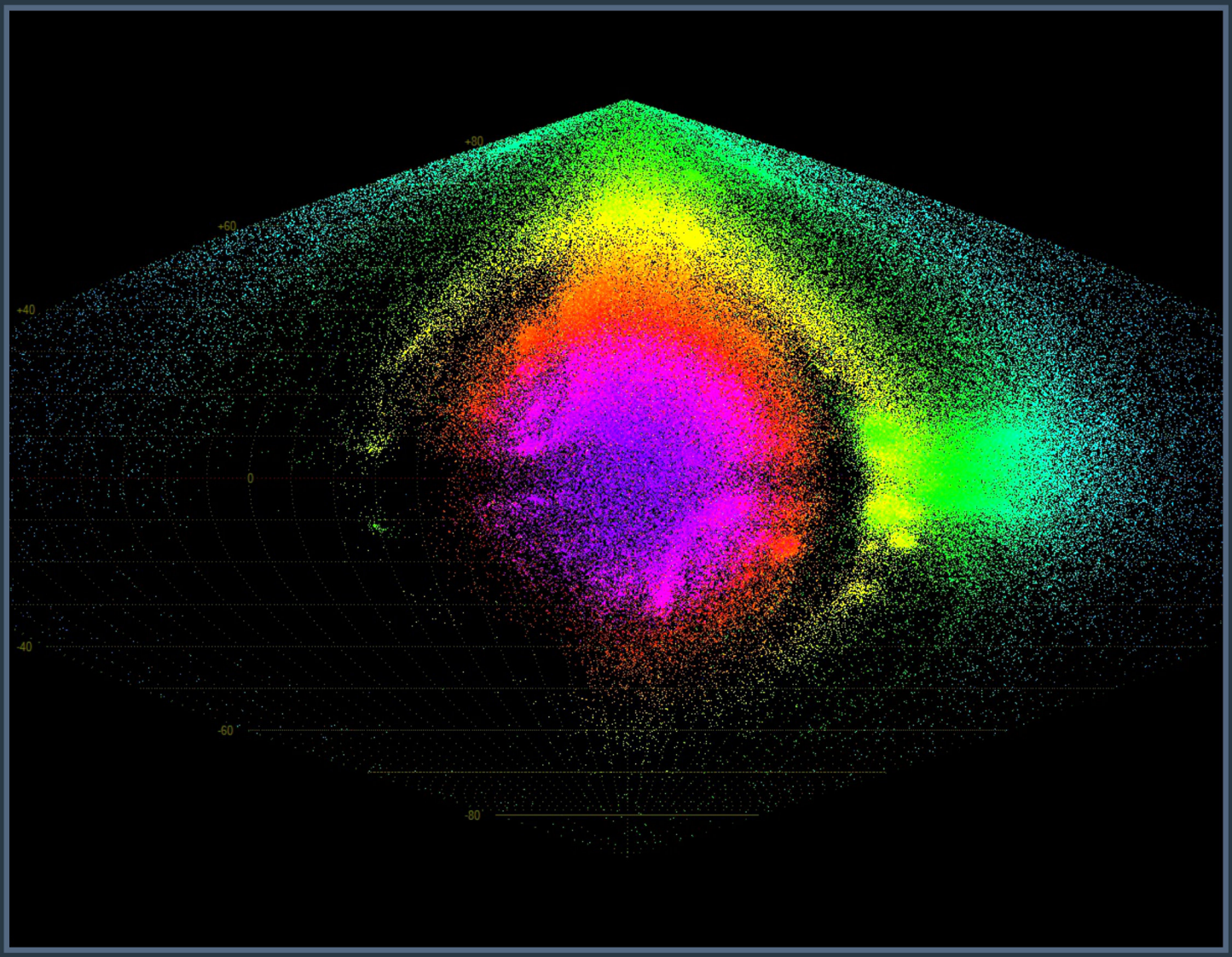

Radiants of multi-station meteor orbits recorded in the EDMOND v5.05 database. A Hammer projection with a Sun-centered ecliptic coordinate system is used for display (credit: Jakub Koukal)

- Forecast 46P/Wirtanen
- First 46P/Wirtanen meteors
- EDMOND v5.05
- CAMS reports
- Radio meteor work
- ML radio echo detection

Contents

Forecast of possible activity of the comet 46P/Wirtanen meteor stream in December 2023 and (especially) in 2024

Mikhail Maslov

skjeller@yandex.ru

This is the forecast for possible meteor activity of the meteor stream related to the comet 46P/Wirtanen. This comet hasn't produced any known meteor activity on Earth. However, it's orbit has been relatively close to the Earth's one since 1986 and the analysis of its trail's evolution showed that there is a slight possibility of meteor activity from the 1967 and 1974 trails in 2023 and some reasonable chance for a small outburst in 2024 due to the encounter with the 1974 trail of comet 46P/Wirtanen.

1 Introduction

The comet 46P/Wirtanen orbit has been relatively close to the orbit of the Earth since the year 1986, when its orbit was pulled by Jupiter closer to the Earth's one. Its perihelion distance decreased from 1.61 AU in 1967 to 1.08 in 1986. After that the orbit of comet 46P/Wirtanen remained relatively stable, its last perihelion was in 2018 and the next one is expected in 2024, both at nearly the same perihelion distance of ~1.055 AU with the MOID of ~0.071 AU.

Such a distance is still quite large to hope for encounters with most dense dust material close to the comet but some particles with higher ejection velocities could reach the Earth. Such particles are smaller and not so abundant as the particles with low ejection velocities which are usually situated closer to the parent comet, but as the comet 46P/Wirtanen is relatively large and active it could produce enough numbers of particles with high ejection velocity allowing some detectable activity when the Earth encounters its trail parts formed by such particles.

The computation of the orbital evolution was made using the software program Comet's Dust 2.0 made by S. Shanov and S. Dubrovsky. The result of this computations show that particles ejected by the comet 46P/Wirtanen showed that in 2023 and 2024 the Earth is expected to encounter some dust trails of the comet 46P/Wirtanen.

For 2023 two encounters are found at 20^h55^m UT on December 10 and at 17^h54^m UT on December 12, but for both of them the parameters are not favorable, so it is very likely that no activity would occur. But still, it is desirable to check them.

For 2024 one encounter is found at 2^h21^m UT on December 13. The activity prospects look to be much more favorable for this encounter and while no high activity is expected the chances for small but still observable activity with a rough ZHR estimation of 10–20 seem to be reasonably high.

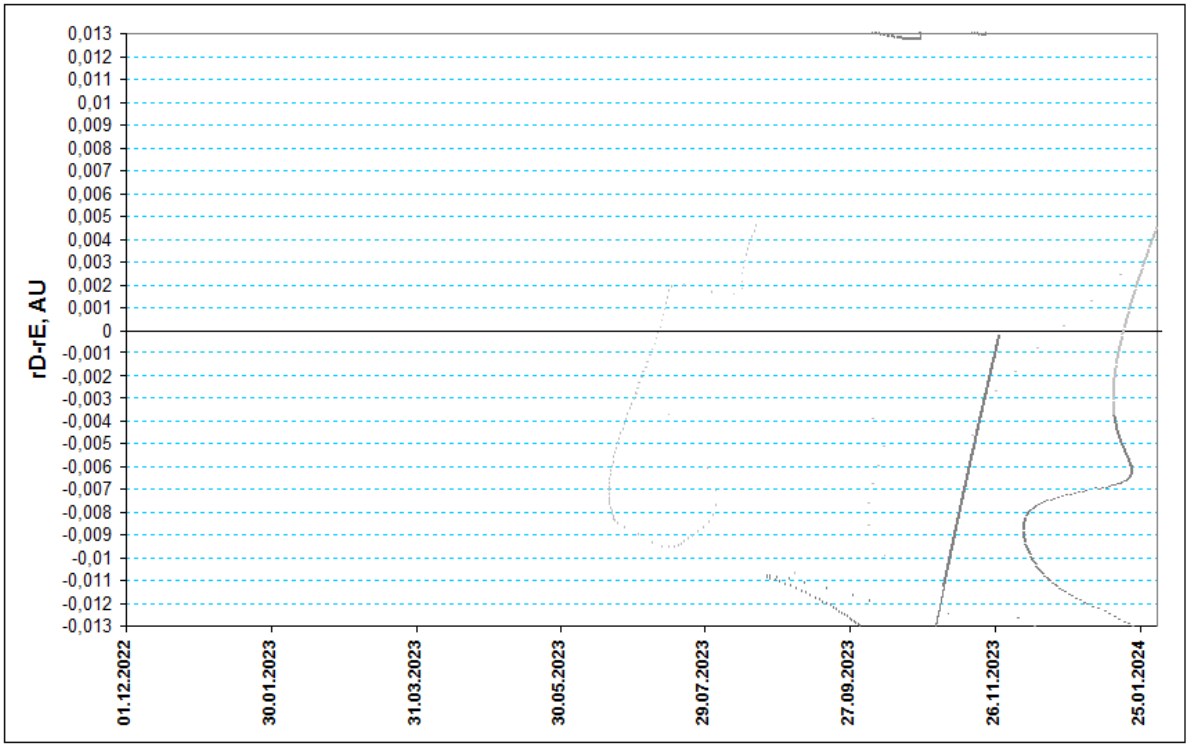

Figure 1 – Space-temporal projection of 46P-ids trail parts onto their minimal distance passages in 2023 before perihelion.

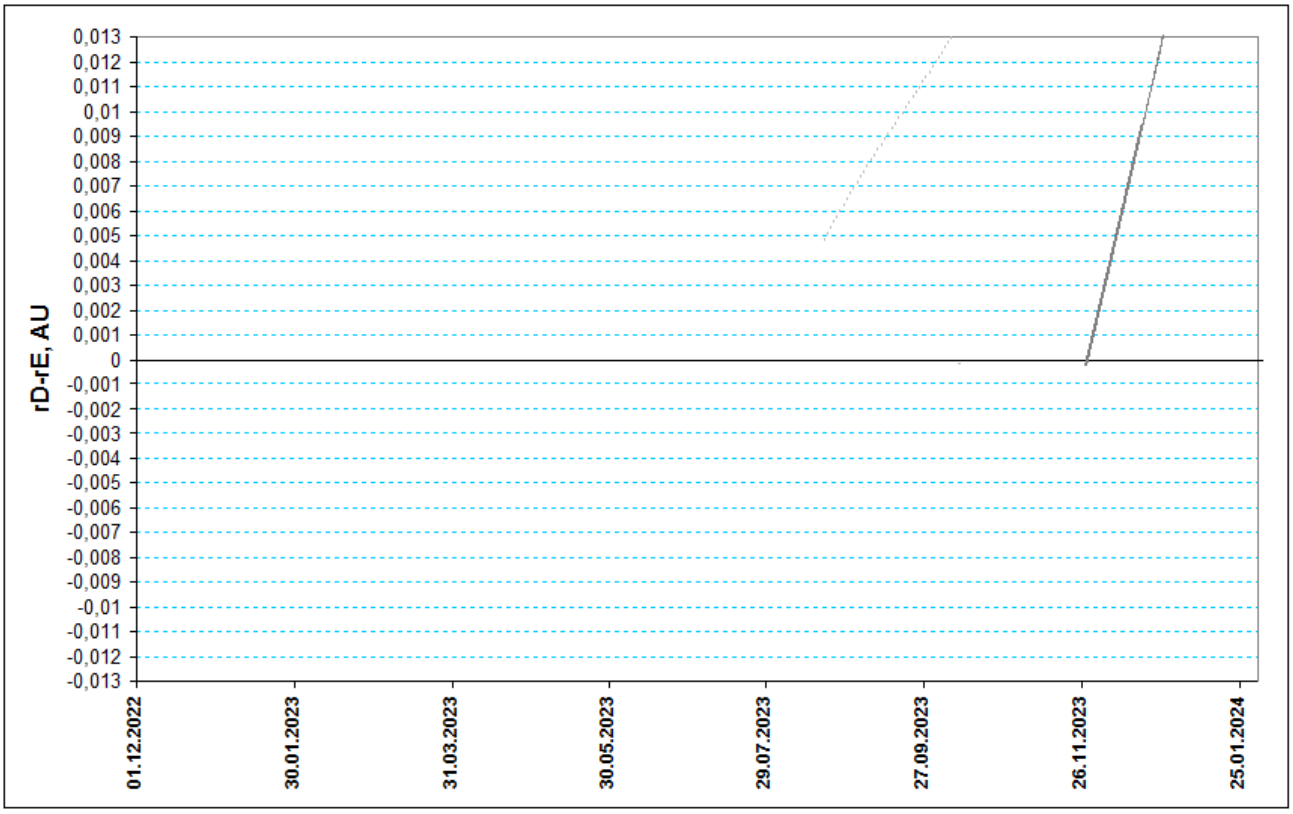

Figure 2 – Space-temporal projection of 46P-ids trail parts onto their minimal distance passages in 2023 after perihelion.

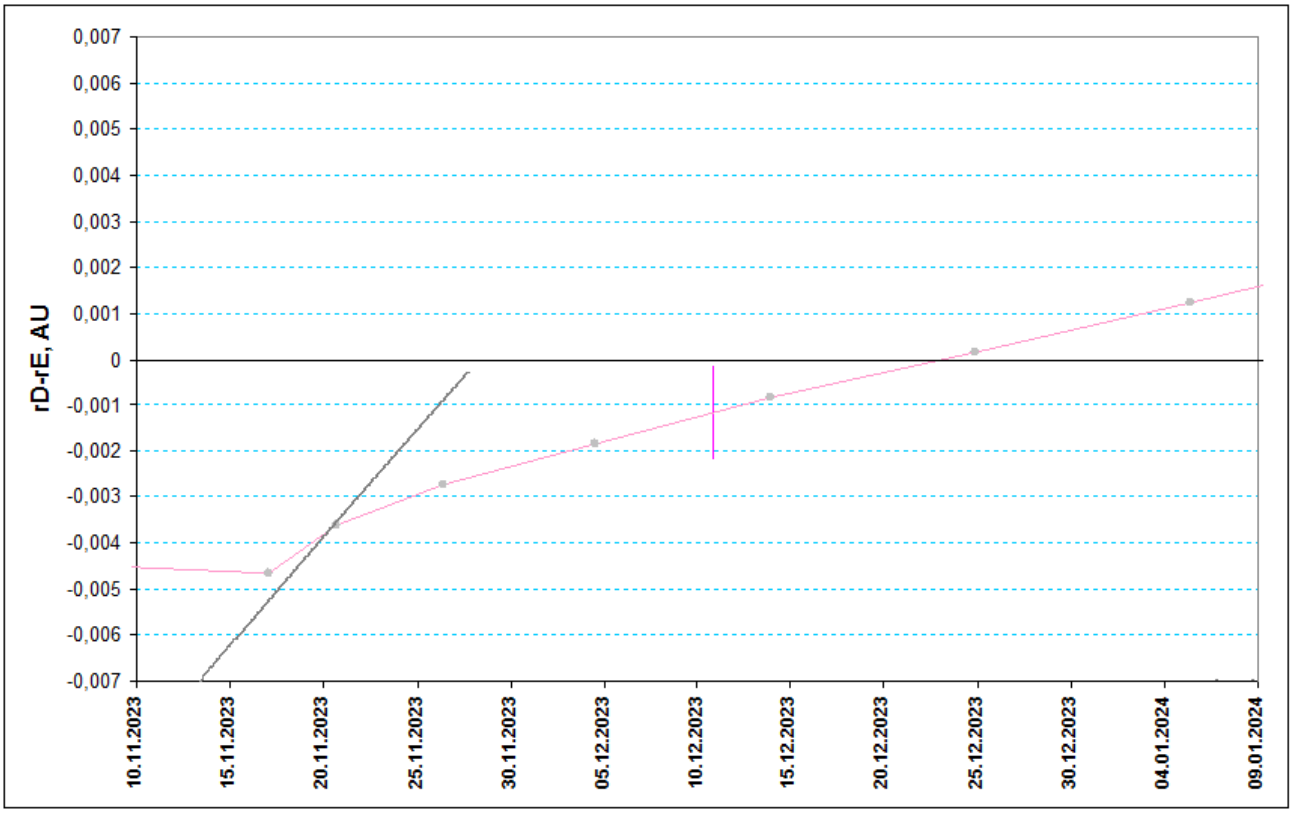

Figure 3 – Detailed space-temporal projection of the 1967 trail parts onto their minimal distance passages in 2023.

2 Forecast 2023

Two remarkable encounters of the Earth with dust trails of the comet 46P/Wirtanen were found for 2023. The first of them is the encounter with particles of the 1967 trail (see *Figure 3*).

Computed maximum time for the 1967 trail is 20^h55^m UT on December 10 from the radiant at RA = 346.5°, Dec = +27.4°. The Earth is to pass from a quite small distance from the trail, which is 0.0016 AU. However, ejection velocity of this trail particles is 58.7 m/s which is quite high meaning that particles sizes are small, so meteors from it are expected to be very faint. Also, the density of

this part of 1967 is very low, it is about 1.8% of the density of the 1 revolution Leonid's trail. Considering these parameters chances for any detectable activity from this trail is low but any observations still seem to be desirable.

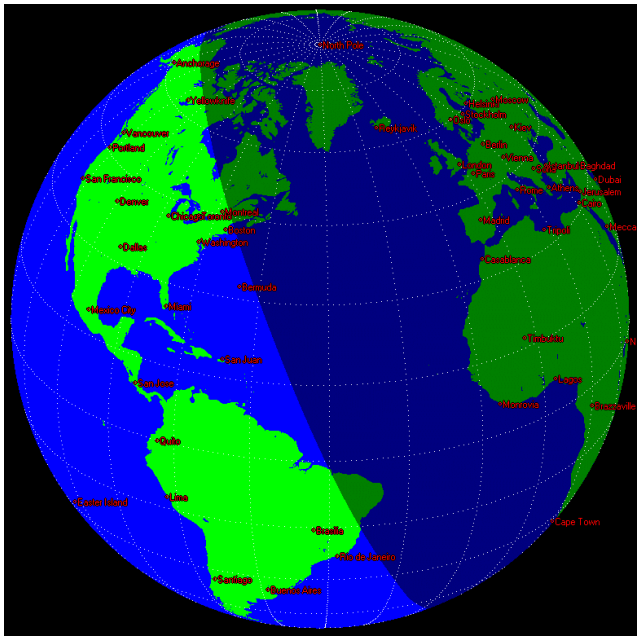

Figure 4 – The Earth as seen from the coming 46P-ids meteors (RA = 346.5°, Dec = +27.4°) during the expected maximum time of the outburst from the 1967 trail at 20^h55^m UT 10 December. The image is made using the software program Xearth 1.1.0 by Hewgill G.

When activity from the 1967 trail occurs at the computed time the best time to observe would be the western part of Africa and Western Europe. In Eastern Europe the radiant would be also above horizon but lower. The radiant would be quite high above Iceland and Greenland.

The second trail encountering the Earth in 2023 is the 1974 trail (see *Figure 5*).

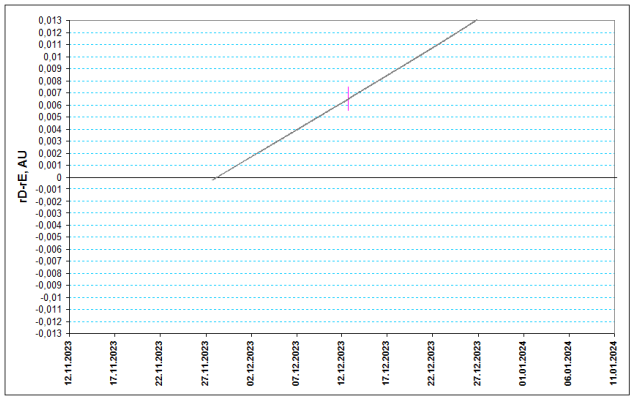

Figure 5 – Detailed space-temporal projection of the 1974 trail parts onto their minimal distance passages in 2023.

The computed time of maximum for this trail is 17^h54^m UT on December 12 with the radiant at RA = 7.7°, Dec = –40.0°. The orbit of comet 46P changed significantly in perihelia from 1967 to 1974 therefore there is a large difference between the orbits of respective trails as well as between their radiant positions in the sky, especially in declinations. At the same time the 1974 trail is considerably denser, 170 times, than the 1967 trail while ejection velocity is much slower, 27.2 m/s, which is also a positive factor for activity perspectives. The main problems with this encounter questioning any perspectives of activity at all, is the significant distance to the Earth at which this trail passes: 0.00646 AU. Nevertheless, it is also desirable to check this case with observations.

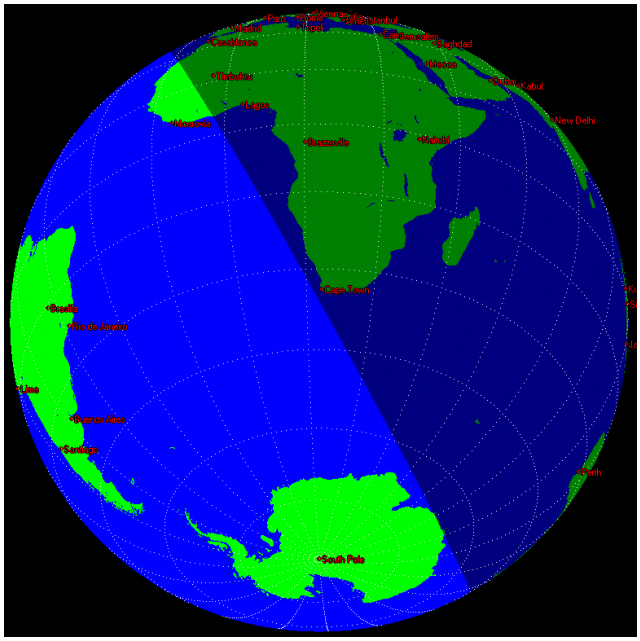

Figure 6 – The Earth as seen from coming 46P-ids meteors (RA = 7.7°, Dec = –40.0°) during the expected maximum time of the outburst from the 1974 trail at 17^h54^m UT 12 December. The image is made using the software program Xearth 1.1.0 by Hewgill G.

As the radiant of this trail is deep in the southern hemisphere its visibility is also worse. It would be visible only in Africa, excluding its western, southern and northern edges, as well as on adjacent territories like the Madagascar island and Arabian Peninsula.

3 Forecast 2024

In 2024 the Earth is expected to pass close to the 1974 trail of the comet 46P. The computed time of the maximum is 2^h21^m UT on December 13 with the radiant RA = 340.9°, Dec = +28.3°. Distance to the trail is 0.00165 AU, trail density is 54.6% of that for a 1 revolution Leonid's trail, ejection velocity is 59.12 m/s. These parameters are in general more favorable than those for the 2023 encounters and considering the quite large size of the comet 46P, there are good chances for some low but detectable activity with mainly faint meteors though. Unfortunately, this encounter is expected to occur under almost full Moon so bright moonlight will create additional problems for observations. However even despite these observations are highly recommended as meteor activity of the comet 46P stream has not yet been observed ever before.

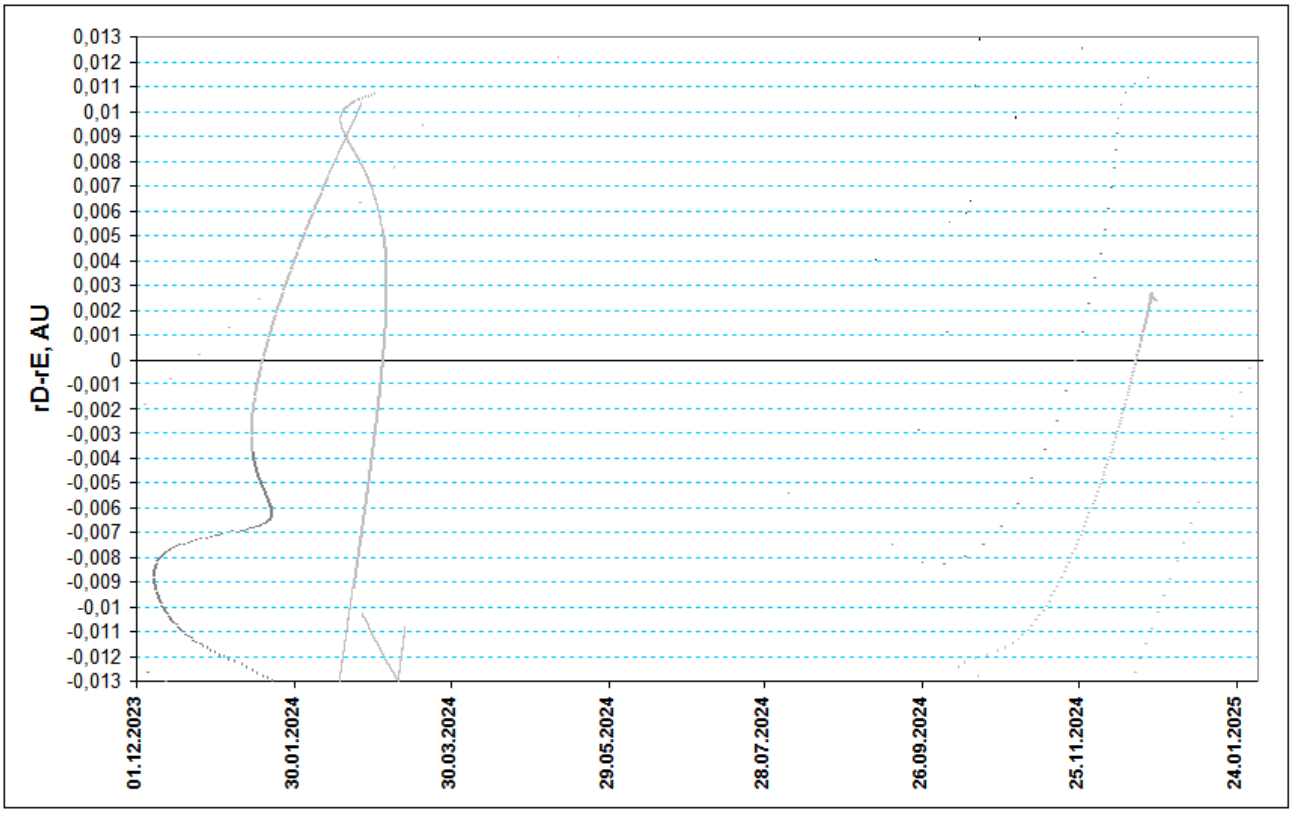

Figure 7 – Space-temporal projection of 46P-ids trail parts onto their minimal distance passages in 2024.

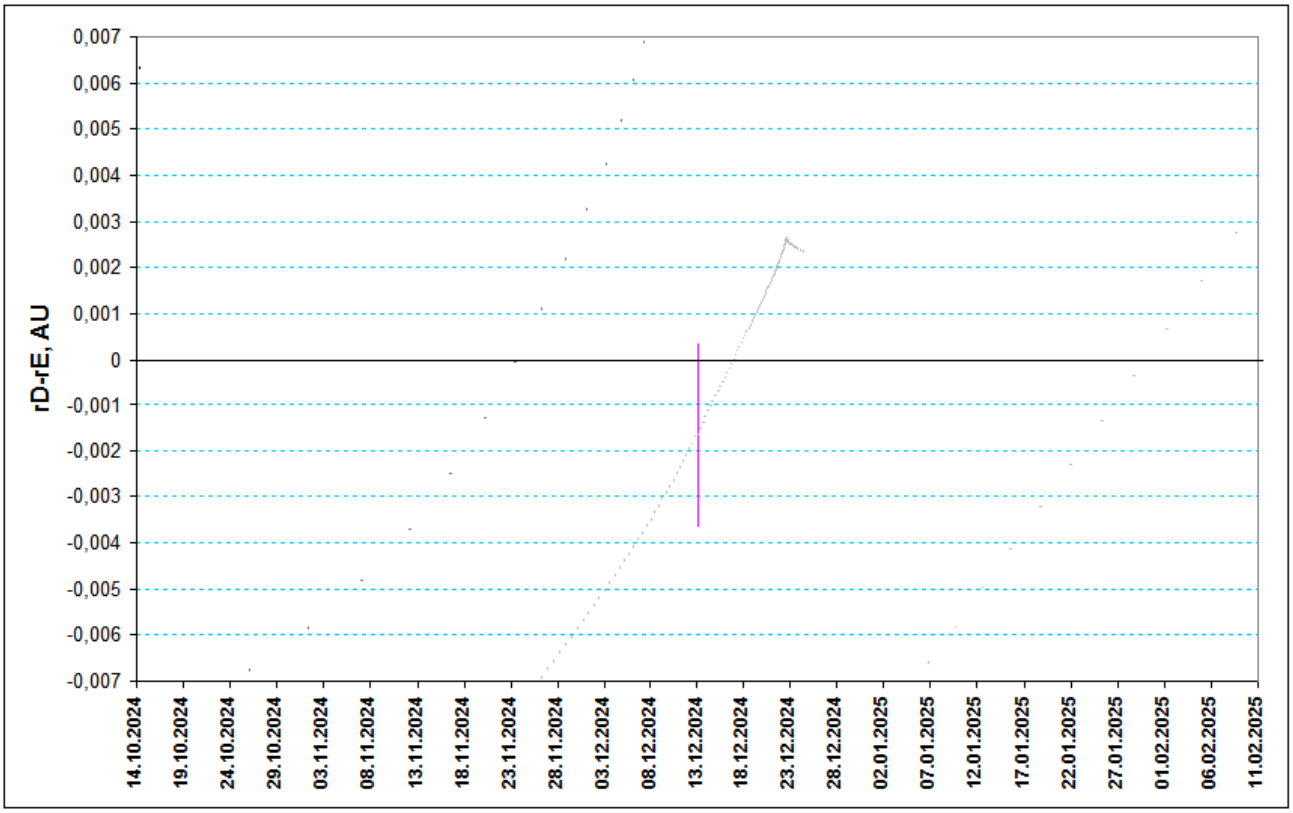

Figure 8 – Detailed space-temporal projection of 1974 trail parts onto their minimal distance passages in 2024.

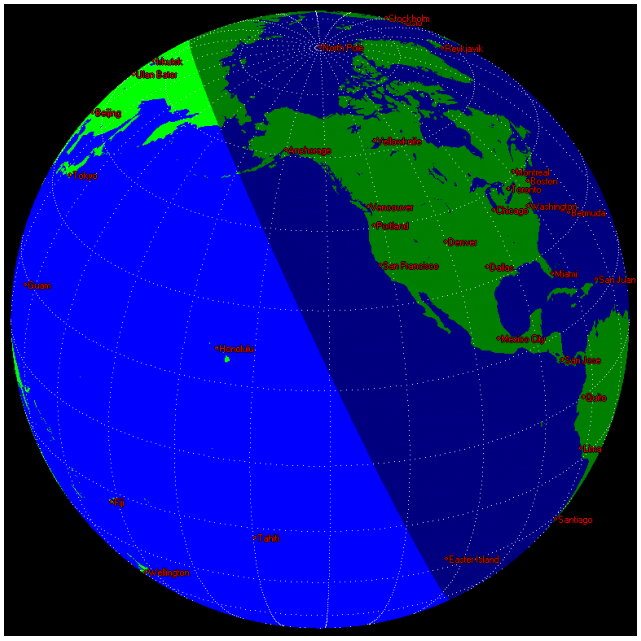

Figure 9 – The Earth as seen from coming 46P-ids meteors (RA = 340.9°, Dec = +28.3°) during the expected maximum time of outburst from the 1974 trail at 2^h21^m UT on 13 December. The image is made using the software program Xearth 1.1.0 by Hewgill G.

In case the activity takes place at the predicted time, it could be observed best in Northern and Central Americas excluding perhaps Alaska.

The forecasts for 2023[1] and 2024[2] are also published at my website.

References

Lyytinen E, van Flandern T. (1998). "Predicting the strength of Leonid outbursts". *Earth, Moon, and Planets*, **82/83**, 149–166.

Jenniskens P. (2006). Meteor showers and their parent comets. Cambridge, US, 780 p.

Kasuo Kinoshita, http://jcometobs.web.fc2.com/ [Orbital elements of the comet 46P/Wirtanen]

[1] http://feraj.ru/Radiants/Predictions/46p-ids2023eng.html

[2] http://feraj.ru/Radiants/Predictions/46p-ids2024eng.html

First observed meteors from comet 46P/Wirtanen (lambda-Sculptorids, LSC)

Paul Roggemans[1], Denis Vida[2], James M. Scott[3], Peter Jenniskens[4], Damir Šegon[5], and David Rollinson[6]

[1] **Pijnboomstraat 25, 2800 Mechelen, Belgium**
paul.roggemans@gmail.com

[2] **Department of Physics and Astronomy, University of Western Ontario, London, Ontario, N6A 3K7, Canada**
dvida@uwo.ca

[3] **University of Otago, Department of Geology, Dunedin, New Zealand**
james.scott@otago.ac.nz

[4] **SETI Institute, 339 Bernardo Ave, Mountain View, CA 94043, USA**
pjenniskens@seti.org

[5] **Astronomical Society Istra Pula, Park Monte Zaro 2, 52100 Pula, Croatia**
damir@astro.hr

[6] **Perth Observatory Volunteer Group, Bickley, Western Australia**

A meteor shower outburst caused by a predicted encounter with the 1974 trail of the Jupiter-family comet 46P/Wirtanen was optically observed above the southwest Pacific, close to the forecast time on the evening of December 12, 2023. 24 multi-station meteor orbits were computed using data from GMN and CAMS stations in New Zealand and Australia, with a radiant at R.A. 7.1° and Decl. –38.8°, located in the Sculptorid constellation. These observations confirm the predictions of its occurrence published earlier by Vauballion et al. (2023). The observed ZHR is low (~0.5 meteors/h) and is due to the slow in-atmosphere velocity of the shower meteoroids (~15 km/s). The average size of the observed meteoroids is ~4 mm, while most of the activity has been predicted in <mm sizes. The large video meteor camera arrays (> 100 cameras) hosted by amateur astronomers in New Zealand and Australia played a critical role in confirming this new meteor shower, as it would have otherwise been missed.

1 Introduction

In 1972, comet 46P/Wirtanen[3] (*Figure 1*) made a pass within 0.276 astronomical units of Jupiter, and another approach in 1984 came within 0.467 AU (*Figure 2*), *Figure 3* shows the current orbit of the comet. Known to be just over 1.5 km wide (Lejoly et al., 2022), 46P/Wirtanen is a Jupiter-family comet that orbits the Sun every 5.4 years. It was originally the target for the Rosetta mission before the mission was delayed and resulted in a change of target to 67P/Churyumov–Gerasimenko. The comet was long known as a potential parent body of a meteor shower due to its closeness to Earth's orbit (e.g., review by Ye and Jenniskens, 2022).

No meteor shower associated with this comet has been observed in the past, but Maslov (2024) published a forecast for possible activity from this comet in 2023 and 2024. He alerted observers about a possible first encounter at 20^h55^m UT on December 10, 2023 ($\lambda_\odot = 258.20°$) with particles from the 1967 trail and a second encounter at 17^h54^m UT on December 12, 2023 ($\lambda_\odot = 260.11°$) from the 1974 trail. Although the chances of meteoroids entering the atmosphere were not favorable for both encounters, the author asked observers to check for possible activity. He predicted a more favorable encounter for 2024 at 2^h21^m UT on December 13.

Figure 1 – 46P Wirtanen, photographed in 2018 by Rolf Carstens (Geyserland Observatory).

In another work, Vaubaillon et al. (2023) also calculated that an encounter with a new meteoroid stream above the Southwestern Pacific could be detected in 2023. Their simulations have shown that it is probable that no meteor activity occurred in the recent past, and 2023 would be the

[3] https://hubblesite.org/contents/media/images/2018/63/4300-Image.html

first year with any activity with a maximum on December 12, 2023, between 8^h00^m and 12^h30^m UT ($\lambda_\odot$ 259.689°–259.879°) with a radiant area near the star λ-Sculptoris ($7.5° < \alpha_g < 9.2°$, $-38° < \delta_g < -43°$). The low geocentric velocity (v_g ~10 km/s) and the relatively small sizes of the meteoroids make this a rather difficult shower for any visual observations (Vaubaillon et al., 2023). The predicted radiant position is in perfect agreement with the forecast by Maslov but the time of the maximum activity for the 1974 dust trail by Vaubaillon et al. (2023), is more than 6 hours earlier than forecast by Maslov.

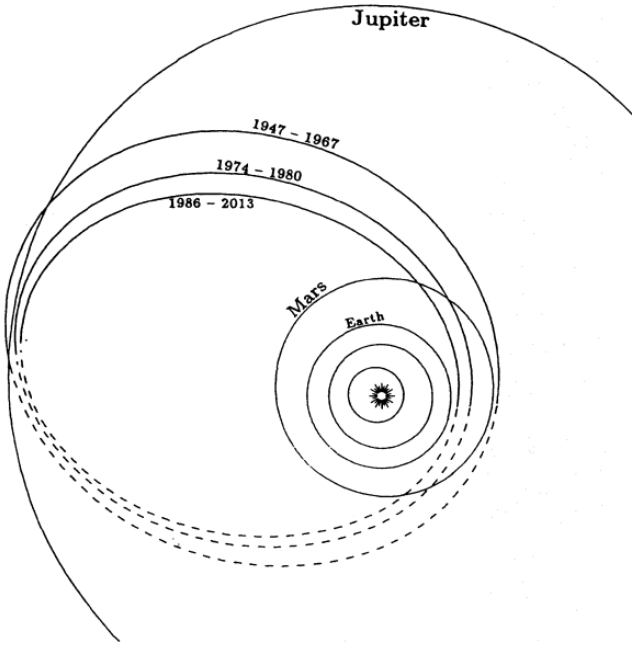

Figure 2 – 46P/Wirtanen, changes in its orbit in 1972 and 1984. (Reproduced from: Królikowska and Sitarski, 1996).

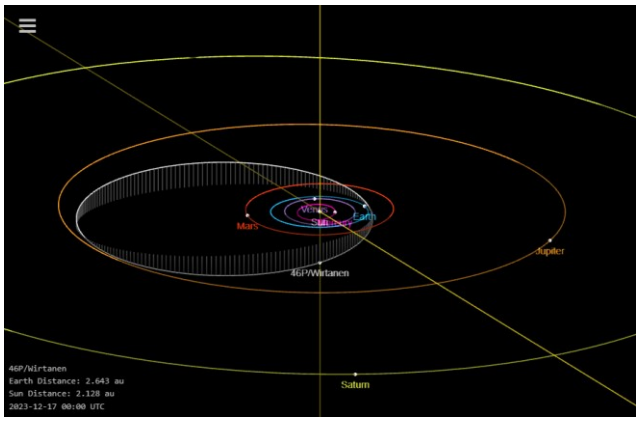

Figure 3 – The current orbit of the parent comet 46P/Wirtanen relative to the planets[4].

2 Radio observations

The first indication of unusual activity appeared on the webpages of IPRMO maintained by Hiroshi Ogawa and Hirofumi Sugimoto[5] which suggested likely enhanced activity recorded by radio observers. However, some caution is warranted since radio forward-scattering observations cannot identify the direction of observed meteor echoes but only provide raw counts. The final compilation of radio observations shows a broader and shallower peak lasting until solar longitude 260.3° (*Figure 4*). The graph is calculated using the factors for the Geminids and not for 46P/Wirtanen. Further investigation is required to determine the cause of this rate enhancement which will be treated in a separate report.

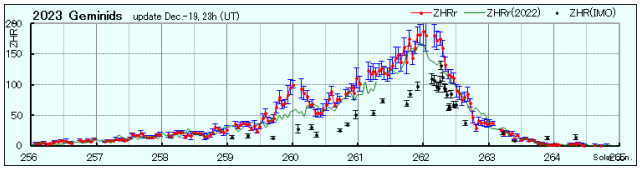

Figure 4 – First indication for a possible meteor activity caused by particles from 46P/Wirtanen, extracted from the website on December 19, status 23^h UT (credit Hirofumi Sugimoto).

3 Video observations

Figure 5 – December 12th night sky image collected NZ0017 in Rotorua, New Zealand. This stacked night image comprises mostly Geminid meteors and a couple of lambda-Sculptorid meteors (Credit: Peter McKellar).

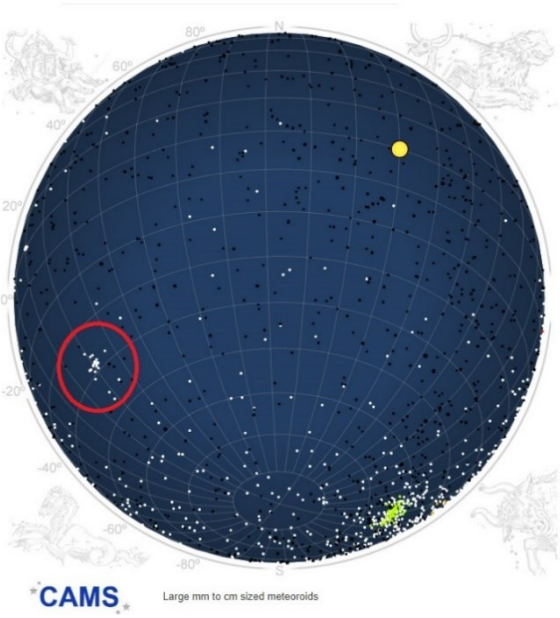

Figure 6– Plot for 2023 December 13 taken from the CAMS website[6]. The region with the radiant produced by particles that were released by comet 46P/Wirtanen is marked with red.

CAMS Chile (Jenniskens et al., 2011) detected a single

[4] https://ssd.jpl.nasa.gov/tools/sbdb_lookup.html#/?des=46P&view=VOP

[5] https://www.iprmo.org/flash/gem-2023.html

[6] http://cams.seti.org/FDL/

meteor associated with this new shower in the hours leading up to this peak (see *Table 1*), but CAMS New Zealand on the South Island was clouded out.

The Global Meteor Network (GMN; Vida et al., 2019, 2020, 2021) cameras on the North Island of New Zealand (coordinated by J. Scott at the University of Otago) successfully recorded 10 meteors within the predicted range of radiants (*Figures 5 and 9*). A CBET telegram was issued following this confirmation (Jenniskens et al., 2023).

Further 12 meteors were detected by the cameras of Global Meteor Network in Australia (coordinated by D. Rollinson) (*Figures 10 and 11*), and 4 were also detected by the CAMS cameras of the CAMS Australia network (coordinated by H. Devillepoix at Curtin University).

The main activity at optical sizes occurred between 259.76° and 260.08° in solar longitude (or December, 12, 9^h40^m and 17^h10^m UTC) with 24 meteor orbits captured within this interval. One of these 24 was recorded from Bulgaria and another from South Korea, both with a D-criterion $D_D < 0.01$ (Drummond, 1981). Apart from the CAMS orbit recorded in Chile, 3 more orbits with very similar elements were recorded before the main group of 24 orbits, two from the UK and one from Bulgaria. One more orbit was detected in New Zealand about 20 hours after the main group.

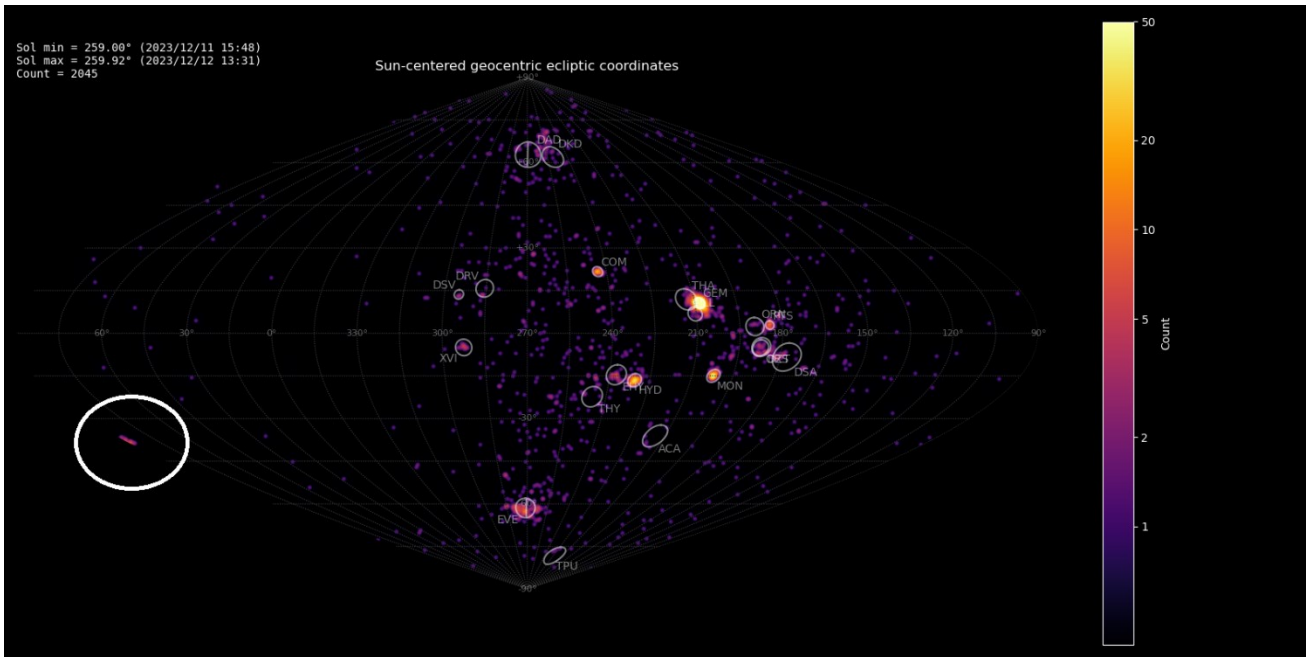

Figure 7 – Heat map for 2045 Sun-centered ecliptic radiants obtained by GMN during the time interval 259.00° < λ_O < 259.92°.

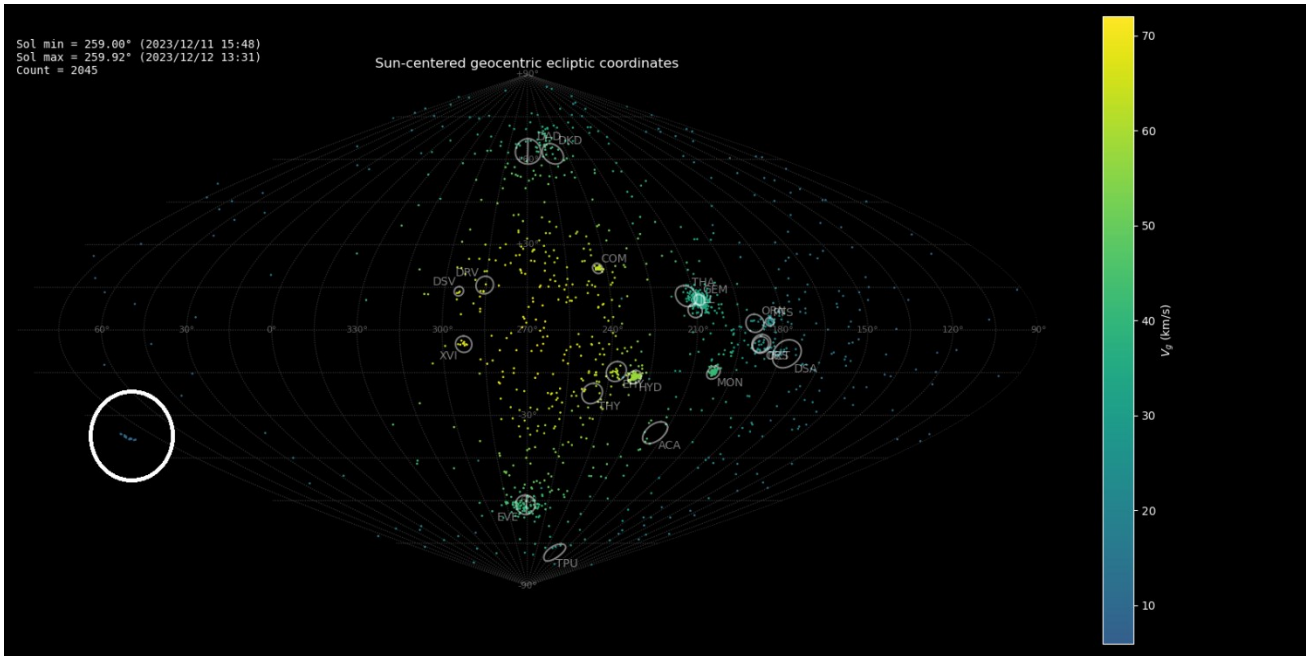

Figure 8 – Velocity distribution for 2045 Sun-centered ecliptic radiants obtained by GMN during the time interval 259.00° < λ_O < 259.92°.

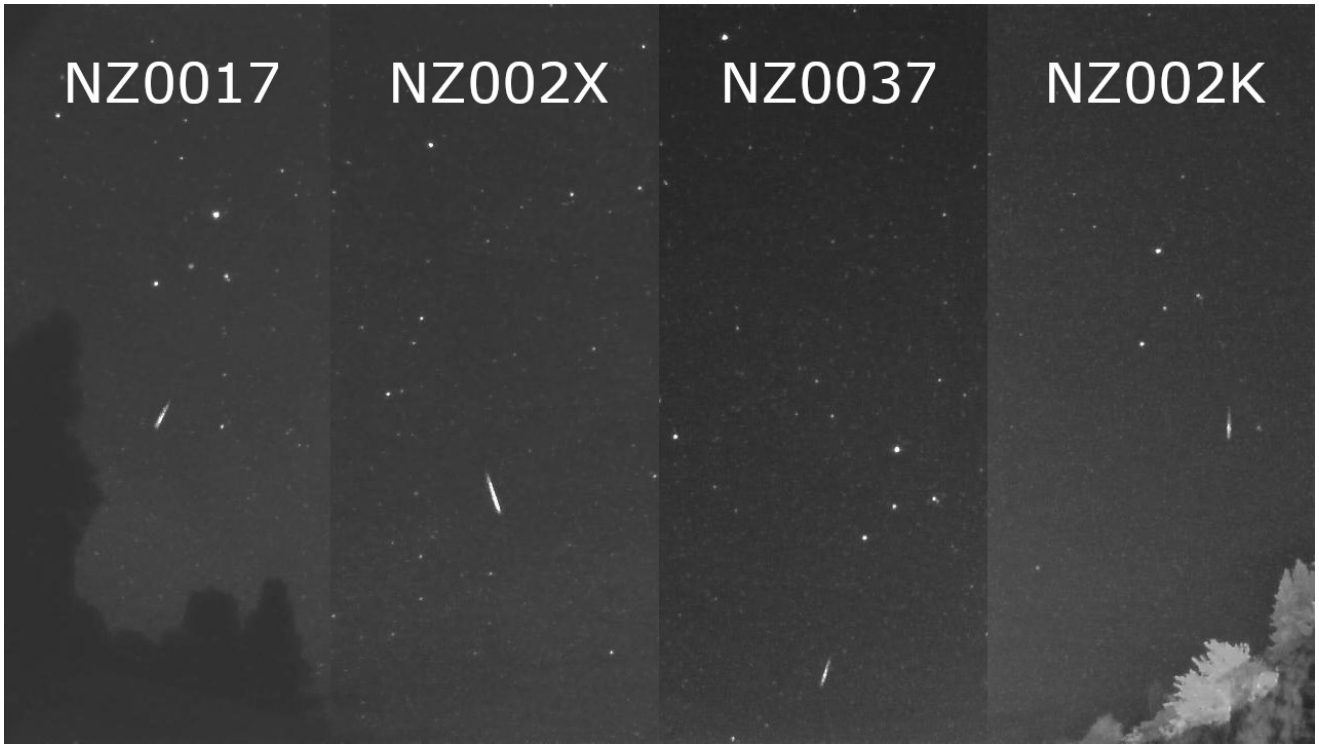

Figure 9 – A lambda-Sculptorid as recorded on 12 December, 2023, at $11^h05^m58^s$ UT from 4 locations by GMN cameras in New Zealand. NZ0017 is Kaharoa, Rotorua, NZ002X is Maharakeke Road 1, Waipukurau, NZ0037 Welcome Bay 2, Tauranga, NZ002K Western Heights High School, Rotorua.

Figure 10 – A lambda-Sculptorid meteor recorded by AU001D at Darkan, Western Australia at $13^h21^m43.1^s$ UT on 12 December 2023.

Figure 11 – A lambda-Sculptorid meteor recorded by AU002C at Pemberton, Western Australia at $13^h21^m43.1^s$ UT on 12 December 2023.

Figures 6, 7 and 8 show that the usual number of meteor radiants near the antapex is very low. The antapex is the direction opposite to the direction of Earth's motion around the Sun, which is at the edge of the plot in *Figures 7 and 8*. The reason is that these meteoroids come from the rear into the Earth atmosphere which moves away at about 30 km/s. Meteoroids entering the atmosphere from this direction must catch up to the Earth and have enough velocity relative to our planet to produce enough energy to cause ionization and become visible as a meteor. Experienced meteor observers know that the local evening hours display low meteor activity compared to the morning sky when our planet catches meteoroids 'head-on'. For example, typical evening meteor showers such as the Andromedids and October Draconids produce very slow meteors from a very dispersed apparent radiant, comparable to meteors from 46P/Wirtanen. Hypothetically, if the Earth encountered the same meteoroids head-on at much higher velocities (the radiant would be near the apex), a particle of the same size would produce much brighter meteors thanks to the energy being proportional to the square of the impact velocity.

4 Mean radiant and orbit

An analysis with an iterative procedure to locate the best-fitting mean orbit for a concentration of similar orbits has been applied to a sample of GMN orbits selected as follows:

- $258° < \lambda_\odot < 261°$
- $350° < \alpha_g < 20°$
- $-46° < \delta_g < -36°$
- $v_g < 12$ km/s

9717 orbits, recorded by GMN in 2023, were available for the above-mentioned time interval in solar longitude. The method used for this search has been described before (Roggemans et al., 2019) and combines three classic

discrimination criteria, considering different classes for the degree of similarity. The discrimination criteria used in this method are that of Southworth and Hawkins (1963), identified as D_{SH}, Drummond (1981), identified as D_D, and Jopek (1993), identified as D_H. The method to compute the mean orbit at each step during the iteration process has been described by Jopek et al. (2006). We define five different classes with specific threshold levels of similarity:

- Low: $D_{SH} < 0.25$ & $D_D < 0.105$ & $D_H < 0.25$;
- Medium low: $D_{SH} < 0.2$ & $D_D < 0.08$ & $D_H < 0.2$;
- Medium high: $D_{SH} < 0.15$ & $D_D < 0.06$ & $D_H < 0.15$;
- High: $D_{SH} < 0.1$ & $D_D < 0.04$ & $D_H < 0.1$.
- Very high: $D_{SH} < 0.05$ & $D_D < 0.02$ & $D_H < 0.05$.

The procedure converged at a mean orbit derived from 28 similar orbits with the median radiant almost exactly at the predicted position (*Table 1*). For this type of orbit, we consider only orbits with a high threshold of similarity ($D_D < 0.04$) in order to exclude random sporadic orbits. The first meteor was recorded by 9 cameras in the UK at $\lambda_\odot = 258.18°$, followed at $\lambda_\odot = 259.054°$ by a second meteor by two GMN cameras in Bulgaria. The next of these orbits was recorded at $\lambda_\odot = 259.122°$ by four cameras in the UK. Then there is a pause until 24 more orbits were detected during the interval $259.76° < \lambda_\odot < 260.08°$, 10 by cameras in New Zealand, 12 by cameras in Australia, one from Bulgaria and one from South Korea, all except four with $D_{SH} < 0.03$ and $D_D < 0.02$. It seems no activity was detected between the first three cases, and the cluster of 24 very similar orbits, although cameras were successfully capturing in between from different geographic locations.

Table 1 – The orbital elements of the parent comet[7], and mean orbital parameters of the meteors based on CAMS (Jenniskens, 2023) and GMN data.

	46P/Wirtanen	CAMS	GMN
Epoch	JD 2458465	J2000.0	J2000.0
$\lambda_\odot$ (°)	–	259.402	259.93
α_g (°)	–	4.6±0.5	7.1±1.7
δ_g (°)	–	–36.4±0.9	–38.8±0.8
v_g (km/s)	–	8.6±0.1	10.0±0.2
$\lambda - \lambda_\odot$ (°)	–	–	88.3±1.4
β (°)	–	–	–37.8±1.0
H_b (km)	–	–	90.2±1.1
H_e (km)	–	–	78.9±3.2
a (AU)	3.09	4.1	2.90±0.16
q (AU)	1.05536	0.968	0.9846
e	0.6588	0.766	0.661±0.002
ω (°)	356.340	343.7	359.84±0.75
Ω (°)	82.158	79.4	79.92
i (°)	11.75	7.6	9.17±0.32
Π (°)	78.5	63.1	79.76±0.74
T_j	2.82	2.40	2.90±0.09
N	–	1	24

[7] https://wirtanen.astro.umd.edu/46P/46P_orbit.shtml

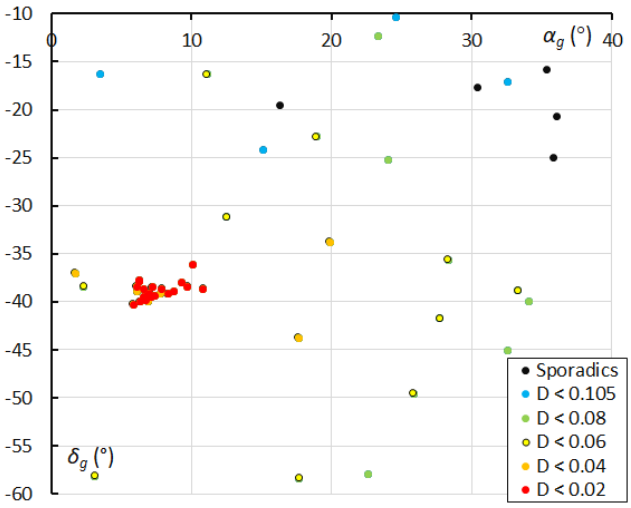

Figure 12 – The 46P/Wirtanen meteor radiant in geocentric equatorial coordinates (GMN orbit data).

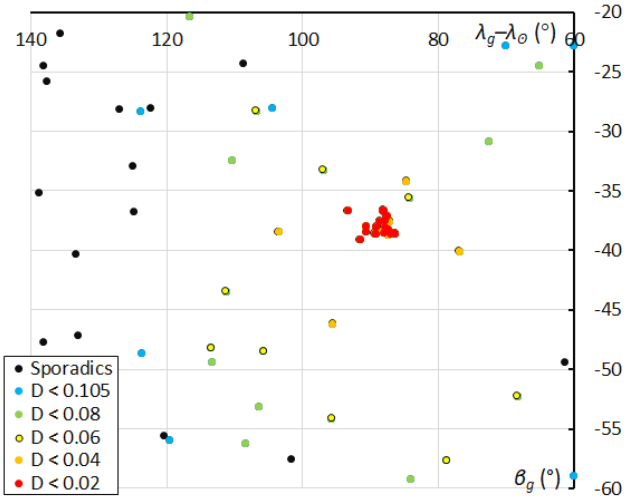

Figure 13 – The 46P/Wirtanen meteor radiant in geocentric Sun-centered ecliptic coordinates (GMN orbit data).

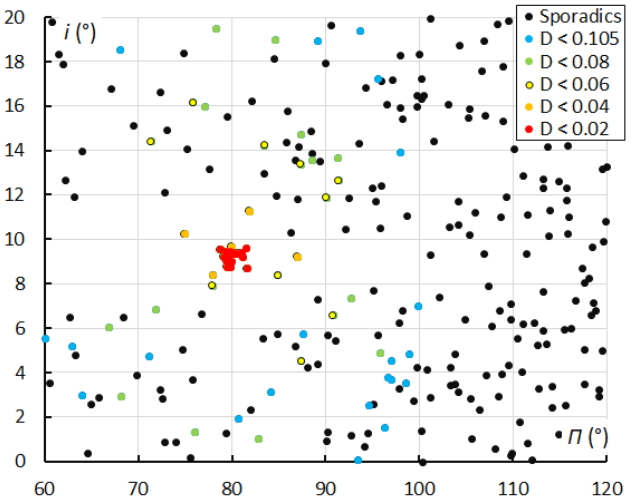

Figure 14 – The distribution of the inclination i against the longitude of perihelion Π for the 46P/Wirtanen meteoroid orbits (GMN orbit data).

The Solar System is filled with very old meteoroids on orbits at low inclination which have evolved over time far away from the orbits of their parent bodies, and which

cannot be associated with any meteoroid stream. These meteoroids are classified as sporadic. Sometimes it may be difficult to differentiate between a sporadic on a very similar orbit to a shower meteor and a dispersed meteoroid stream member. Therefore, we decided to use only the 24 orbits in a tight cluster within time of the predicted activity. The values given for GMN data in *Table 1* are based on this cluster.

The radiant plot in equatorial coordinates (*Figure 12*) shows a very compact radiant area with only 3 events separated from the main radiant concentration. The same situation appears in the plot with the Sun-centered ecliptic coordinates (*Figure 13*). Looking at the distribution of the inclination i against the longitude of perihelion Π, we see the same concentration (*Figure 14*). We can conclude that there is sufficient evidence that Earth encountered a concentration of particles which confirm the presence of dust produced by the 1974 dust trail of comet 46P/Wirtanen.

The black dots in *Figures 12, 13 and 14* are sporadic orbits. For the computation of the mean orbit only the red and orange dots were considered ($D_D < 0.04$). The compact concentration of these orbits is obvious from these distributions. For reason of completeness, we also plot the "less" similar orbits color-coded as yellow, green and blue. In our limited analysis, we cannot assess if these are dispersed particles associated with 46P/Wirtanen or are simply nearby sporadics.

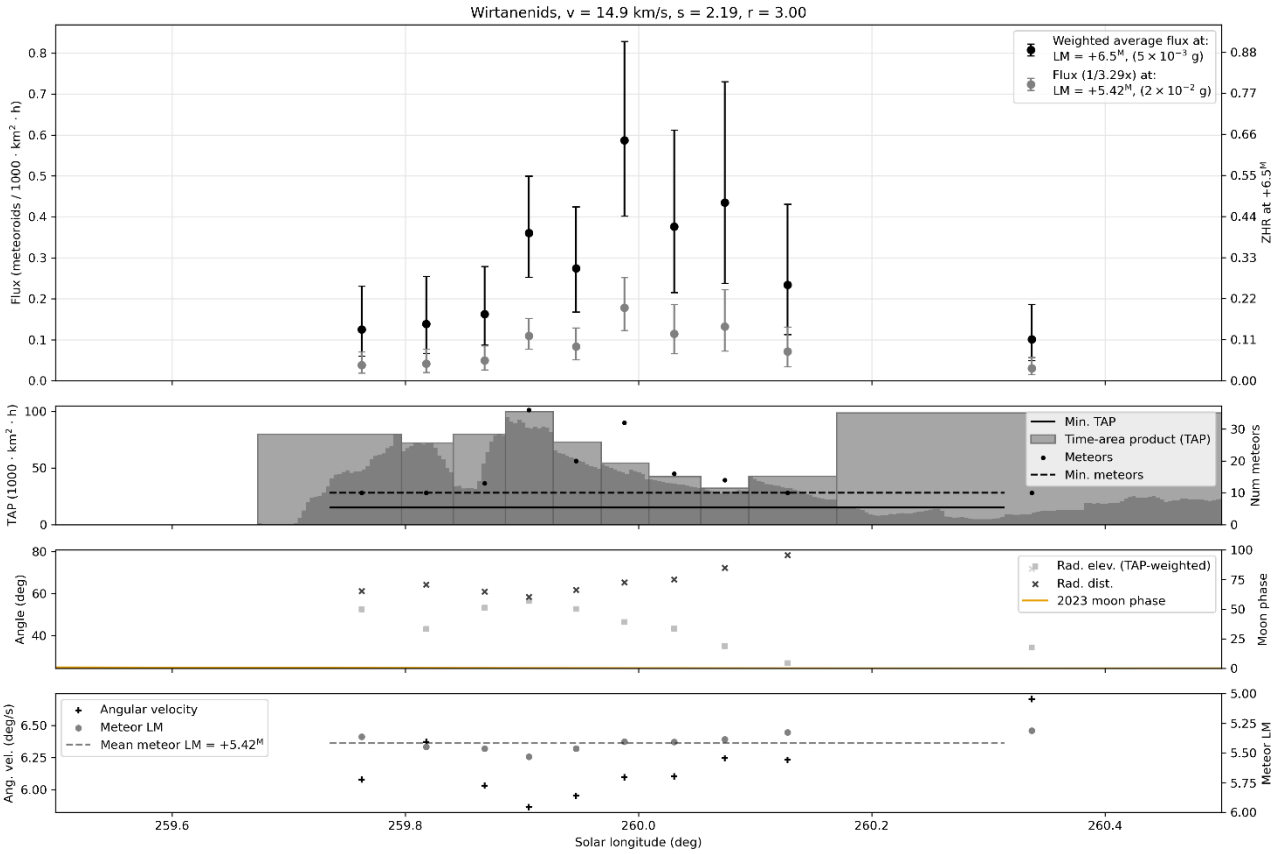

Figure 15 – The flux and corresponding ZHR profile (Vida et al., 2022) for the lambda-Sculptorids based on GMN data collected during 2023.

We also checked for possible activity from the first encounter forecasted by Mikail Maslov, at 20^h55^m UT on December 10 ($\lambda_\odot = 258.20°$) with particles from the 1967 trail. We found only 3 orbits at this node with $D_D < 0.04$, dispersed over about a day and which cannot be excluded as sporadics.

A search among meteor orbit data of previous years resulted in a number of similar orbits with $D_D < 0.04$ using the mean orbit from *Table 1* as a reference orbit. The search was applied on 471583 orbits by CAMS (2010–2016), 508266 orbits by EDMOND (2001–2023), 722314 orbits by GMN (2018–2022) and 443196 orbits by SonotaCo network (2007–2022), 2145359 orbits in total. All positive matches were dispersed in time and in radiants, with no obvious clustering. We conclude that they can be explained as sporadics and that there is no indication of any activity from this source in the past, in line with the findings by Vaubaillion et al. (2023).

5 Activity profile

The meteor shower flux profile based on ~150 single-station meteors reported by the GMN (*Figure 15*) shows that the peak ZHR of the shower was around 0.5 meteors/h, which is well below the detectability threshold for visual observers. In other words, without a large-scale network of video cameras, this activity would have passed completely unnoticed. On average, each camera observed around one lambda-Sculptorid meteor during the entire night.

The mean limiting mass of the flux observations was around 0.02 grams, translating to meteoroids of 4 mm in diameter assuming a cometary meteoroid bulk density of 500 kg/m^3.

According to the stream modelling, the shower should have been mainly produced by small particles with a size of less than 1 mm, just under the detectability limit of wide-field GMN cameras but detectable by radio. There is some enhancement in radio meteor activity during the lambda-Sculptorids video activity, but it is unclear if this is due to this meteor shower or some other source. The outstanding question is whether any enhanced activity in radio echoes can be confirmed.

6 Conclusion

Radio observers contributing to IPRMO were the first to indicate possible meteor activity related to the 1974 dust trail released by 46P/Wirtanen, but it remains to be confirmed which source caused this enhancement. The visual (video) counterpart confirmed the meteor activity from the predicted radiant position, but with a low activity level (ZHR around 0.5 meteors/h).

The radiant position predicted by Maslov (2024) and Vaubaillon et al. (2023) matches the observed position. The time of the observed activity occurred a few hours later than predicted by Vaubaillon et al. (2023) and a few hours earlier than predicted by Maslov (2024), indicating possible improvements in the shower model parameters.

The new meteor shower has been added to the IAU MDC[8] meteor shower list with preliminary designation M2023-Y1. Once established, it will be given the currently provisional name of lambda-Sculptorids (LSC).

According to Maslov (2024), another possible opportunity to see this shower may occur next year 2024 on December 13, 2^{h}21^m UT from a radiant at RA = 340.9°, Dec = +28.3°.

Acknowledgment

The authors thank all the camera operators and people involved in the Global Meteor Network and CAMS. The Global Meteor Network (GMN) data are released under the following license[9].

The Global Meteor Network results were obtained thanks to the efforts of the following volunteers: *Adam Mullins, Aden Walker, Adrian Bigland, Adriana Roggemans, Alain Marin, Alaistar Brickhill, Alan Beech, Alan Maunder, Alan Pevec, Alan Pickwick, Alan Decamps, Alan Cowie, Alastair Emerson, Aled Powell, Alejandro Barriuso, Aleksandar Merlak, Alex Bell, Alex Haislip, Alex Hodge, Alex Jeffery, Alex Kichev, Alex McConahay, Alex Pratt, Alex Roig, Alex Aitov, Alexander Wiedekind-Klein, Alexandre Alves, Alfredo Dal' Ava Júnior, Alison Scott, Amy Barron, Anatoly Ijon, Andre Rousseau, Andre Bruton, Andrea Storani, Andrei Marukhno, Andres Fernandez, Andrew Campbell-Laing, Andrew Challis, Andrew Cooper, Andrew Fiamingo, Andrew Heath, Andrew Moyle, Andrew Washington, Andrew Fulher, Andrew Robertson, Andy Stott, Andy Sapir, Ange Fox, Angel Sierra, Angélica López Olmos, Anna Johnston, Ansgar Schmidt, Anthony Hopkinson, Anthony Pitt, Anthony Kesterton, Anton Macan, Anton Yanishevskiy, Antony Crowther, Anzhari Purnomo, Arie Blumenzweig, Arie Verveer, Arnaud Leroy, Attila Nemes, Barry Findley, Bart Dessoy, Bela Szomi Kralj, Bernard Côté, Bernard Hagen, Bev M. Ewen-Smith, Bill Cooke, Bill Wallace, Bill Witte, Bill Carr, Bill Thomas, Bob Evans, Bob Greschke, Bob Hufnagel, Bob Marshall, Bob Massey, Bob Zarnke, Bob Guzik, Brenda Goodwill, Brendan Cooney, Brendon Reid, Brian Chapman, Brian Murphy, Brian Rowe, Brian Hochgurtel, Wyatt Hochgurtel, Brian Mitchell, Bruno Bonicontro, Callum Potter, Carl Elkins, Carl Mustoe, Carl Panter, Charles Thody, Charlie McCormack, Chris Baddiley, Chris Blake, Chris Dakin, Chris George, Chris James, Chris Ramsay, Chris Reichelt, Chris Chad, Chris O'Neill, Chris White, Chris Jones, Chris Sale, Christian Wanlin, Christine Ord, Christof Zink, Christophe Demeautis, Christopher Coomber, Christopher Curtis, Christopher Tofts, Christopher Brooks, Chuck Goldsmith, Chuck Pullen, Ciaran Tangney, Claude Boivin, Claude Surprenant, Clive Sanders, Colin Graham, Colin Marshall, Colin Nichols, Con Stoitsis, Craig Young, Creina Beaman, Daknam Al-Ahmadi, Damien Lemay, Damien McNamara, Damir Matković, Damir Šegon, Damjan Nemarnik, Dan Klinglesmith, Dan Pye, Daniel Duarte, Daniel J. Grinkevich, Daniela Cardozo Mourão, Danijel Reponj, Danko Kočiš, Dario Zubović, Dave Jones, Dave Mowbray, Dave Newbury, Dave Smith, David Akerman, David Attreed, David Bailey, David Brash, David Castledine, David Hatton, David Leurquin, David Price, David Rankin, David Robinson, David Rollinson, David Strawford, David Taylor, David Rogers, David Banes, David Johnston, David Rees, David Cowan, David Greig, David Hickey, David Colthorpe, Dean Moore, Debbie Godsiff, Denis Bergeron, Denis St-Gelais, Dennis Behan, Derek Poulton, Didier Walliang, Dimitris Georgoulas, Dino Čaljkušić, Dmitrii Rychkov, Dominique Guiot, Don Anderson, Don Hladiuk, Dorian Božičević, Dougal Matthews, Douglas Sloane, Douglas Stone, Dustin Rego, Dylan O'Donnell, Ed Breuer, Ed Harman, Edd Stone, Edgar Mendes Merizio, Edison José Felipe Pérezgómez Álvarez, Edson Valencia Morales, Eduardo Fernandez Del Peloso, Edward Cooper, Ehud Behar, Eleanor Mayers, Emily Barraclough, Enrico Pettarin, Enrique Arce, Enrique Chávez Garcilazo, Eric Lopez, Eric Toops, Errol Balks, Erwin van Ballegoij, Erwin Harkink, Eugene Potapov, Ewan Richardson, Fabricio Borges, Fernando Dall'Igna, Fernando Jordan, Fernando Requena, Filip Matković, Filip Mezak, Filip Parag, Fiona Cole, Florent Benoit, Francis Rowsell, François Simard, Frank Lyter, Frantisek Bilek, Gabor Sule, Gaétan Laflamme, Gareth Brown, Gareth Lloyd, Gareth Oakey, Garry Dymond, Gary Parker, Gary Eason, Gavin Martin, Gene Mroz, Geoff Scott, Georges Attard, Georgi*

[8] https://www.ta3.sk/IAUC22DB/MDC2022/Roje/roje_lista.php?corobic_roje=0&sort_roje=0

[9] https://creativecommons.org/licenses/by/4.0/

Momchilov, Germano Soru, Gilton Cavallini, Gordon Hudson, Graeme Hanigan, Graeme McKay, Graham Stevens, Graham Winstanley, Graham Henstridge, Graham Atkinson, Graham Palmer, Greg Michael, Greg Parker, Gustav Frisholm, Gustavo Silveira B. Carvalho, Guy Létourneau, Guy Williamson, Guy Lesser, Hamish Barker, Hamish McKinnon, Haris Jeffrey, Harri Kiiskinen, Hartmut Leiting, Heather Petelo, Heriton Rocha, Hervé Lamy, Herve Roche, Holger Pedersen, Horst Meyerdierks, Howard Edin, Hugo González, Iain Drea, Ian Enting Graham, Ian Lauwerys, Ian Parker, Ian Pass, Ian A. Smith, Ian Williams, Ian Hepworth, Ian Collins, Igor Duchaj, Igor Henrique, Igor Macuka, Igor Pavletić, Ilya Jankowsky, Ioannis Kedros, Ivan Gašparić, Ivan Sardelić, Ivica Ćiković, Ivica Skokić, Ivo Dijan, Ivo Silvestri, Jack Barrett, Jacques Masson, Jacques Walliang, Jacqui Thompson, James Davenport, James Farrar, James Scott, James Stanley, James Dawson, Jamie Allen, Jamie Cooper, Jamie McCulloch, Jamie Olver, Jamie Shepherd, Jan Hykel, Jan Wisniewski, Janis Russell, Janusz Powazki, Jason Burns, Jason Charles, Jason Gill, Jason van Hattum, Jason Sanders, Javor Kac, Jay Shaffer, Jean Francois Larouche, Jean Vallieres, Jean Brunet, Jean-Baptiste Kikwaya, Jean-Fabien Barrois, Jean-Louis Naudin, Jean-Marie Jacquart, Jean-Paul Dumoulin, Jean-Philippe Barrilliot, Jeff Holmes, Jeff Huddle, Jeff Wood, Jeff Devries, Jeffrey Legg, Jeremy Taylor, Jesse Stayte, Jesse Lard, Jessica Richards, Jim Blackhurst, Jim Cheetham, Jim Critchley, Jim Fordice, Jim Gilbert, Jim Rowe, Jim Seargeant, Jochen Vollsted, Jocimar Justino, John W. Briggs, John Drummond, John Hale, John Kmetz, John Maclean, John Savage, John Thurmond, John Tuckett, John Waller, John Wildridge, John Bailey, Jon Bursey, Jonathan Alexis Valdez Aguilar, Jonathan Eames, Jonathan Mackey, Jonathan Whiting, Jonathan Wyatt, Jonathon Kambulow, Jorge Augusto Acosta Bermúdez, Jorge Oliveira, Jose Carballada, Jose Galindo Lopez, José María García, José-Luis Martín, Josip Belas, Josip Krpan, Jost Jahn, Juan Luis Muñoz, Jure Zakrajšek, Jürgen Dörr, Jürgen Ketterer, Justin Zani, Karen Smith, Karl Browne, Kath Johnston, Kees Habraken, Keith Maslin, Keith Biggin, Keith Christie, Ken Jamrogowicz, Ken Lawson, Ken Gledhill, Kevin Gibbs-Wragge, Kevin Morgan, Kevin Faure, Klaas Jobse, Korado Korlević, Kyle Francis, Lachlan Gilbert, Larry Groom, Laurent Brunetto, Laurie Stanton, Lawrence Saville, Lee Hill, Leith Robertson, Len North, Leslie Kaye, Lev Pustil'Nik, Lexie Wallace, Lisa Holstein, Llewellyn Cupido, Logan Carpenter, Lorna McCalman, Louw Ferreira, Lovro Pavletić, Lubomir Moravek, Luc Turbide, Lucia Dowling, Luciano Miguel Diniz, Ludger Börgerding, Luis Fabiano Fetter, Maciej Reszelsk, Magda Wisniewska, Manel Colldecarrera, Marc Corretgé Gilart, Marcel Berger, Marcelo Domingues, Marcelo Zurita, Marcio Malacarne, Marco Verstraaten, Margareta Gumilar, Marián Harnádek, Mariusz Adamczyk, Mark Fairfax, Mark Gatehouse, Mark Haworth, Mark McIntyre, Mark Phillips, Mark Robbins, Mark Spink, Mark Suhovecky, Mark Williams, Mark Ward, Marko Šegon, Marshall Palmer, Marthinus Roos, Martin Breukers, Martin Richmond-Hardy, Martin Robinson, Martin Walker, Martin Woodward, Martin Connors, Martyn Andrews, Mary Waddingham, Mary Hope, Mason McCormack, Mat Allan, Matej Mihelčić, Matt Cheselka, Matthew Howarth, Megan Gialluca, Mia Boothroyd, Michael Cook, Michael Mazur, Michael O'Connell, Michael Krocil, Michael Camilleri, Michael Kennedy, Michał Warchoł, Michel Saint-Laurent, Miguel Diaz Angel, Miguel Preciado, Mike Breimann, Mike Hutchings, Mike Read, Mike Shaw, Mike Ball, Milan Kalina, Minesh Patel, Miranda Clare, Mirjana Malarić, Muhammad Luqmanul Hakim Muharam, Murray Forbes, Murray Singleton, Murray Thompson, Myron Valenta, Nalayini Brito, Nawaz Mahomed, Ned Smith, Nedeljko Mandić, Neil Graham, Neil Papworth, Neil Waters, Neil Petersen, Nelson Moreira, Neville Vann, Nial Bruce, Nicholas Hill, Nicholas Ruffier, Nick Howarth, Nick James, Nick Moskovitz, Nick Norman, Nick Primavesi, Nick Quinn, Nick Russel, Nick Powell, Nick Wiffen, Nicola Masseroni, Nigel Bubb, Nigel Evans, Nigel Owen, Nigel Harris, Nikola Gotovac, Nikolay Gusev, Nikos Sioulas, Noah Simmonds, Norman Izsett, Ollie Eisman, Pablo Canedo, Paraksh Vankawala, Pat Devine, Patrick Franks, Patrick Poitevin, Patrick Geoffroy, Patrik Kukić, Paul Cox, Paul Dickinson, Paul Haworth, Paul Heelis, Paul Kavanagh, Paul Ludick, Paul Prouse, Paul Pugh, Paul Roche, Paul Roggemans, Paul Stewart, Paul Huges, Pedro Augusto Hay Day, Penko Yordanov, Pete Graham, Pete Lynch, Peter G. Brown, Peter Campbell-Burns, Peter Davis, Peter Eschman, Peter Gural, Peter Hallett, Peter Jaquiery, Peter Kent, Peter Lee, Peter McKellar, Peter Meadows, Peter Stewart, Peter Triffitt, Peter Leigh, Peter Felhofer, Pető Zsolt, Phil James, Philip Gladstone, Philip Norton, Philippe Schaak, Phillip Wilhelm Maximilian Grammerstorf, Pierre Gamache, Pierre de Ponthière, Pierre-Michael Micaletti, Pierre-Yves Pechart, Pieter Dijkema, Predrag Vukovic, Przemek Nagański, Radim Stano, Rajko Sušanj, Raju Aryal, Ralph Brady, Raoul van Eijndhoven, Raul Truta, Raul Elias-Drago, Reinhard Kühn, Remi Lacasse, Renato Cássio Poltronieri, René Tardif, Richard Abraham, Richard Bassom, Richard Croy, Richard Davis, Richard Fleet, Richard Hayler, Richard Johnston, Richard Kacerek, Richard Payne, Richard Stevenson, Richard Severn, Rick Fischer, Rick Hewett, Rick James, Ricky Bassom, Rob Agar, Rob de Corday Long, Rob Saunders, Rob Smeenk, Robert Longbottom, Robert McCoy, Robert Saint-Jean, Robert D. Steele, Robert Veronneau, Robert Peledie, Robin Boivin, Robin Earl, Robin Rowe, Roel Gloudemans, Roger Banks, Roger Morin, Roland Idaczyk, Rolf Carstens, Romulo Jose, Ron James Jr, Roslina Hussain, Ross Skilton, Ross Dickie, Ross Welch, Russell Jackson, Russell Brunton, Ryan Frazer, Ryan Harper, Salvador Aguirre, Sam Green, Sam Hemmelgarn, Sam Leaske, Sarah Tonorio, Scott Kaufmann, Sebastian Klier, Seppe Canonaco, Seraphin Feller, Serge Bergeron, Sergio Mazzi, Sevo Nikolov, Simon Cooke-Willis, Simon Holbeche, Simon Maidment, Simon McMillan, Simon Minnican, Simon Parsons, Simon Saunders, Simon Fidler, Simon Oosterman, Simon Peterson, Simon lewis, Sofia Ulrich, Srivishal Sudharsan, Stacey Downton, Stan Nelson, Stanislav Korotkiy, Stanislav Tkachenko, Stef Vancampenhout, Stefan Frei, Stephane Zanoni, Stephen Grimes, Stephen Nattrass, Steve Berry, Steve Bosley, Steve

Carter, Steve Dearden, Steve Homer, Steve Kaufman, Steve Lamb, Steve Rau, Steve Tonkin, Steve Trone, Steve Welch, Steve Wyn-Harris, Steven Shanks, Steven Tilley, Stewart Doyle, Stuart Brett, Stuart Land, Stuart McAndrew, Sue Baker Wilson, Sylvain Cadieux, Tammo Jan Dijkema, Terry Pundiak, Terry Richardson, Terry Simmich, Terry Young, Thiago Paes, Thomas Blog, Thomas Schmiereck, Thomas Stevenson, Tihomir Jakopčić, Tim Burgess, Tim Claydon, Tim Cooper, Tim Gloudemans, Tim Havens, Tim Polfliet, Tim Frye, Tioga Gulon, Tobias Westphal, Tom Warner, Tom Bell, Tommy McEwan, Tommy B. Nielsen, Torcuill Torrance, Tosh White, Tracey Snelus, Trevor Clifton, Ubiratan Borges, Urs Wirthmueller, Uwe Glässner, Vasilii Savtchenko, Ventsislav Bodakov, Victor Acciari, Viktor Toth, Vincent McDermott, Vladimir Jovanović, Waily Harim, Warley Souza, Washington Oliveira, Wenceslao Trujillo, William Perkin, William Schauff, William Stewart, William Harvey, William Hernandez, Wullie Mitchell, Yakov Tchenak, Yfore Scott, Yohsuke Akamatsu, Yong-Ik Byun, Yozhi Nasvadi, Yuri Stepanychev, Zach Steele, Zané Smit, Zbigniew Krzeminski, Željko Andreić, Zhuoyang Chen, Zoran Dragić, Zoran Knez, Zoran Novak, Asociación de Astronomía de Marina Alta, Costa Blanca Astronomical Society, Perth Observatory Volunteer Group, Royal Astronomical Society of Canada Calgary Centre.

References

Drummond J. D. (1981). "A test of comet and meteor shower associations". *Icarus*, **45**, 545–553.

Jenniskens P., Gural P. S., Dynneson, L., Grigsby, B. J., Newman, K. E., Borden, M., Koop, M., Holman D. (2011). "CAMS: Cameras for Allsky Meteor Surveillance to establish minor meteor showers". *Icarus*, **216**, 40–61.

Jenniskens P., Sugimoto H., Scott J., Vida D. (2023). "Meteors from comet 46P/Wirtanen". CBET 5324, D.W.E. Green (ed.), 2023 December 13.

Jopek T. J. (1993). "Remarks on the meteor orbital similarity D-criterion". *Icarus*, **106**, 603–607.

Krolikowska M., Sitarski G. (1996). "Evolution of the orbit of comet 46P/Wirtanen during 1947-2013". *Astronomy and Astrophysics*, **310**, 992–998.

Lejoly C., Harris W., Samarasinha N., Mueller B. E. A., Howell E., Bodnarik J., Springmann A., Kareta T., Sharkey B., Noonan J., Bedin L. R., Bosch J. -G., Brosio A., Bryssinck E., de Vanssay J. -B., Hambsch F. -J., Ivanova O., Krushinsky V., Lin Z. -Y., Manzini F., Maury A., Moriya N., Ochner P., Oldani V. (2022). "Radial Distribution of the Dust Comae of Comets 45P/Honda-Mrkos-Pajdušáková and 46P/Wirtanen". *The Planetary Science Journal*, **3**, Issue 1, id.17.

Maslov M. (2024). "Forecast of possible activity of the comet 46P/Wirtanen meteor stream in December 2023 and (especially) in 2024". *eMetN*, **9**, 1–5.

Roggemans P., Johannink C. and Cambell-Burns P. (2019). "October Ursae Majorids (OCU#333)". *eMetN*, **4**, 55–64.

Southworth R. B. and Hawkins G. S. (1963). "Statistics of meteor streams". *Smithsonian Contributions to Astrophysics*, **7**, 261–285.

Vaubaillon J., Ye Q.-Z., Egal A., Sato M., and Moser D. E. (2023). "A new meteor shower from comet 46P/Wirtanen expected in December 2023". Submitted for publication in Astronomy & Astrophysics (https://arxiv.org/pdf/2312.02636.pdf)

Vida D., Gural P., Brown P., Campbell-Brown M., Wiegert P. (2019). "Estimating trajectories of meteors: an observational Monte Carlo approach - I. Theory". *Monthly Notices of the Royal Astronomical Society*, **491**, 2688–2705.

Vida D., Gural P., Brown P., Campbell-Brown M., Wiegert P. (2020). "Estimating trajectories of meteors: an observational Monte Carlo approach - II. Results". *Monthly Notices of the Royal Astronomical Society*, **491**, 3996–4011.

Vida D., Šegon D., Gural P. S., Brown P. G., McIntyre M. J. M., Dijkema T. J., Pavletić L., Kukić P., Mazur M. J., Eschman P., Roggemans P., Merlak A., Zubrović D. (2021). "The Global Meteor Network – Methodology and first results". *Monthly Notices of the Royal Astronomical Society*, **506**, 5046–5074.

Vida D., Blaauw Erskine R.C., Brown P.G., Kambulow J., Campbell-Brown M. and Mazur M.J. (2022). "Computing optical meteor flux using global meteor network data". *Monthly Notices of the Royal Astronomical Society*, **515**, 2322–2339.

Ye Q. and Jenniskens P. (2022). "Comets and meteor showers". arXiv e-prints, arXiv:2209.10654.

EDMOND v5.05

Jakub Koukal[1,2], Jiří Srba[1] and Libor Lenža[1,2]

[1] **Valašské Meziříčí Observatory, Vsetínská 78, CZ75701 Valašské Meziříčí, Czech Republic**
jkoukal@astrovm.cz, libor.lenza@astrovm.cz

[2] **J. Heyrovský Institute of Physical Chemistry, Academy of Sciences of the Czech Republic**
Dolejškova 3, CZ18223 Prague 8, Czech Republic

EDMOND (European viDeoMeteOr Network Database) is a database of meteor orbits that aggregates video data from observations of meteors from 15 independent national networks and 2 multinational databases. These networks and databases employ different methods and systems for detecting meteors as well as calculating their orbits. EDMOND v5.05 is the fifth version of the database, containing continuous video meteor data from the year 2000 to 2023. The database's goal is to continuously collect video data and ensure continuity with respect to upcoming new systems for recording video meteors. Currently, the database has compiled data on 7462700 single-station meteors, creating 978006 orbits. After reduction using the applied criteria, EDMOND v5.05 contains a total of 480190 orbits of multi-station meteors.

1 EDMOND

The use of video technology for monitoring and recording meteors began in the 1970s and has since undergone rapid development. Although initially the domain of professional astronomers, amateur observers, especially in Japan and the Netherlands, started developing systems suitable for amateur conditions in the 1980s. Subsequent development of amateur observation stations continued at a fast pace, primarily in connection with the improvement and innovation of CCD or CMOS technology, and the increasing accessibility of this equipment to amateur astronomers.

Initially fragmented national networks or isolated observers in Europe, Australia, North America, and South America were consolidated into the centralized database of meteor orbits called EDMOND (European viDeoMeteOr Network Database), which was established in 2011 (Kornoš et al., 2013, 2014a, 2014b).

The first pioneer in video meteor observation on a larger scale was the IMO VMN network (International Meteor Organization Video Meteor Network). The first video observations within this network were carried out in the year 2000, and the network utilizes the MetRec system for data recording and processing (Molau, 2001). Observations from this network have been incorporated into the EDMOND v5.05 database from the year 2000 to 2019, with the IMO VMN contributing 55.5% to the overall count of single-station meteors in the database.

Starting from 2007, the software UFO Capture (SonotaCo, 2009) began to be used for recording video meteors, with the UFO Analyzer as an add-on for processing and UFO Orbit for calculating the orbits of multi-station meteors. The percentage of stations using UFO Capture in the total count of single-station meteors in the database is 34.8%. The Croatian network CMN (Croatian Meteor Network / Hrvatska Meteorska Mreza) and the Danish network Stjerneskud use (or used) their own detection software, contributing 5.7% to the overall count of single-station meteors in the EDMOND database.

Since 2018, a new worldwide network, GMN (Global Meteor Network), has been established, utilizing the open-source RMS system for data recording and processing (Vida et al., 2020; 2021). The percentage of stations using RMS in the total count of single-station meteors in the database is 4.0%, and it constitutes the national subsite CSMON (Czech and Slovak Meteor Observation Network).

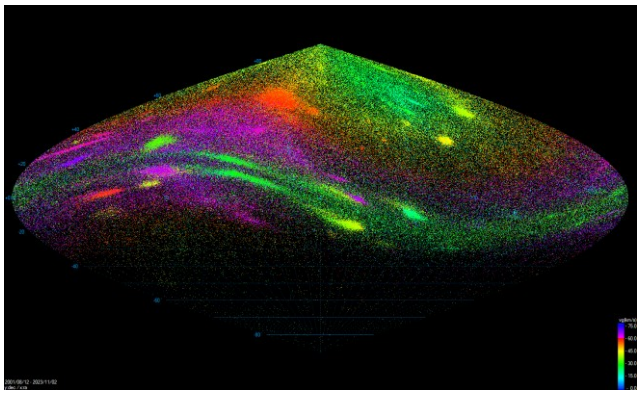

Figure 1 – Radiants of multi-station meteor orbits recorded in the EDMOND v5.05 database. A Hammer projection with an equatorial coordinate system is used for display.

Table 1 – Overview of national or multinational networks included in the EDMOND v5.05 database.

Network ID	Network name	State	Beg.	End	Software
BOAM	Base des Observateurs Amateurs de Metéores	France	2010	2020	UFO Capture
BosNet	Bosnian Network	Bosnia and Herzegovina	2012	2014	UFO Capture
BRAMON	BRAzilian MeteOr Network	Brazil	2014	2017	UFO Capture
CEMeNt	Central European Meteor Network	Czechia	2009	TP	UFO Capture
CMN	Croatian Meteor Network Hrvatska Meteorska Mreza	Croatia	2007	2011	own
CSMON	Czech and Slovak Meteor Observation Network	Czechia	2019	TP	RMS
FMA	Fachgruppe Meteorastronomie	Switzerland	2014	TP	UFO Capture
HMN	Hungary Meteor Network Magyar Hullócsillagok Egyesulet	Hungary	2009	TP	MetRec UFO Capture
IMO VMN	IMO Video Meteor Network	Worldwide	2000	2019	MetRec
ITMN	Italian Meteor and TLE Network	Italy	2007	2017	UFO Capture
MeteorsUA	Група відеоспостереження метеорів	Ukraine	2013	TP	UFO Capture
NEMETODE	Network for Meteor Triangulation and Orbit Determination	Great Britain	2010	2016	UFO Capture
PFN	Polish Fireball Network Pracownia Komet i Meteorów	Poland	2011	2013	MetRec UFO Capture
-	Stjerneskud	Denmark	2012	2016	own
SVMN	Slovak Video Meteor Network	Slovakia	2007	2016	UFO Capture
UKMON	UK Meteor Observation Network	Great Britain	2012	2022	UFO Capture
-	independent observers	Serbia	2012	2013	UFO Capture

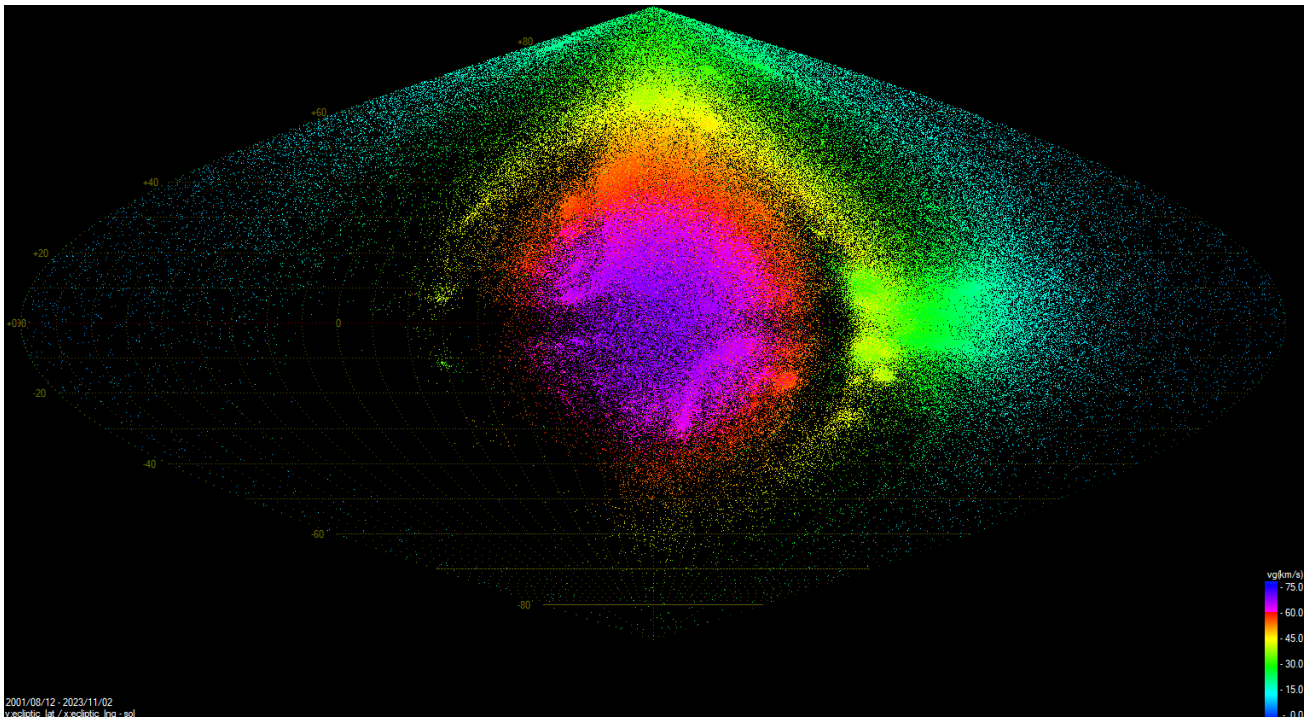

Figure 2 – Radiants of multi-station meteor orbits recorded in the EDMOND v5.05 database. A Hammer projection with a Sun-centered ecliptic coordinate system is used for display.

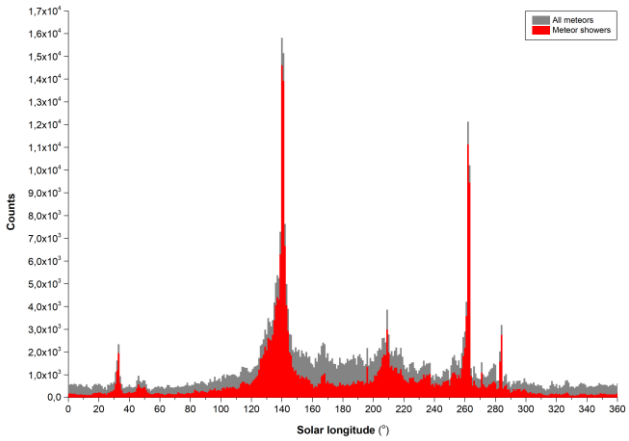

Figure 3 – Distribution of multi-station meteor orbits in the EDMOND v5.05 database based on solar longitude (1-degree bins).

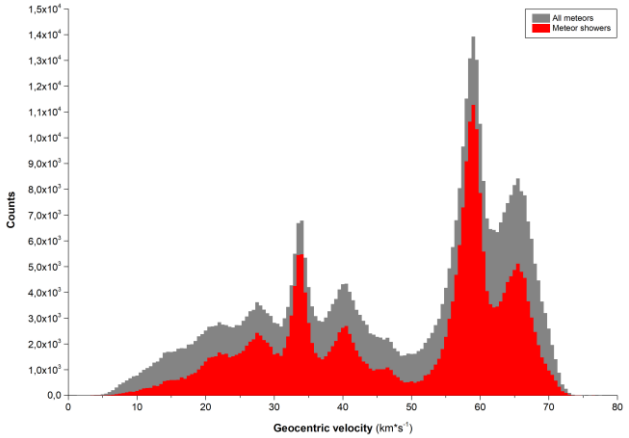

Figure 4 – Distribution of multi-station meteor orbits in the EDMOND v5.05 database based on geocentric velocity (0.5 km/s bins).

2 Detection equipment

Most amateur stations use sensitive analog CCTV cameras built with Sony CCD chips (1/2" ExView HAD, 1/3" Super HAD II) with a standard resolution of 720 × 576 pixels for the PAL B system (720 × 480 pixels for the NTSC M system). These cameras have varifocal lenses with a focal length ranging from 3 to 8 mm and aperture between f/0.8 and f/1.4. Fixed focus lenses with a focal length of 4 to 6 mm and similar aperture (f/0.8 to f/1.4) are also commonly used. For GMN, since the network's inception, cameras with Sony Starvis IMX291 or IMX307 CMOS chips with a full HD resolution of 1920 × 1080 pixels have been used. The resolution is reduced to 1280 × 720 pixels during processing. Many original stations using (or used) analog CCD cameras are transitioning to operating with digital CMOS cameras, utilizing Sony Starvis chips, as well as OmniVision or Aptina chips.

In the case of spectrographs under the administration of Valašské Meziříčí Observatory, monochromatic cameras such as PointGrey Grasshopper3 GS3-U3-32S4M-C with a Sony Pregius IMX252 (1/1.8") CMOS sensor and a resolution of 2048 × 1536 pixels are used. These cameras are equipped with a megapixel lens from VS Technology (5 Mpx) with a aperture of f/1.4 and a focal length of 6 mm. The field of view of the spectrograph, when using the VS Technology lens ($F = 6$mm), is 60 × 45°. Holographic gratings with a density of 1000 lines per mm are used due to the resolution of the installed chip and the size of the field of view.

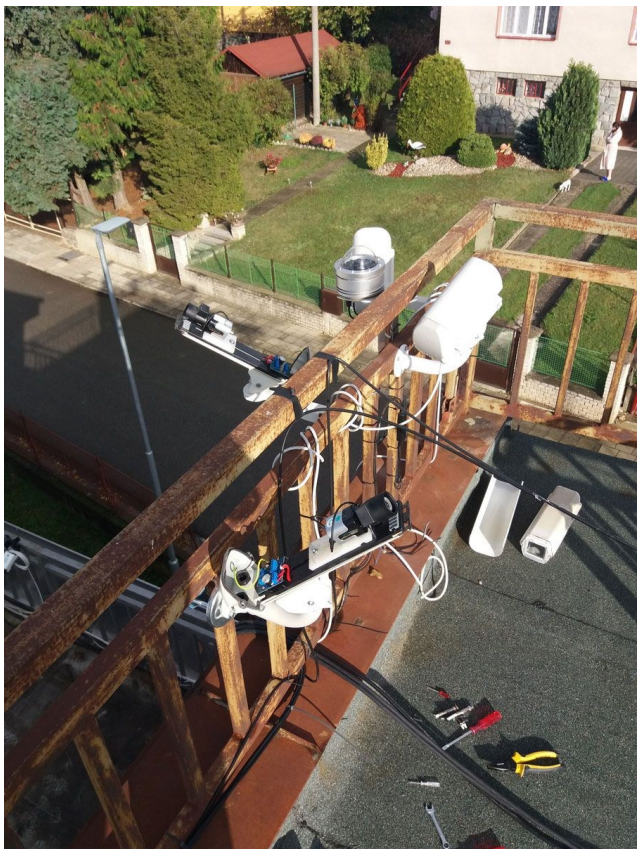

Figure 5 – Demonstration of the installed systems of the CEMeNt and CSMON network at the Ždánice Observatory (Czech Republic).

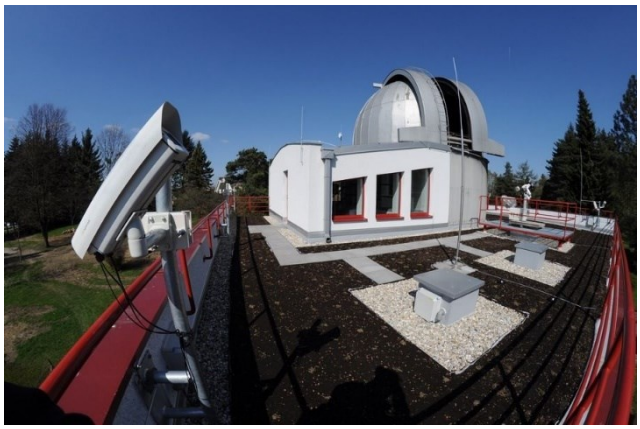

Figure 6 – Sample of installed spectroscopic and survey systems of the CEMeNt network at the Valašské Meziříčí Observatory (Czech Republic).

The fundamental limit for the accuracy of evaluating camera recordings in the EDMOND database is the absolute resolution of the imaging elements (CCD or CMOS chips) depending on the field of view. The absolute resolution of PAL system cameras (720 × 576 pixels) with a typical field of view of ~80 degrees is around 7 arcminutes per pixel. The resolution of 1.2MPx CMOS cameras (e.g., QHY5L-IIM with a resolution of 1280 × 960 pixels) with a typical field of view of ~70 degrees is around 3.5 arcminutes per

pixel. For 2MPx CMOS cameras (e.g., the mentioned Sony Starvis chips with a resolution of 1920 × 1080 pixels) with a typical field of view of ~85 degrees, it is around 2.5 arcminutes. Finally, the resolution of 3MPx CMOS cameras (e.g., PointGrey Grasshopper3 GS3-U3-32S4M-C with a resolution of 2048 × 1536 pixels) with a typical field of view of ~60 degrees is around 1.8 arcminutes per pixel. In the case of CMOS cameras equipped with Sony Starvis chips within the GMN network, the resolution is reduced to 1280 × 720 pixels, and the absolute resolution is lower, around 4 arcminutes per pixel, while maintaining the field of view size.

3 Major meteor showers

The total number of multi-station trajectories in the EDMOND database allows for the calculation of the mean orbits of major regular meteor showers using a large number of trajectories that meet relatively strict criteria for orbital similarity. Drummond's criteria for comparing orbits (Drummond, 1981) were employed, with an upper limit of $D_D < 0.6$. This criterion was chosen for its greater universality in combining prograde and retrograde meteor showers. The identification of individual stream members for calculating the mean orbit was carried out using the method of independent clustering (Rudawska, 2015). The resulting mean orbits of the meteor shower were then compared with data provided in the IAU MDC meteor shower list (Jopek et al., 2011, 2014, 2017; Jenniskens et al., 2020; Neslušan et al., 2020).

For the calculations, primarily major regular meteor showers were selected, or meteor showers with the highest representation of multi-station orbits in the EDMOND v5.05 database. Four meteor showers have parent bodies belonging to the group represented by the long-period comet 1P/Halley (0006 LYR, 0007 PER, 0008 ORI, 0013 LEO). The Tisserand invariant with respect to Jupiter classifies members of these showers into the HT (Halley type) group. The parent body of the Southern Taurid meteor shower (0002 STA) is the comet 2P/Encke. The Tisserand invariant with respect to Jupiter classifies members of this shower into the JFC (Jupiter family comets) or AST (asteroidal) group. The last strong meteor shower in the selection (0004 GEM), with the parent body being the asteroid (3200) Phaethon, is one of the two strongest regular meteor showers together with the Perseids. The Tisserand invariant with respect to Jupiter classifies members of this shower into the AST (asteroidal) group.

Table 2a – Overview of orbital parameters of mean orbits of major meteor showers and their comparison with parameters included in the IAU MDC (International Astronomical Union Meteor Data Center) meteor shower list (2023). Meteor shower name and code is mentioned with following parameters: $\lambda\odot$ – Solar longitude of shower maximum, RA, DEC – radiant position, ΔRA, ΔDEC – daily radiant motion, v_g – geocentric velocity, a – semimajor axis, q – perihelion distance, e – eccentricity, ω – argument of perihelion, Ω – ascending node, i – inclination, N – number of orbits in the IAU MDC.

Shower	0002 STA			0004 GEM			0006 LYR		
Element	EDMOND 2023	Shiba 2022	Jenniskens 2016	EDMOND 2023	Shiba 2023	Jenniskens 2016	EDMOND 2023	Shiba 2023	Jenniskens 2016
$\lambda\odot$ (°)	220.628	221.600	216.000	261.303	-	262.000	32.089	32.180	32.000
RA (°)	51.22	51.80	47.90	113.08	-	113.50	271.89	272.20	272.00
ΔRA (°)	0.82	0.70	0.99	0.98	-	1.15	1.02	0.78	0.66
DEC (°)	13.16	13.70	12.80	32.33	-	32.30	33.28	33.40	33.40
ΔDEC (°)	0.19	0.13	0.26	-0.18	-	-0.16	-0.28	-0.21	0.02
v_g (km/s)	27.22	27.40	26.60	33.67	-	33.80	46.45	46.80	46.70
a (AU)	1.98	2.03	1.95	1.28	-	1.31	14.68	25.10	10.80
q (AU)	0.374	0.374	0.353	0.144	-	0.145	0.919	0.921	0.921
e (-)	0.811	0.816	0.798	0.887	-	0.889	0.937	0.963	0.956
ω (°)	113.122	112.700	116.600	324.698	-	324.300	214.249	214.000	214.000
Ω (°)	42.245	41.600	34.400	261.396	-	261.700	32.104	32.200	32.300
i (°)	5.21	5.40	5.30	22.84	-	22.90	79.21	79.70	79.40
N	1894	1212	916	12528	-	5103	2027	601	258

Table 2a – Overview of orbital parameters of mean orbits of major meteor showers and their comparison with parameters included in the IAU MDC (International Astronomical Union Meteor Data Center) meteor shower list (2023). Meteor shower name and code is mentioned with following parameters: $\lambda_\odot$ – Solar longitude of shower maximum, RA, DEC – radiant position, ΔRA, ΔDEC – daily radiant motion, v_g – geocentric velocity, a – semimajor axis, q – perihelion distance, e – eccentricity, ω – argument of perihelion, Ω – ascending node, i – inclination, N – number of orbits in the IAU MDC.

Shower	0007 PER			0008 ORI			0013 LEO		
Element	EDMOND 2023	Shiba 2023	Jenniskens 2016	EDMOND 2023	Shiba 2023	Jenniskens 2016	EDMOND 2023	Shiba 2023	Jenniskens 2016
$\lambda_\odot$ (°)	139.081	138.060	140.000	208.398	210.170	209.000	235.945	236.570	235.000
RA (°)	46.92	45.50	48.20	95.43	97.00	95.90	154.07	154.60	153.80
ΔRA (°)	1.24	1.45	1.40	0.64	0.80	1.03	0.62	0.64	0.99
DEC (°)	57.81	57.50	58.10	15.65	15.70	15.70	21.64	21.40	21.80
ΔDEC (°)	0.24	0.21	0.26	-0.03	0.03	-0.05	-0.38	-0.40	-0.36
v_g (km/s)	58.90	59.10	59.10	66.06	66.30	66.30	70.17	70.50	70.20
a (AU)	14.47	19.30	9.57	8.84	12.10	6.87	7.33	9.56	6.63
q (AU)	0.948	0.949	0.949	0.574	0.572	0.578	0.983	0.983	0.983
e (-)	0.935	0.951	0.950	0.935	0.953	0.944	0.866	0.897	0.867
ω (°)	150.074	150.600	150.400	82.860	82.700	82.200	173.132	173.500	170.800
Ω (°)	139.085	138.100	139.300	28.400	30.200	28.300	235.956	236.600	234.500
i (°)	112.91	112.90	113.10	163.77	164.00	163.90	162.29	162.40	162.20
N	24796	8862	4367	4187	3909	3024	1208	1507	268

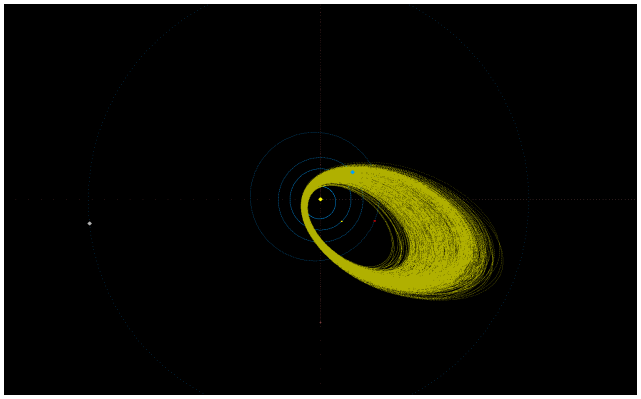

Figure 7 – Multi-station orbits of meteoroids belonging to the meteor shower 0002 STA ($D_D < 0.06$).

The Southern Taurid meteor shower (0002 STA) is part of an extensive complex of showers that are active from late August to early January. While the comet 2P/Encke is often mentioned as the parent body, the meteor shower is also associated with several asteroids, such as 2003 WP21, 2005 UR, or 2015 TX24 (Devillepoix et al., 2021). The northern branch of the complex (Northern Taurids, 0017 NTA) is associated with the asteroid 2004 TG10. When applying the method of independent clustering, several associations emerge during the activity of the Southern Taurids due to the long period of activity and the size of the radiant. For the calculation of the mean orbit of the meteoroid stream, the association with the largest number of members was used (1894 orbits), with a total of 2903 orbits in all associations of the meteor shower 0002 STA ($D_D < 0.06$). The initiation altitude of the ablation trajectory for a 1 g mass object is 94.8 km, while the termination altitude for an object of the same mass lies at 78.2 km.

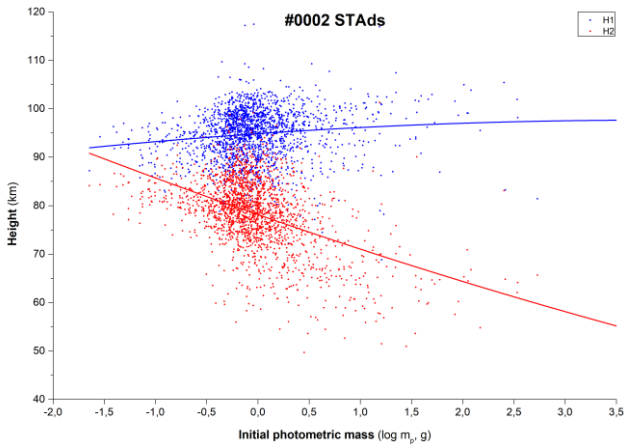

Figure 8 – Dependency of the initial and final heights of the ablation trajectory for Southern Taurids on the photometric mass of the body (log m_p).

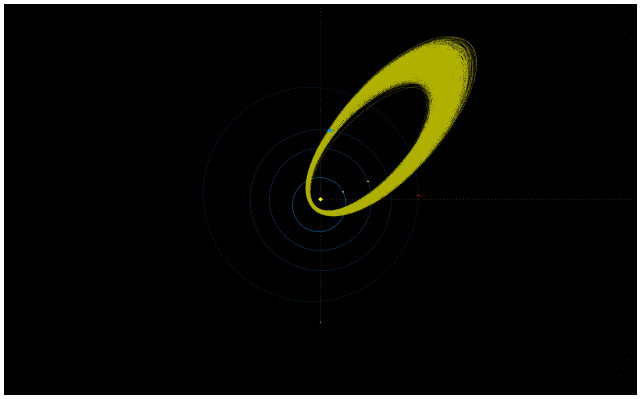

Figure 9 – Multi-station orbits of meteoroids belonging to the meteor shower 0004 GEM ($D_D < 0.06$).

The Geminid meteor shower (0004 GEM) is currently the strongest regular meteor shower with a zenithal hourly rate (ZHR) reaching up to 150 meteors per hour. The meteor shower is associated with the asteroid (3200) Phaethon, as well as asteroids 2005 UD and 1999 YC (Jewitt et al., 2006). The origin of the shower has been investigated in terms of possible cometary activity of the parent body or through the parent body's breakup (Cukier et al., 2023). The destructive theory of the meteor shower's origin appears to be more likely, even considering the existence of smaller asteroids that are also associated with the Geminids.

For the calculation of the mean orbit of the meteoroid stream, 12528 orbits were used, with a total of 22901 orbits associated ($D_D < 0.10$) with the Geminid meteor shower for the mean orbit from the IAU MDC catalog (Jenniskens, 2016). The initiation altitude of the ablation trajectory for a 1 g mass object is 94.2 km, while the termination altitude for an object of the same mass lies at 77.8 km. This value is practically identical to that of the Southern Taurid meteor shower (0002 STA).

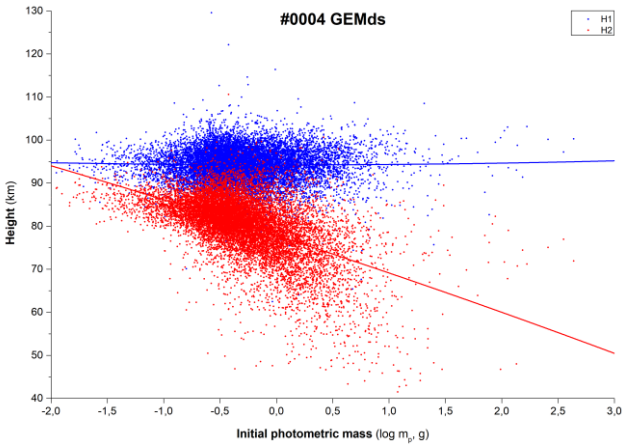

Figure 10 – Dependency of the initial and final heights of the ablation trajectory for Geminids on the photometric mass of the body (log m_P).

The Lyrid meteor shower (0006 LYR) is one of the oldest known meteor showers, observed as far back as 687 BC, and it is associated with the comet C/1861 G1 (Thatcher). For most of the years, the meteor shower is relatively inactive. However, in years corresponding to multiples of 12 (or 60), its activity increases (Arter et al., 1997). Lyrids belong to prograde meteor showers, but their parent comet belongs to the group of long-period comets, specifically HT (Halley type).

For the calculation of the mean orbit of the meteoroid stream, 2027 orbits were used, with a total of 2502 orbits associated ($D_D < 0.10$) with the Lyrid meteor shower for the mean orbit from the IAU MDC catalog (Jenniskens, 2016). The initiation altitude of the ablation trajectory for a 1 g mass object is 105.3 km, while the termination altitude for an object of the same mass lies at 84.1 km.

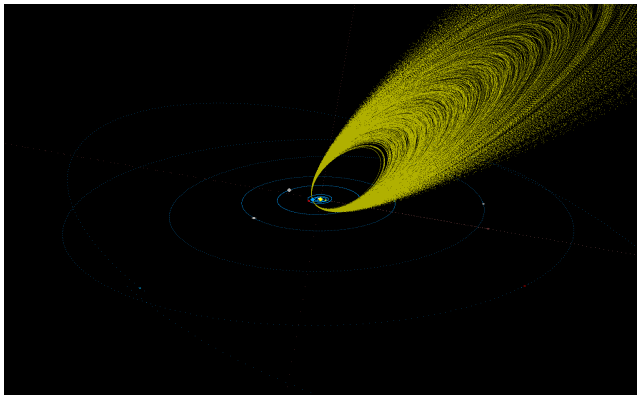

Figure 11 – Multi-station orbits of meteoroids belonging to the meteor shower 0006 LYR ($D_D < 0.06$).

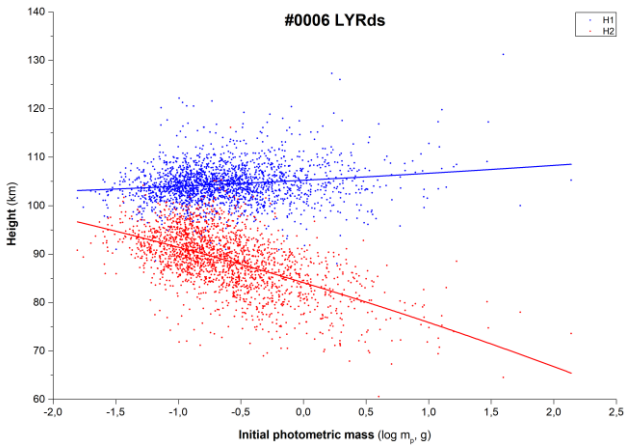

Figure 12 – Dependency of the initial and final heights of the ablation trajectory for Lyrids on the photometric mass of the body (log m_P).

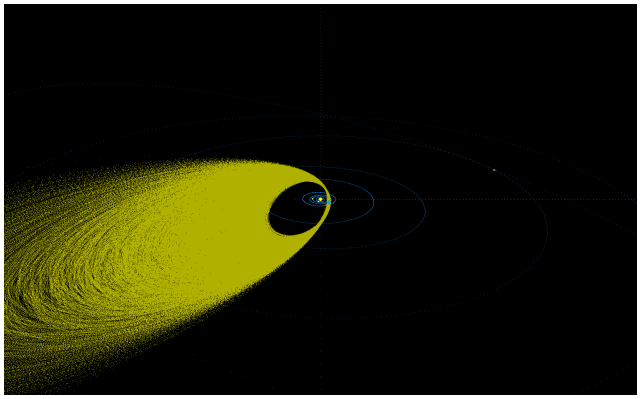

Figure 13 – Multi-station orbits of meteoroids belonging to the meteor shower 0007 PER ($D_D < 0.06$).

The Perseid meteor shower (0007 PER) is, along with the Geminids, one of the most active regular meteor showers,

and its parent body is the comet 109P/Swift-Tuttle. The Perseids are a retrograde meteor shower, and their parent comet belongs to the group of long-period comets, specifically HT (Halley type).

For the calculation of the mean orbit of the meteoroid stream, 24796 orbits were used, with a total of 44373 orbits associated ($D_D < 0.10$) with the Perseid meteor shower for the mean orbit from the IAU MDC catalog (Jenniskens, 2016). The initiation altitude of the ablation trajectory for a 1 g mass object is 108.9 km, while the termination altitude for an object of the same mass lies at 86.3 km.

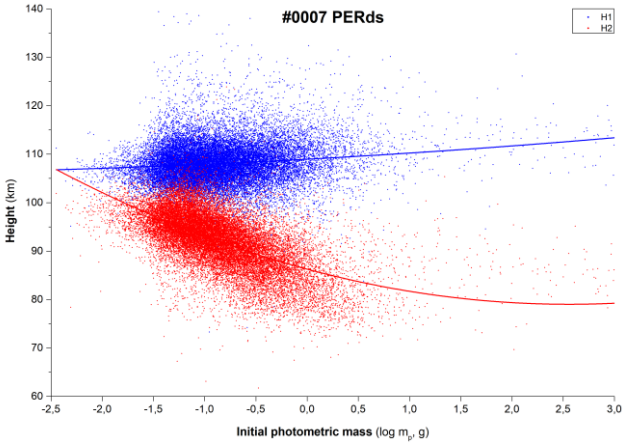

Figure 14 – Dependency of the initial and final heights of the ablation trajectory for Perseids on the photometric mass of the body (log m_p).

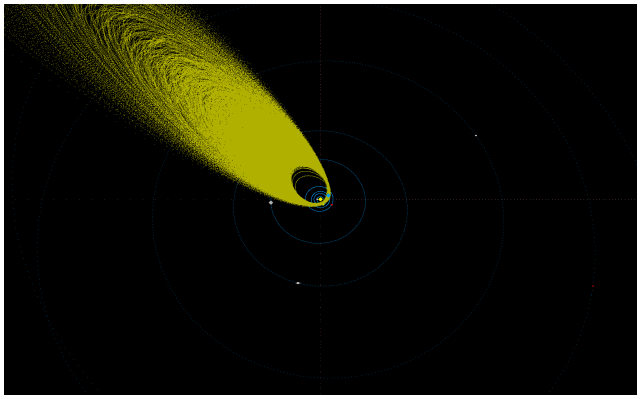

Figure 15 – Multi-station orbits of meteoroids belonging to the meteor shower 0008 ORI ($D_D < 0.06$).

The Orionid meteor shower (0008 ORI), along with the Eta Aquariids (0031 ETA), is produced by the comet 1P/Halley. The Orionids are a retrograde meteor shower, and their parent comet has given its name to the entire group of long-period comets, specifically the group of Halley type (HT) comets.

For the calculation of the mean orbit of the meteoroid stream, 4187 orbits were used, with a total of 8791 orbits associated ($D_D < 0.10$) with the Orionid meteor shower for the mean orbit from the IAU MDC catalog (Jenniskens, 2016). The initiation altitude of the ablation trajectory for a 1 g mass object is 112.3 km, while the termination altitude for an object of the same mass lies at 93.4 km.

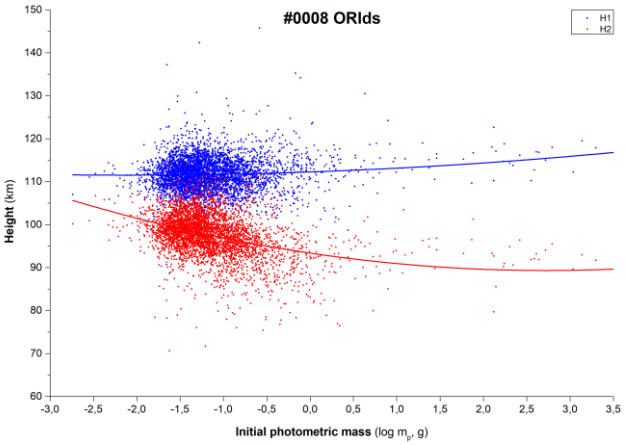

Figure 16 – Dependency of the initial and final heights of the ablation trajectory for Orionids on the photometric mass of the body (log m_p).

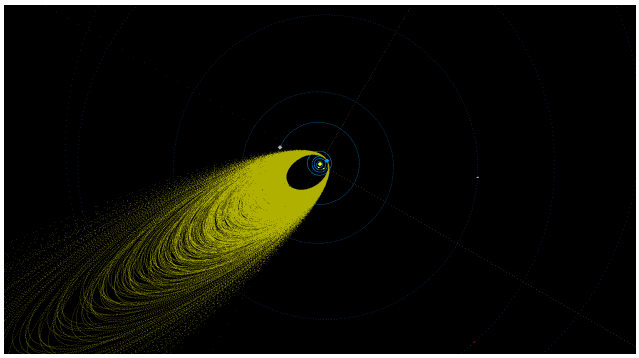

Figure 17 – Multi-station orbits of meteoroids belonging to the meteor shower 0013 LEO ($D_D < 0.06$).

The Leonid meteor shower (0013 LEO) is known for its powerful meteor storms (Asher, 1999), and its parent body is the comet 55P/Tempel-Tuttle, which belongs to the HT (Halley type) group of comets, specifically long-period comets. The Leonids are a retrograde meteor shower, and the mean orbit was calculated for the entire period covered in the EDMOND database, from 2001 to 2023. Since the strong activity from 1998–2000 is not included in the database, and the activity in 2001 is only marginally included, the mean orbit can be considered as the mean orbit of a regular shower with typical activity in the peak ranging between 10–15 meteors per hour.

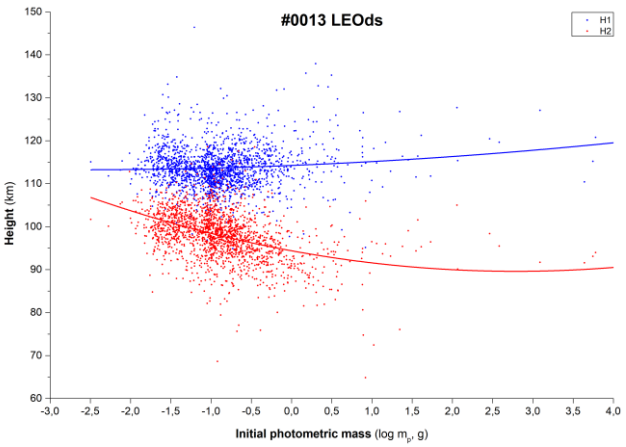

Figre 18 – Dependency of the initial and final heights of the ablation trajectory for Leonids on the photometric mass of the body (log m_p).

For the calculation of the mean orbit of the meteoroid stream, 1208 orbits were used, with a total of 2097 orbits associated ($D_D < 0.10$) with the Leonid meteor shower for the mean orbit from the IAU MDC catalog (Jenniskens, 2016). The initiation altitude of the ablation trajectory for a 1 g mass object is 114.2 km, while the termination altitude for an object of the same mass lies at 94.3 km.

4 Conclusion

The EDMOND database version 5.05 is the result of processing more than 7.4 million single-station meteors, from which over 480000 multi-station orbits were derived. The new version of the EDMOND database (v5.05) is freely available for download on the MeteorNews e-zine website[10]. It is provided in the form of archives (zip files) for each year, containing CSV files in the standard output format of UFO Orbit v2.52. Please note that the mentioned version of the database is not yet complete; for example, data from the IMO VMN is currently available only up to the year 2019.

The calculation of mean heliocentric orbits and final parameters of atmospheric trajectories has revealed the potential of the database, which will be utilized for the analysis of minor meteor showers (either confirming or excluding them from the IAU MDC list). Another potential direction for analysis is to determine the properties of meteor showers listed in the IAU MDC as day-time. The final parameters of atmospheric paths for multi-station meteors indicate differences in the profiles for more massive particles, dependent on the input (geocentric) velocity.

Acknowledgments

Thank you to the operators of all national networks and independent databases whose long-term and precise work enabled the creation of the EDMOND database.

Further thanks go to all involved institutions for supporting the activities and growth of the CEMeNt network. The RPOS project (Development of a Cross-Border Observation Network) was co-financed by the Small Project Fund program of Interreg V-A Slovakia – Czech Republic 2014–2020, call code 5/FMP/11b, reg. no. CZ/FMP/11b/05/058. The KOSOAP (Cooperative Network in the Field of Astronomical Research-Observation Programs) and RPKS (Development of a Cross-Border Cooperative Network for Professional Work and Education) projects were implemented by the Valašské Meziříčí Observatory (Czech Republic) and Kysucké Nové Mesto Observatory (Slovakia) in cooperation with SMPH (Society for Interplanetary Matter). The projects were co-financed by the Microproject Fund of the Operational Program for Cross-Border Cooperation Slovakia – Czech Republic 2007–2013. The project for the purchase and operation of high-resolution spectroscopic cameras is partially funded by the Program for Regional Cooperation of the Czech Academy of Sciences, reg. no. R200401521, grant APVV-0517-12 (FMFI UK), and internal grant no. 994316 of the J. Heyrovský Institute of Physical Chemistry. The acquisition of instrumental equipment at the Valašské Meziříčí Observatory, p. o., was also contributed to by the companies DEZA, a. s., and CS CABOT, spol. s r. o.

References

Arter T. R., and Williams I. P. (1997). “Periodic behaviour of the April Lyrids”. *Monthly Notices of the Royal Astronomical Society*, **286**, 163–172.

Asher D. J. (1999). “The Leonid meteor storms of 1833 and 1966”. *Monthly Notices of the Royal Astronomical Society*, **307**, 919–924.

Cukier W. Z., Szalay J. R. (2023). “Formation, structure, and detectability of the Geminids meteoroid stream”. *The Planetary Science Journal*, **4**, id.109.

Devillepoix H. A., Jenniskens P., Bland P. A., Sansom E. K., Towner M. C., Shober P., Cupák M., Howie R. M., Hartig B. A. D., Anderson S., Jansen-Sturgeon T. and Albers, J. (2021). “Taurid stream# 628: a reservoir of large cometary impactors”. *The Planetary Science Journal*, **2**, id.223.

Drummond J. D. (1981). “A test of comet and meteor shower associations”. *Icarus*, **45**, 545–553.

Jenniskens P., Nénon Q., Albers J., Gural P. S., Haberman B., Holman D., Morales R., Grigsby B. J., Samuels D. and Johannink C. (2016). “The established meteor showers as observed by CAMS”. *Icarus*, **266**, 331–354.

Jenniskens P., Jopek T.J., Janches D., Hajduková M., Kokhirova G.I., Rudawska R. (2020). “On removing showers from the IAU Working List of Meteor Showers”. *Planetary and Space Science*, **182**, id. 104821.

Jewitt D., and Hsieh H. (2006). “Physical observations of 2005 UD: A mini-Phaethon”. *The Astronomical Journal*, **132**, 1624.

Jopek T. J. and Kaňuchová Z. (2017). “IAU Meteor Data Center - the shower database: A status report”. *Planetary and Space Science*, **143**, 3–6.

Jopek T. J., Kaňuchová Z. (2014). “Current status of the IAU MDC Meteor Shower Database”. In Jopek T. J., Rietmeijer F. J. M., Watanabe J., Williams I. P., editors, Proceedings of the Meteoroids 2013 Conference, Poznań, Poland, Aug. 26-30, 2013. A.M. University, pages 353–364.

Jopek T. J. and Jenniskens P. M. (2011). “The Working Group on Meteor Showers Nomenclature: A

[10] https://www.meteornews.net/edmond/edmond/edmond-database/

History, Current Status and a Call for Contributions". In Meteoroids: The Smallest Solar System Bodies, *Proceedings of the Meteoroids Conference* held in Breckenridge, Colorado, USA, May 24-28, 2010. Edited by W.J. Cooke, D.E. Moser, B.F. Hardin, and D. Janches, NASA/CP-2011-216469., 7–13.

Kornoš L., Koukal J., Piffl R., and Tóth J. (2013). "Database of meteoroid orbits from several European video networks". In Gyssens M., Roggemans P., editors, Proceedings of the International Meteor Conference, La Palma, Canary Islands, Spain, 20-23 September 2012, International Meteor Organization, pages 21–25.

Kornoš L., Koukal J., Piffl R., and Tóth J. (2014a). "EDMOND Meteor Database". In Gyssens M., Roggemans P. and Zoladek P., editors, Proceedings of the International Meteor Conference, Poznan, Poland, 22-25 August 2013, International Meteor Organization, pages 23–25.

Kornoš L., Matlovič P., Rudawska R., Tóth J., Hajduková M. Jr., Koukal J. and Piffl R. (2014). "Confirmation and characterization of IAU temporary meteor showers in EDMOND database". In Jopek T. J., Rietmeijer F. J. M., Watanabe J., Williams I. P., editors, Proceedings of the Meteoroids 2013 Conference, Poznań, Poland, Aug. 26-30, 2013. A.M. University, pages 225–233.

Molau S. (2001). The AKM video meteor network. In Barbara Warmbein, editor, Proceedings of the Meteoroids 2001 Conference, 6-10 August 2001, Kiruna, Sweden. ESA SP-495, Noordwijk: ESA Publications Division, ISBN 92-9092-805-0, 2001, pages 315–318.

Neslušan L., Poručan V., Svoreň J., Jakubík M. (2020). "On the new design of the IAU MDC portal". *WGN, Journal of the International Meteor Organization*, **48**, 168–169.

Rudawska R., Matlovič P., Tóth J., Kornoš L. (2015). "Independent identification of meteor showers in EDMOND database". *Planetary and Space Science*, **118**, 38–47.

Shiba Y. (2022). "Jupiter family meteor showers by SonotaCo network observations". *WGN, Journal of the International Meteor Organization*, **50**, 38–61.

Shiba Y. (2023). "Halley type and long period meteor shower luminous altitude characteristics". *WGN, Journal of the International Meteor Organization*, **51**, in print.

SonotaCo (2009). "A meteor shower catalog based on video observations in 2007–2008". *WGN, Journal of the IMO*, **37**, 55–62.

Vida D., Gural P., Brown P., Campbell-Brown M., Wiegert P. (2019). "Estimating trajectories of meteors: an observational Monte Carlo approach - I. Theory". *Monthly Notices of the Royal Astronomical Society*, **491**, 2688–2705.

Vida D., Šegon D., Gural P. S., Brown P. G., McIntyre M. J. M., Dijkema T. J., Pavletić L., Kukić P., Mazur M. J., Eschman P., Roggemans P., Merlak A., Zubrović D. (2021). "The Global Meteor Network – Methodology and first results". *Monthly Notices of the Royal Astronomical Society*, **506**, 5046–5074.

October 2023 report CAMS-BeNeLux

Carl Johannink

Am Ollenkamp 4, 48599 Gronau, Germany
c.johannink@t-online.de

A summary of the activity of the CAMS-BeNeLux network during the month of October 2023 is presented. This month we collected a total of 24636 multi-station meteors resulting in 7404 orbits.

1 Introduction

Sporadic meteor activity is near its peak this month. Some major showers, Orionids and Taurids, are also visible and meanwhile observations are possible for more than 12 hours from our latitudes. These facts make October one of the finest months for meteor observing.

Interesting to see what this month would bring this year.

2 October 2023 statistics

To be clear: October was a very unsettled month with a lot of rain in the first half of the month, especially in the Netherlands. (*Figure 1*).

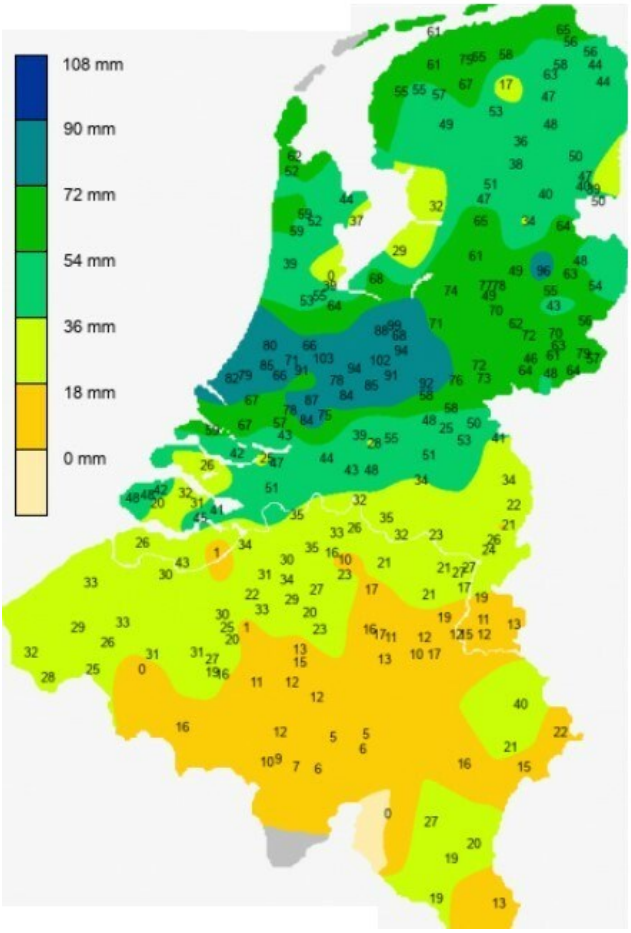

Figure 1 – Amount of rain in Belgium and the Netherlands during October 2023 (Source: total rain in October KNMI online).

Fortunately, Belgium and northern France had far better circumstances. But in general, we see that the different totals in *Table 1* are lower than in September. On average 98 cameras were active this month, this is 6% lower than in September. At least 78 cameras (night October 13–14) and at most 112 cameras were active this month. In September we had at least 89 cameras active. These totals prove that we didn't have an optimal month for observing.

But there is another reason why these totals are lower than last month. Several stations faced technical problems during some nights. Most of them were solved soon, but some are still waiting for a solution.

We could welcome *Rob Smeenk* (Assen, the Netherlands) as a new participant in our network. He now delivers data from his RMS NL000P as CAMS 3196 to our network. There are now 38 locations where cameras are monitoring the skies over the BeNeLux.

In Grapfontaine the number of cameras was expanded with two new RMS cameras (RMS BE000P and BE000Q as CAMS 3843 and 3844). Furthermore, RMS BE0001 (3814) was moved to another position, and now delivers data with CAMS id 3845.

CAMS-BeNeLux captured 24636 multi-station meteors, resulting in 7404 orbits. For reasons mentioned earlier, this is ~25% less than in October 2022. (see *Figure 2*). No orbits were obtained during the night October 23–24. The night October 22–23 had the highest score: 1072 orbits. This is the second time that a night in October produced more than 1000 orbits since the Draconid outburst October 8–9 in 2018. Furthermore, we have collected more than 600 orbits during the nights October 10–11, 14–15, 15–16 and 24–25. So, in these 5 nights more than 50% of all the orbits for this month were obtained.

In *Figure 3* we see a plot of all the radiants obtained during the night October 22–23 with as many as 1072 orbits and thus radiant points. The Orionid activity is very prominent, and also both Taurid branches are clearly visible.

Table 1 and *Figure 2* show an overview of all data for this month compared with the month of October in previous years.

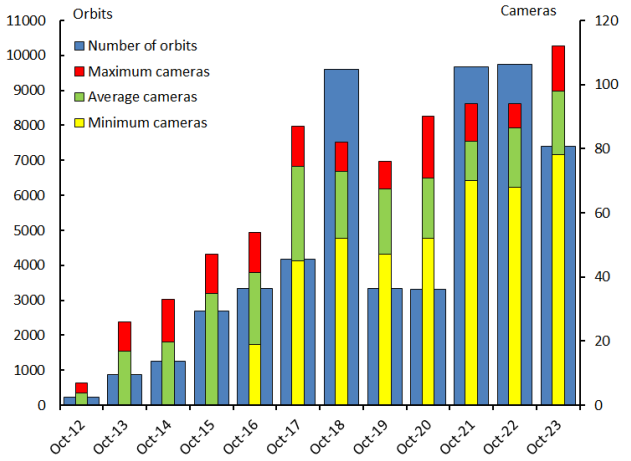

Figure 2 – Comparing October 2023 to previous months of October in the CAMS-BeNeLux history. The blue bars represent the number of orbits, the red bars the maximum number of cameras capturing in a single night, the green bars the average number of cameras capturing per night and the yellow bars the minimum number of cameras.

Table 1 – Number of orbits and active cameras in the BeNeLux during the month of October in the period 2012–2023.

Year	Nights	Orbits	Stations	Max. Cams	Min. Cams	Mean Cams
2012	16	220	6	7	–	3.9
2013	20	866	10	26	–	16.8
2014	22	1262	14	33	–	19.7
2015	24	2684	15	47	–	34.8
2016	30	3335	19	54	19	41.3
2017	29	4163	22	87	45	74.4
2018	29	9611	21	82	52	73.0
2019	29	3344	20	76	47	67.5
2020	29	3305	23	90	52	70.9
2021	29	9669	26	94	70	82.2
2022	30	9749	31	94	68	86.4
2023	30	7404	38	112	78	97.9
Total	317	55612				

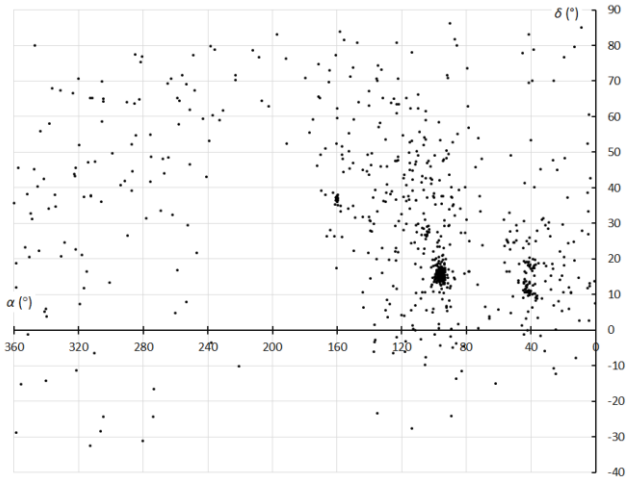

Figure 3 – Plot of all radiants for October 22–23, 2023 (data CAMS-BeNeLux).

3 Conclusion

Results for October 2023 were the fourth best for this month in CAMS-BeNeLux.

Acknowledgement

Many thanks to all participants in the CAMS-BeNeLux network for their dedicated efforts. The CAMS-BeNeLux team was operated by the following volunteers during the month of October 2023: *Stéphane Barré* (Colombey-Les-Belles, France, RMS 3907), *Hans Betlem* (Woold, Netherlands, Watec 3071, 3072, 3073, 3074, 3075, 3076, 3077 and 3078), *Felix Bettonvil* (Utrecht, Netherlands, Watec 376), *Jean-Marie Biets* (Wilderen, Belgium, Watec 379, 380 and 381), *Ludger Boergerding* (Holdorf, Germany, RMS 3801), *Günther Boerjan* (Assenede, Belgium, RMS 3823), *Martin Breukers* (Hengelo, Netherlands, Watec 320, 321, 322, 323, 324, 325, 326 and 327, RMS 319, 328 and 329), *Seppe Canonaco* (Genk, RMS 3818 and 3819), *Pierre de Ponthiere* (Lesve, Belgium, RMS 3816 and 3826), *Bart Dessoy* (Zoersel, Belgium, Watec 804, 805, 806 and RMS 3827), *Tammo Jan Dijkema* (Dwingeloo, Netherlands, RMS 3199), *Isabelle Ansseau, Jean-Paul Dumoulin, Dominique Guiot* and *Christian Wanlin* (Grapfontaine, Belgium, Watec 814, 815, RMS 3814, 3817, 3843, 3844 and 3845), *Uwe Glässner* (Langenfeld, Germany, RMS 3800), *Roel Gloudemans* (Alphen aan de Rijn, Netherlands, RMS 3197), *Luc Gobin* (Mechelen, Belgium, Watec 3890, 3891, 3892 and 3893), *Tioga Gulon* (Nancy, France, Watec 3900 and 3901), *Robert Haas* (Alphen aan de Rijn, Netherlands, Watec 3160, 3161, 3162, 3163, 3164, 3165, 3166 and 3167), *Robert Haas* (Texel, Netherlands, Watec 811 and 812), *Kees Habraken* (Kattendijke, Netherlands, RMS 3780, 3781, 3782 and 3783), *Klaas Jobse* (Oostkapelle, Netherlands, Watec 3030, 3031, 3032, 3033, 3034, 3035, 3036 and 3037), *Carl Johannink* (Gronau, Germany, Watec 3100, 3101, 3102), *Reinhard Kühn* (Flatzby, Germany, RMS 3802), *Hervé Lamy* (Dourbes, Belgium, Watec 394 and 395, RMS 3825 and 3841), *Hervé Lamy* (Humain, Belgium, RMS 3821 and 3828), *Hervé Lamy* (Ukkel, Belgium, Watec 393 and 817), *Hartmut Leiting* (Solingen, Germany, RMS 3806), *Horst Meyerdierks* (Osterholz-Scharmbeck, Germany, RMS 3807), *Koen Miskotte* (Ermelo, Netherlands, Watec 3051, 3052, 3053 and 3054), *Pierre-Yves Péchart* (Hagnicourt, France, RMS 3902, 3903, 3904 and 3905), *Eduardo Fernandez del Peloso* (Ludwigshafen, Germany, RMS 3805), *Tim Polfliet* (Gent, Belgium, Watec 396, RMS 3820 and 3840), *Steve Rau* (Oostende, Belgium, RMS 3822), *Steve Rau* (Zillebeke, Belgium, Watec 3850 and 3852, RMS 3851 and 3853), *Paul and Adriana Roggemans* (Mechelen, Belgium, RMS 3830 and 3831, Watec 3832, 3833, 3834, 3835, 3836 and 3837), *Philippe Schaack* (Roodt-sur-Syre, Luxemburg, RMS 3952), *Hans Schremmer* (Niederkruechten, Germany, Watec 803), *Rob Smeenk* (Assen, Netherlands, RMS 3196), *Erwin van Ballegoij* (Heesh, Netherlands Watec 3148 and 3149), *Stef Vancampenhout* (Vorselaar, Belgium, RMS 3842), *Andy Washington* (Clapton, England, RMS 3702).

November 2023 report CAMS-BeNeLux

Carl Johannink

Am Ollenkamp 4, 48599 Gronau, Germany
c.johannink@t-online.de

A summary of the activity of the CAMS-BeNeLux network during the month of November 2023 is presented. This month we collected a total of 11211 multi-station meteors resulting in 3991 orbits.

1 Introduction

In November the chance for many clear nights is rather small. A series of clear nights can only exist in special meteorological circumstances. Meteor activity this month, is high, so one can be sure that under good conditions the number of orbits will reach several hundred in one night. Beside the sporadic activity, we also see activity from the major streams Taurids and Leonids. That makes November one of the most interesting months for meteor observing.

2 November 2023 statistics

November 2023 was a somber month. Only a handful of complete clear nights occurred in large parts of the BeNeLux. Although the number of cameras and stations increased significantly compared to November months in the past, we have captured only 3991 orbits, resulting from 11211 captured meteors.

In night of November 26–27 we couldn't capture any orbit at all, but on the other hand, there was only a small number of nights in which we could collect more than 100 orbits. So, we got only a modest result this year. See *Figure 1*.

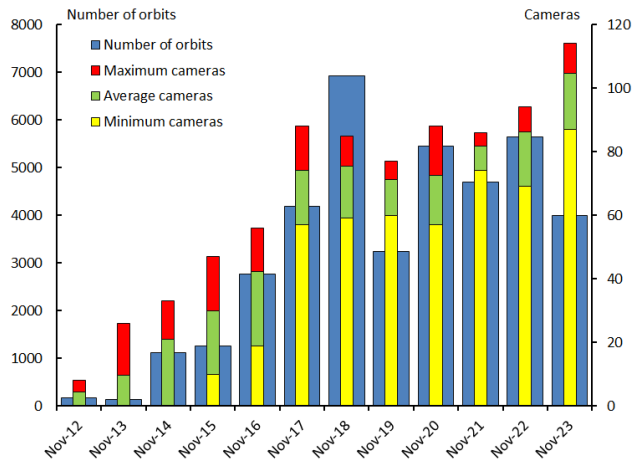

Figure 1 – Comparing November 2023 to previous months of November in the CAMS-BeNeLux history. The blue bars represent the number of orbits, the red bars the maximum number of cameras capturing in a single night, the green bars the average number of cameras capturing per night and the yellow bars the minimum number of cameras.

Table 1 – Number of orbits and active cameras in the BeNeLux during the month of November in the period 2012–2023.

Year	Nights	Orbits	Stations	Max. Cams	Min. Cams	Mean Cams
2012	14	165	6	8	–	4.4
2013	13	142	10	26	–	9.8
2014	24	1123	14	33	–	21.1
2015	23	1261	15	47	10	29.8
2016	24	2769	19	56	19	42.2
2017	26	4182	22	88	57	74.2
2018	28	6916	21	85	59	75.3
2019	27	3237	20	77	60	71.1
2020	28	5441	23	88	57	72.6
2021	24	4691	26	86	74	81.6
2022	29	5635	31	94	69	86.2
2023	29	3991	41	114	87	104.7
Total	289	39553				

The highest number of orbits in one night has been captured during the nights of November 10–11 and November 21–22, approximately 400 orbits. As said earlier, compared with November 2022, the number of stations, and consequently the number of active cameras, has increased significantly (see *Figure 1* and *Table 1*). Most new cameras were installed in France.

Pierre-Yves Péchart at Hagnicourt, added two extra RMS cameras (numbers 3906 and 3908) to our network. Besides two Watecs, *Tioga Gulon* added an RMS camera (number 3910) operating at Chassignolles. New stations appeared at Fontenay le Marmion (number 3911, operated by *Jean Brunet*), and at Gretz-Armainvilliers (number 3909, operated by *Arnoud Leroy*).

After his move to a new house, Jim Rowe picked up his activities again from Eastbourne in England (number 3703). This month, only 43.3% of all simultaneous meteors were captured by more than two stations. This confirms the bad weather this month. In *Table 2*, the number of captured meteors per camera during the last six November months are given. From this overview, we see that November 2023 was distinctly the least productive November.

Table 2 – The total number of meteors in CAMS-BeNeLux, and the number of meteors per camera in the last 6 November months. 'Cameras' = mean number of active cameras during this month.

November	Meteors	Cameras	Meteors per camera
2018	38556	75.3	512.0
2019	21143	71.1	297.4
2020	31080	72.6	428.1
2021	25832	81.6	316.6
2022	34128	86.2	395.9
2023	27091	104.7	258.7

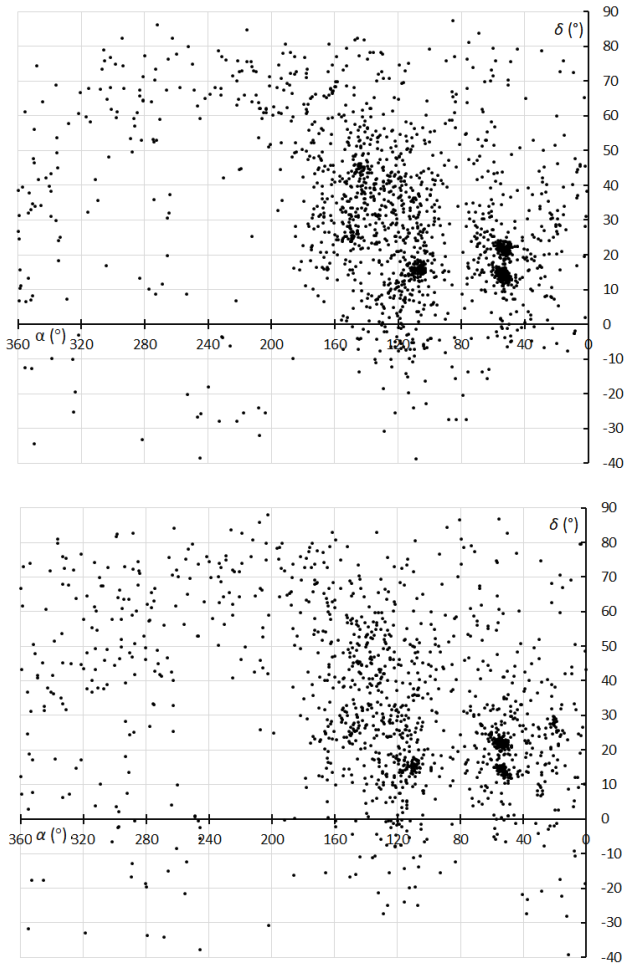

Figure 2 – The radiant plot of all orbits captured during November 1 – 10 for 2022 with 1915 orbits (top) and 2023 with 1444 orbits (bottom) (data CAMS-BeNeLux).

Table 3 – The total number of meteors in CAMS-BeNeLux, and the number of meteors per camera in the last three months. 'Cameras' = mean number of active cameras in this month.

2023	Meteors	Cameras	Meteors per camera
September	72445	104.1	695.9
October	46284	97.9	472.8
November	27091	104.7	258.7

Also, when we compare results for this month with the results for September and October 2023, we see the same picture: although nights are significantly shorter in September, we have captured about 2.5 times more meteors than in November with the same mean number of cameras active each night (*Table 3*).

So, it is no wonder that we could hardly see the activity pattern for the major streams Taurids and Leonids this year. *Figure 2* shows the Taurid activity during November 1-10 for 2022 and 2023. At least we can say that in 2023 the activity from the southern Taurid branch when compared with the northern branch was less than in 2022.

On average, more than 104 cameras at 41 stations were active during this month. Every night, at least 87 cameras captured meteors. The highest number of active cameras was 114 for a single night. These numbers are significantly higher than last year (*Figure 1* and *Table 1*). Unfortunately, the number of orbits was hampered by bad weather.

3 Conclusion

Results for November 2023 are, when compared to other years, rather modest, although the number of cameras increased significantly.

Acknowledgement

Many thanks to all participants in the CAMS-BeNeLux network for their dedicated efforts. The CAMS-BeNeLux team was operated by the following volunteers during the month of November 2023: *Stéphane Barré* (Colombey-Les-Belles, France, RMS 3907), *Hans Betlem* (Woold, Netherlands, Watec 3071, 3072, 3073, 3074, 3075, 3076, 3077 and 3078), *Jean-Marie Biets* (Wilderen, Belgium, Watec 379, 380 and 381), *Ludger Boergerding* (Holdorf, Germany, RMS 3801), *Günther Boerjan* (Assenede, Belgium, RMS 3823), *Martin Breukers* (Hengelo, Netherlands, Watec 320, 321, 322, 323, 324, 325, 326 and 327, RMS 319, 328 and 329), *Jean Brunet* (Fontenay le Marmion, France, RMS 3911), *Seppe Canonaco* (Genk, RMS 3818 and 3819), *Pierre de Ponthiere* (Lesve, Belgium, RMS 3816 and 3826), *Bart Dessoy* (Zoersel, Belgium, Watec 804, 805, 806), *Tammo Jan Dijkema* (Dwingeloo, Netherlands, RMS 3199), *Isabelle Ansseau, Jean-Paul Dumoulin, Dominique Guiot* and *Christian Wanlin* (Grapfontaine, Belgium, Watec 814, 815, RMS 3817, 3843, 3844 and 3845), *Uwe Glässner* (Langenfeld, Germany, RMS 3800), *Roel Gloudemans* (Alphen aan de Rijn, Netherlands, RMS 3197), *Luc Gobin* (Mechelen, Belgium, Watec 3890, 3891, 3892 and 3893), *Tioga Gulon* (Nancy, France, Watec 3900 and 3901), *Tioga Gulon* (Chassignolles, France, RMS 3910), *Robert Haas* (Alphen aan de Rijn, Netherlands, Watec 3160, 3161, 3162, 3163, 3164, 3165, 3166 and 3167), *Robert Haas* (Texel, Netherlands, Watec 811 and 812), *Kees Habraken* (Kattendijke, Netherlands, RMS 3780, 3781, 3782 and 3783), *Klaas Jobse* (Oostkapelle, Netherlands, Watec 3030, 3031, 3032, 3033, 3034, 3035, 3036 and 3037), *Carl Johannink* (Gronau, Germany, Watec 3100, 3101, 3102), *Reinhard Kühn* (Flatzby, Germany, RMS 3802), *Hervé Lamy* (Dourbes, Belgium, Watec 394 and 395, RMS 3825 and 3841), *Hervé Lamy* (Humain, Belgium, RMS 3821 and

3828), *Hervé Lamy* (Ukkel, Belgium, Watec 393 and 817), *Hartmut Leiting* (Solingen, Germany, RMS 3806), *Arnoud Leroy* (Gretz-Armainvielliers, France, RMS3909), *Horst Meyerdierks* (Osterholz-Scharmbeck, Germany, RMS 3807), *Koen Miskotte* (Ermelo, Netherlands, Watec 3051, 3052, 3053 and 3054), *Pierre-Yves Péchart* (Hagnicourt, France, RMS 3902, 3903, 3904, 3905, 3906 and 3908), *Eduardo Fernandez del Peloso* (Ludwigshafen, Germany, RMS 3805), *Tim Polfliet* (Gent, Belgium, Watec 396, RMS 3820 and 3840), *Steve Rau* (Oostende, Belgium, RMS 3822), *Steve Rau* (Zillebeke, Belgium, Watec 3850 and 3852, RMS 3851 and 3853), *Paul and Adriana Roggemans* (Mechelen, Belgium, RMS 3830 and 3831, Watec 3832, 3833, 3834, 3835, 3836 and 3837), *Jim Rowe* (Eastbourne, England, RMS 3703), *Philippe Schaack* (Roodt-sur-Syre, Luxemburg, RMS 3952), *Hans Schremmer* (Niederkruechten, Germany, Watec 803), *Rob Smeenk* (Assen, Netherlands, RMS 3196), *Erwin van Ballegoij* (Heesh, Netherlands Watec 3148 and 3149), *Stef Vancampenhout* (Vorselaar, Belgium, RMS 3842), *Andy Washington* (Clapton, England, RMS 3702).

Meteor detection using Artificial Intelligence and Machine Learning

Wilhelm Sicking

Augustin-Wibbelt-Straße 13, 48712 Gescher, Germany
wil.sicking@gmail.com

In this article I would like to introduce a method that detects meteor echoes based on artificial intelligence. The advantages over conventional object detection are significant:

- The current version can detect meteors of various shapes and distinguish them from interferences and Starlink satellites.
- Echoes that are smaller than the interference level can be detected.
- Because there is no threshold, more echoes are detected than with the conventional method.
- The software also detects echoes that are incomplete for example due to the periodic switching process of the GRAVES antennas.
- A neural network is easy to expand or adapt to new spectrograms or emerging disturbances.

1 Introduction

For some time now I have been developing programs that record and evaluate meteor echoes. Originally it was a real-time version running on a Nvidia-Jetson-Nano-computer. Some time ago I ported the program to Windows 10 and switched to post-processing (Sicking, 2022a; 2022b). The program works well, but has flaws. Traditionally programmed object recognition is never perfect. Detection is inflexible and complicated when high accuracy is desired. Especially when many signals are in the image, echoes are missed. The data often has to be checked manually. Starlink satellites and interferences are constantly increasing. I'm also particularly interested in small echoes to examine the In-Line-Peak (Sicking, 2022a) in more detail. To increase accuracy, I looked for a way to learn to use artificial intelligence (AI) / machine learning (ML) and came across a tutorial and excellent software: The PixelLib[11] by Ayoola Olafenwa (Olafenwa, 2020). Pixellib is a program library that provides all the procedures needed for object recognition using AI methods. The instance segmentation with PixelLib used in this work is based on the MaskRCNN framework (He et al., 2018).

2 Setup

A circularly polarized 4-element cross-Yagi antenna is used to receive the meteor echoes. My antennas are mounted in the attic so the configuration can be easily changed. A low-noise preamplifier with a frequency range of 140-150 MHz and a noise figure of 0.25 dB is connected directly to the antenna. The receiver is an Icom IC-R8600. Spectrum-Lab (SL) from Wolfgang Buescher (DL4YHF) is used as recording software. SL generates plots at 20 second intervals with corresponding date and time in the filename, which are later analyzed using the software described here.

For recording and programming, I use Windows 11 notebooks with i3 or i5 processors. To train the neural network, I use a Windows 10 gaming PC, also with an i5 processor and a GeForce RTX-3060 graphics card (GPU). The GPU has 3840 CUDA cores. This GPU and the corresponding Nvidia software lead to significant acceleration, especially when training the neural network. A bench test is shown below.

3 Setup of the neural network

Pixellib is well documented on the Internet, so only the things that are important to the project are described here.

Before you can start examining objects with AI, a neural network for the objects to be recognized, a model, must be created. Typically, an existing model is retrained. This process is called transfer learning. The Pixellib author used the mask_rcnn_coco model for this. It recognizes pretty much everything we encounter every day. An example of using mask_rcnn_coco is shown below. In her Pixellib tutorial, Ayoola Olafenwa has now retrained this model on two new objects, namely butterflies and squirrels. These two so-called classes are not included in mask_rcnn_coco and are therefore suitable for demonstrating transfer learning.

I followed the tutorial and have now retrained the mask_rcnn_coco model with three new classes. My corresponding line in the training script is:

```
segment_image.inferConfig(num_classes= 3,
class_names= ["BG", "Artificial-Star",
"Background", "Meteor"])
```

[11] https://github.com/ayoolaolafenwa/PixelLib

The first BG belongs to Pixellib. Then my three classes follow.

The classes must be in ascending alphabetical order, otherwise mismatches will occur. The files in my Test and Train folders also start with A, B and the rest are for meteors.

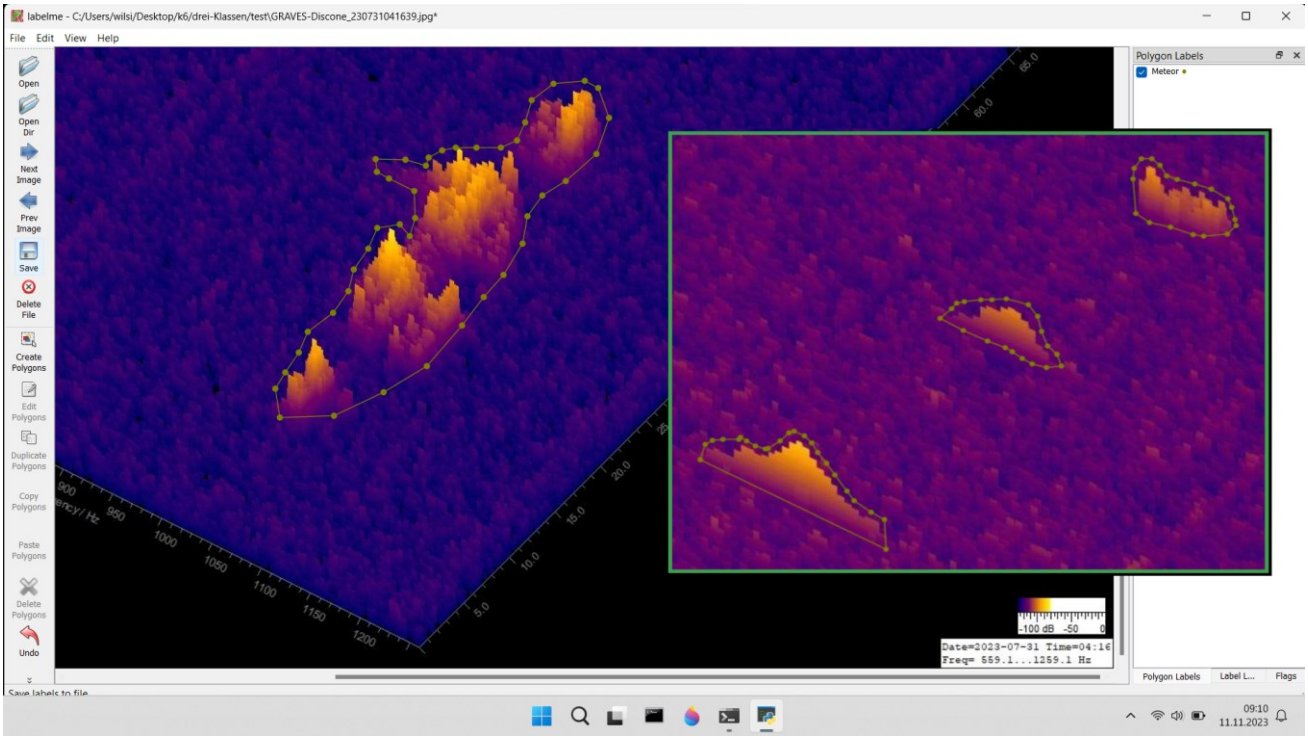

Figure 1 – Screenshot of the Labelme program. The inset shows that the three echoes can be labeled together in one plot. Different classes must not be labeled in one plot.

Labeling the data for the three classes

The main work now consists of collecting images of the three classes Artificial-Stars, Background and Meteor and preparing them for training the model. So far there are over 600 plots that had to be individually labeled by hand. This process is explained for Meteors based on *Figure 1*. Labeling, i.e., creating the border and naming it with the class name, here Meteor, must be carried out for each signal. For demonstration purposes, an inset with three echoes was added to the screenshot. This is intended to show that the 600 plots contain significantly more than just 600 objects, perhaps three or four times as many. The boundary strip around the fragments of the large echo created by the switching process of the GRAVES antennas indicates the algorithm that such or similar echoes must later be viewed as a single meteor, as we see it as observers. The label data generated for each plot are then saved in a .JSON file. Finally, the files are divided into two folders: One third of each class is copied into a folder called TEST, two thirds are copied into the TRAIN folder. This so-called test-train split is used so that the algorithm can check its training with data that are not used in training. The key word for this is backpropagation.

A few details about the actual training and the calculation times can be found in the Benchtest chapter.

Figure 2 illustrates how divided / interrupted objects are treated: The mask_rcnn_coco network is used to analyze two horses that are divided by the picket fence. Of course, the horses are detected as a whole, just as we perceive it. *Figure 2* also shows the short code used to examine the image.

Figure 2 – Two horses are detected using the mask_rcnn_coco network. Only a very short code is required. (The photo was taken by the author.) Source[12].

How well the detection of a soft and fragmented meteor works is shown in *Figure 3*. The following short code would detect the echo in *Figure 3*:

[12] https://pixellib.readthedocs.io/en/latest/Image_instance.html


```
import pixellib
from pixellib.instance import
custom_segmentation
segment_image = custom_segmentation()
segment_image.inferConfig(num_classes= 3,
class_names= ["BG", "Artificial-Star",
"Background", "Meteor"])
segment_image.load_model("mask_rcnn_model.0
75-0.393305.h5")
segment_image.segmentImage("Meteor.jpg",
show_bboxes=True,
output_image_name="Output_Meteor.jpg")
```

In this Python script the three new classes Artificial-Star, Background and Meteor and the self-created neural network mask_rcnn_model.075-0.393305.h5 are used.

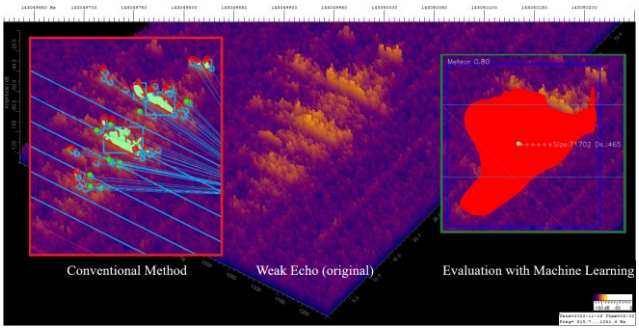

Figure 3 – The image shows the detection of a very soft echo using the conventional method compared to the machine learning method. The conventional method would log many echoes. I would have had to edit such an echo by hand. Further weak echoes that were correctly detected using the AI method are shown in the appendix *Figure A13*.

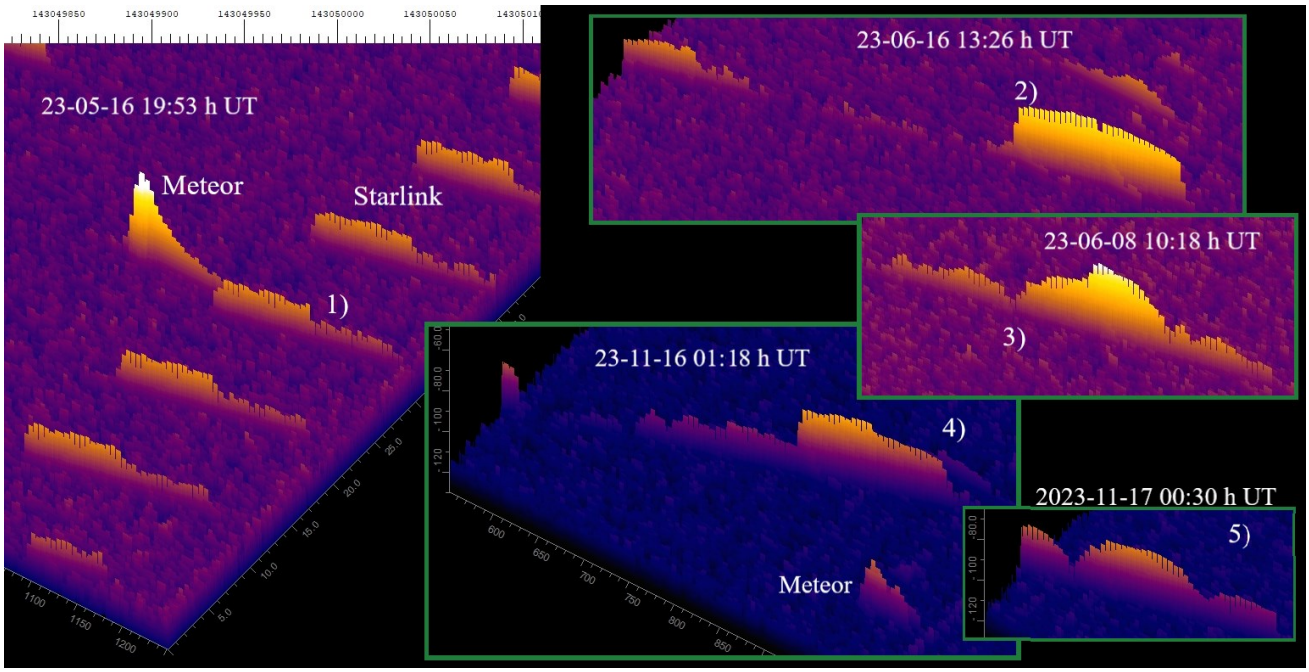

Figure 4 – A meteor and some Starlink satellites are shown on the left side of the image. The steps on the echoes (marked with 1) result from the change in direction of the transmission lobes. Furthermore, 4 echoes are shown on the right in the remaining figures, which presumably come from larger spaceships, see text.

Artificial stars

Starlink satellites are launched into space at short intervals, so that they increasingly appear in the GRAVES radar. Therefore, a separate class called Artificial-Stars was created. Meteors and satellites can be distinguished very well with ML because the metal surface produces a comb-like structure of the echo, see *Figure 4*.

The Starlink satellites basically provide an echo with a straight surface/envelope. The stage on the right of the echoes (labeled with 1) is generated by the switching process of the GRAVES antennas. The remaining satellite echoes (2 – 5) show a more or less curved envelope, indicating a more complex surface.

The image from the Starlink satellites (left in the picture) shows them shortly after release at an altitude of approximately 200 km, see also *Figure 5*. This would explain the small difference in size compared to the other objects if they were space stations. The ISS, for example, flies at an altitude of 400 km.

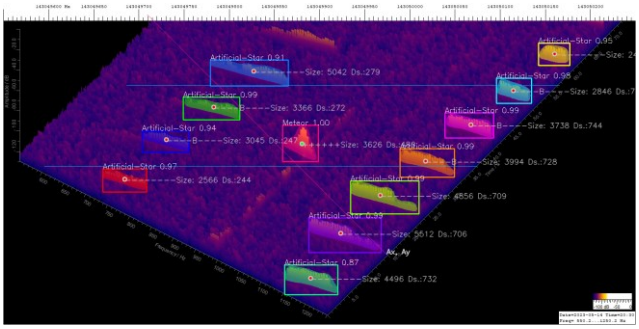

Figure 5 – A meteor in the middle of Starlink satellites was detected using ML. The echoes on the right and left belong to the same satellite. However, due to the switching process of the GRAVES antennas, they are not always exposed. One meteor and five satellites are logged. In this case, that's two too many. However, such accumulations are rare.

Background

A separate class was created to detect interferences. Various crackling impulses and a disturbance carrier are labeled. In an early version I had also labeled the stripes/carriers that are caused by switching power supplies in LED bulbs etc., see *Figure 6*. However, not all types of interference need to be explicitly labeled. By training with images that contain both labeled echoes and unlabeled noise / interference, the model learns that these signals do not belong to the echo. Of course, prior knowledge is also incorporated through transfer learning. The model already knows the recurring frame or label. With the conventional method, everything had to be masked away.

Figure 6 shows that the ML detects the meteor even in presence of strong interference.

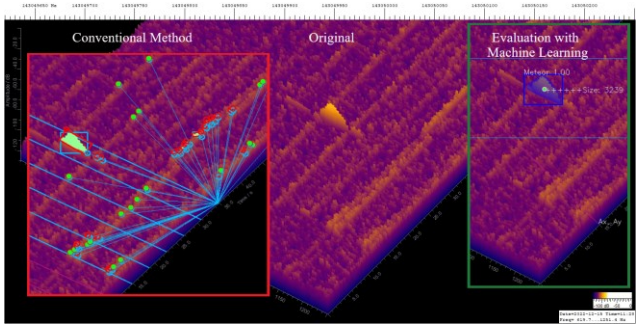

Figure 6 – The ML method can detect the meteor even in presence of strong interferences. With the conventional method, the disturbances trigger many hits and evaluation was no longer possible. With the ML method, evaluation is no problem. Another image (*Figure A14*) with a very small meteor is shown in the appendix.

4 The evaluation

The evaluation software reads all the images addressed by file names and wildcards one after the other, usually those from an entire day. The total recording time per chart is approximately one minute. However, since the plots are saved every 20 seconds, only the contents of a 20-second time window need to be logged. Due to the long recording time, even large echoes that last significantly longer than 20 seconds are still recorded correctly. This is explained in *Figure 7*.

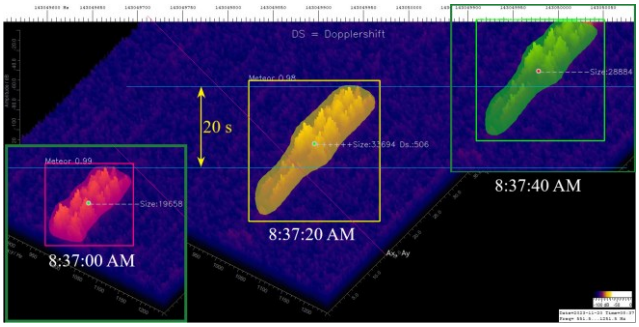

Figure 7 – Logging an Echo. Only the echo from $8^h37^m20^s$ AM (yellow) is logged because the center of gravity is in the 20 s evaluation window. *Figure A15* in the appendix shows an example of another large and soft echo being logged.

Figure 7 is based on a plot from $8^h37^m20^s$ AM. Two insets, one on the left from $8^h37^m00^s$ AM and one from $8^h37^m40^s$ AM on the right edge, were added. So, three recordings are displayed approximately 20 seconds apart. At $8^h37^m00^s$ AM the meteor is partially at the bottom of the image but is not recorded because the center of mass is still below the blue line. At $8^h37^m20^s$ AM the center of gravity is in the 20-second evaluation window and logging takes place. At $8^h37^m40^s$ AM the center of gravity is again outside the evaluation area.

The Pixellib routines shown above then return information about the detected objects to the evaluation program. These are the classes, polygons of the areas, the probabilities and the boxes. The result can be displayed in debug mode. An example is shown in *Figure 8*.

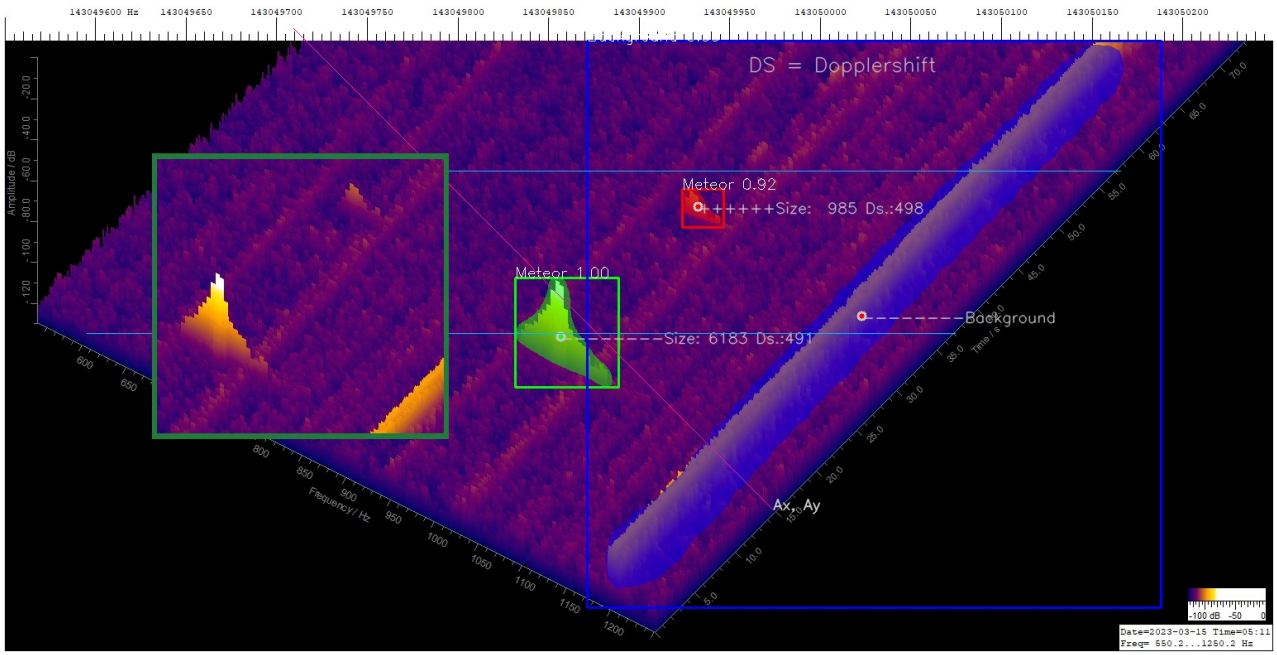

Figure 8 – Detection of two small meteors and a disturbance. In this diagram, only the small upper (red) echo is recorded because it lies between the two horizontal blue lines, i.e. in the 20 second window. The lower echo is in the evaluation window with the next plot. The inset on the left shows the original echoes.

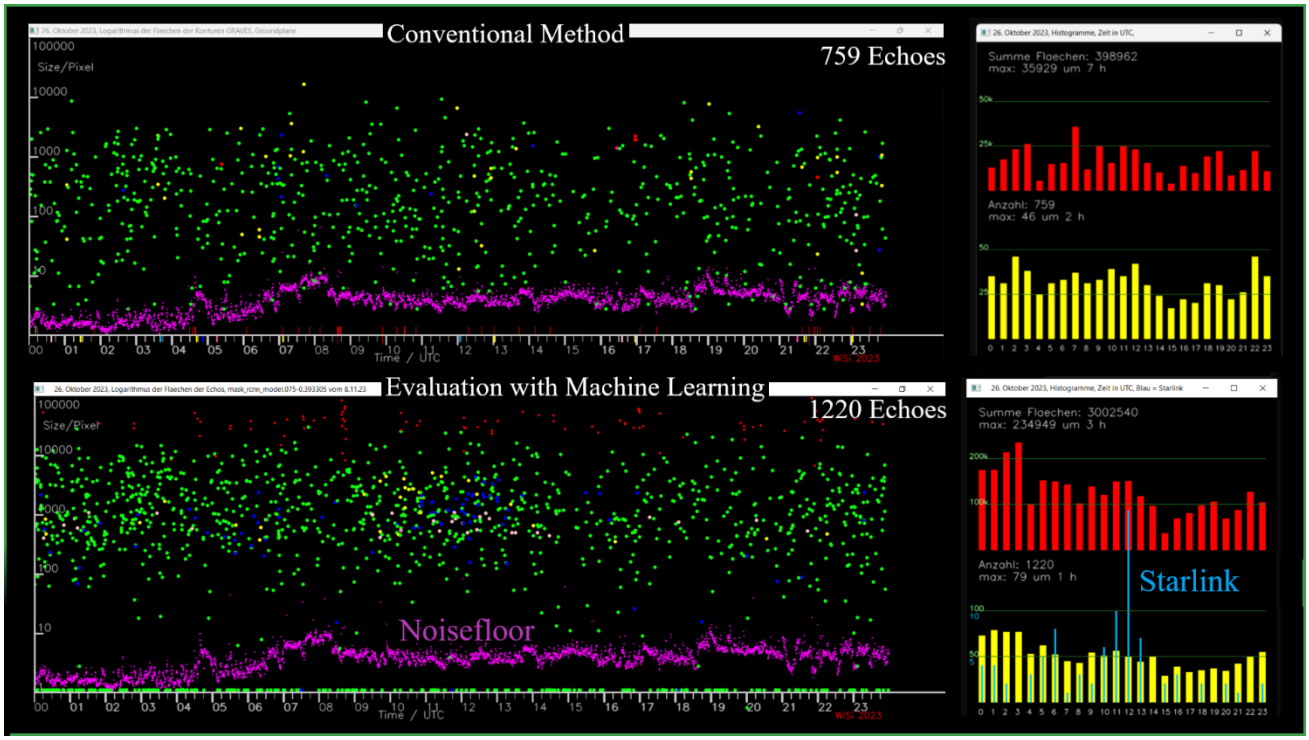

Figure 9 – Measured meteor sizes as a function of time, recorded on 26th October 2023. Each green dot represents an echo. The diagram in the lower half of the image shows that 1220 echoes were recorded using the AI/ML method. The blue dots and the blue histogram represent the Starlink satellites. The red dots are the logged interferences. For comparison, the evaluation using the conventional method is also shown in the upper diagram. Only 759 echoes are logged here, see text. The noise floor is determined by integrating a small area of background.

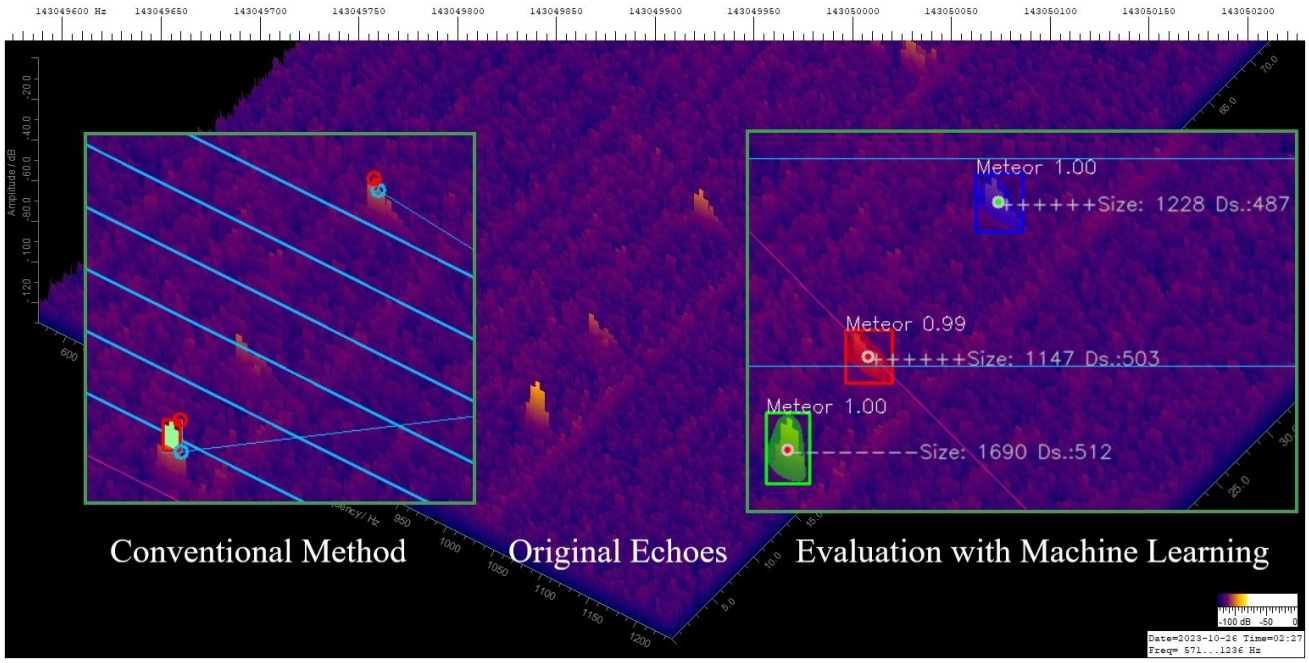

Figure 10 – With the conventional method, the threshold must be high enough so that disturbances do not trigger the recording. The ML method also detects weak signals.

Figure 8 contains two echoes and a disturbance that occurs occasionally and fortunately only on the right edge. I chose this plot to show that such disorders can be reliably detected. The upper small echo is below the level of the interference signal.

This type of AI/ML-investigation is called instance segmentation because multiple instances (meteors) are distinguished in one class. In the case of *Figure 8*, only the upper small meteor is recorded. The evaluation software determines the area and a relative Doppler shift is calculated from the center of gravity of the surface. The lower meteor is in the evaluation window with the next plot. After all plots have been examined, an overview is created, see *Figure 9*.

The points in the lower illustration in *Figure 9* represent the measured echo sizes as a function of time for October 26,

2023 as an example. Around five orders of magnitude of the echo sizes are resolved. 1220 echoes were counted. The yellow histograms show the rate and the red histograms show the rate weighted by the size of the meteor echoes. The blue dots and blue lines represent the Starlink satellites.

To the threshold

Figure 9 shows the evaluation using the conventional method for comparison purposes too. Significantly more echoes are detected with the ML method. The reason for this will now be examined using *Figure 10*. Two echoes are detected using the conventional method. The third middle echo is below the threshold. With the ML method, all three echoes are detected because there is no threshold. The absence of the threshold also means that the echoes are larger by a factor of 10 according to the ML method. (There are 10 times more pixels in the polygon.) The reason for this is that the conventional method only detects the peaks of the echoes that are above the threshold. The ML method also detects the part of the echo that lies in the background or noise. This is one of the big advantages of object detection with ML.

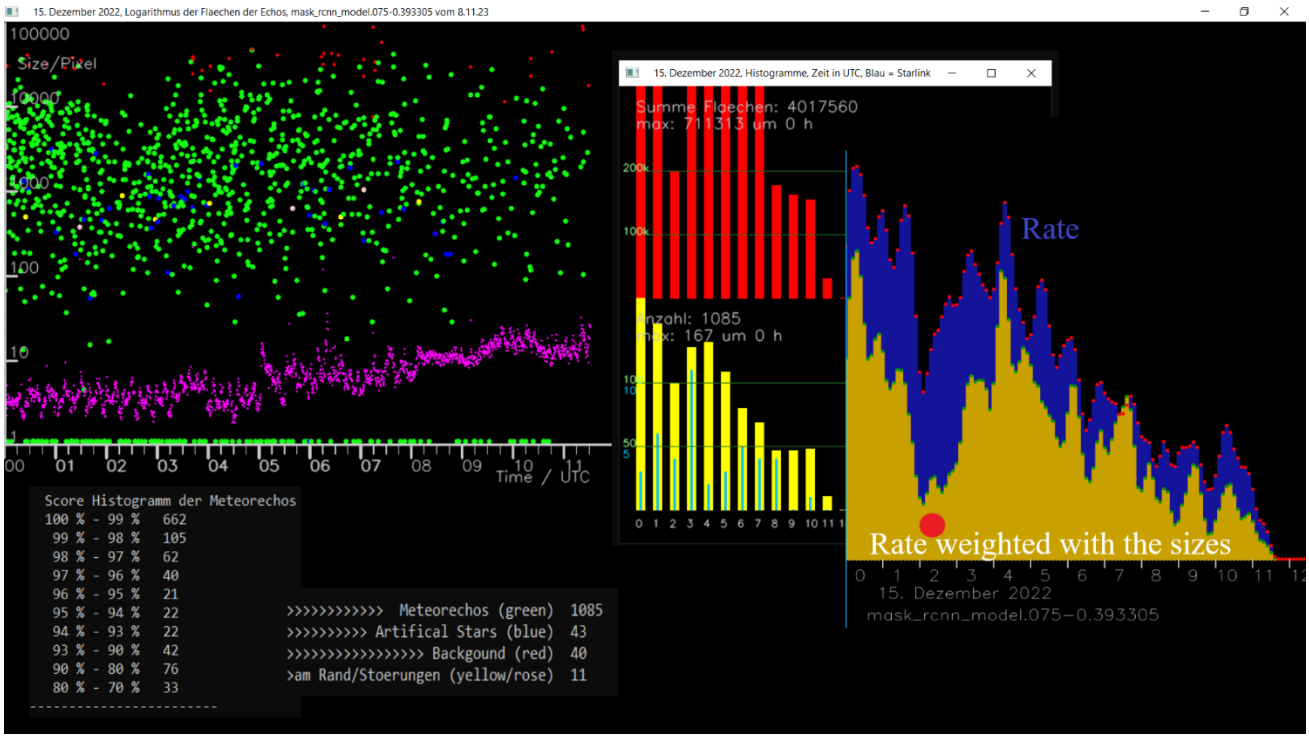

Figure 11 – Recording from December 15, 2022. I canceled the recording because of the interferences. An inset clearly shows the In-Line-Peak, see the red dot.

5 Summary and outlook

Figure 12 – Photo of the OV N62 clubhouse. It is a former NATO radio tower. (The photo was taken by the author.)

The so-called AI, or rather ML, is not a fad or something mystical, but a tool that can deliver very good results. I am particularly interested in the very small echoes in order to further investigate the In-Line-Peak, see *Figure 11*, the red dot. I would also like to investigate particle sorting in streams based on the Poynting-Robertson effect. To do this, small echoes in particular must be detected. The method shown here should help. Because of the interference in my residential area, I will test a new location in the future. It is the clubhouse of the chapter N62 Wüllen of the German Amateur Radio Club, see *Figure 12*. But at the moment it's too cold and too dark, so realistically collecting data probably won't really start until the Perseids in summer.

The project is constantly being developed. I would be happy to pass on the programs, the label data used and the model if anyone would like to participate.

Acknowledgment

Many thanks to *Kerstin Sicking*, *Stefanie Lück* and *Richard Kacerek* for proofreading the article. My special thanks go to *Stefanie Lück* for the many discussions in the Astronomie.de forum.

References

He K., Gkioxari G., Dollár P., Girshick R. (2018). "Mask R-CNN". Facebook AI Research (FAIR). https://arxiv.org/abs/1703.06870.

Sicking W. (2022a). “A Notch in the Arietids Radio Data and a new so called In-Line-Effect”. *eMetN*, **7**, 331–335.

Sicking W. (2022b). “Radio observations on the Perseids and some other showers in August and September 2022”. *eMetN*, **7**, 407–410.

Appendix

Installation, a bench test and a few additional images.

Installation

The important packages are Python3, Pixellib and the CUDA software for the RTX-3060 GPU. Since Pixellib hasn’t been maintained for two years, installing it is a bit tricky, especially on Windows 11. First you have to install Python 3.9.7 with appropriate dependencies. Tensorflow 2.5 is the highest working version with Pixellib.

Tensorflow 2.5 installs an older version of Numpy with a module (scikit-image) that is not compatible in the current version. Another problem under Windows 11 is a bug in the labelme2coco program. It works with the very first version.

These versions and this sequence work on Windows 11 for the author:

```
pip3 install scikit-image==0.18.3
pip3 install numpy==1.19.5
pip3 install tensorflow==2.5.0
pip3 install imgaug……(it is 0.4.0)
pip3 install pixellib -upgrade
pip3 install labelme2coco==0.1.0
```

This is how you can view the installed versions:

```
C:\Users\wilsi>python
```

Python 3.9.7 (tags/v3.9.7:1016ef3, Aug 30 2021, $8^h19^m38^s$ p.m.) [MSC v.1929 64 bit (AMD64)] on win32 Type “help”, “copyright”, “credits” or “license” for more information.

```
>>>import numpy
>>>print (numpy.__version__)
1.19.5
>>>
```

An exception is scikit-image. You import it with:

```
>>> import skimage
>>> print (skimage.__version__)
0.18.3
>>>
```

The installation ran with the default settings on the Windows 10 gaming PC.

If you want to install CUDA code for Nvidia GPUs, you need to know the compute capability of the GPU. My graphics card, the GeForce 3060 laptop GPU, has a compute capability of 8.6. Therefore, cuDNN 8.6 for CUDA 11.2 and the Cuda Toolkit 11.2 were installed.

Tensorflow then calculates in parallel.

Bench test

comparing the gaming PC with the Nvidia 3060 GPU and a normal i5 PC.

A short script from the tutorial is used for training[13].

I calculated 200 epochs to train the current model. I didn’t remember the total computing time, but the last saved epoch was epoch 92. It took an hour and 20 minutes up to that point on the gaming PC. An epoch therefore lasts just under a minute.

However, the model from epoch 92 was not used for the analyzes in this paper, but rather the model from epoch 75 (mask_rcnn_model.075-0.393305.h5) in order to prevent overfitting.

For comparison purposes, I calculated only one epoch on the i5 PC. It lasts 37 minutes. The 92 epochs of the gaming PC would therefore last 56.7 hours, i.e. 2 days and almost 9 hours. The i5 also works with its 4 cores in parallel: the load was up to 100%.

The analysis of the 4320 images from the 24 hours of October 26th, 2023 took 17 minutes on the gaming PC. To compare the analysis times, I only examined one hour of data on both computers: It takes 50 seconds on the gaming PC and 8 minutes on the normal PC, which would mean over 3 hours for data from a day. When analyzing, the GPU load of the gaming PC is in the range of 30%, while the GPU load during training is around 80%. The analysis does not benefit as much from the GPU, as images constantly have to be loaded.

This comparison should show that it is difficult to do machine learning without a GPU. It’s not just a one-off 2 days and 8 hours, but a lot of tests are necessary. I often see where the journey is going after 3-4 epochs. That’s a few minutes of computing time. On the PC it would then be 2 hours.

Supporting images

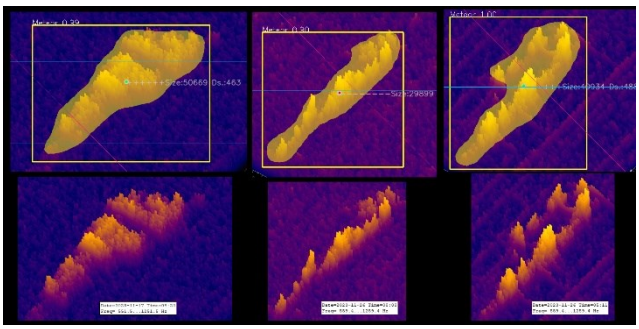

Figure A13 – Further weak echoes that were correctly detected using the AI method.

[13] https://pixellib.readthedocs.io/en/latest/custom_train.html

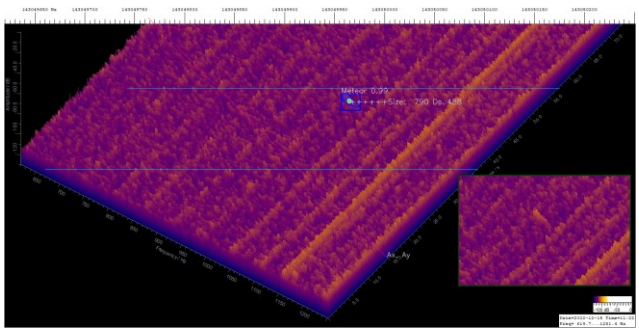

Figure A14 – The ML method can detect the very small meteor even in presence of strong interferences.

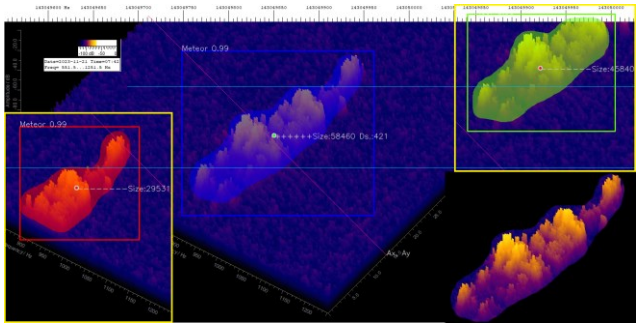

Figure A15 – The picture shows how a soft echo that lasts significantly longer than 20 s is logged correctly. The ++++ show that it was logged.

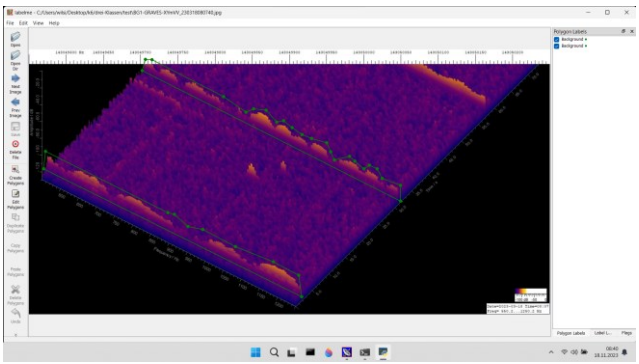

Figure A16 – An example of disturbances/clicking impulses is shown in a Labelme screenshot.

Radio meteors October 2023

Felix Verbelen

Vereniging voor Sterrenkunde & Volkssterrenwacht MIRA, Grimbergen, Belgium
felix.verbelen@gmail.com

An overview of the radio observations during October 2023 is given.

1 Introduction

The graphs show both the daily totals (*Figure 1 and 2*) and the hourly numbers (*Figure 3 and 4*) of "all" reflections counted automatically, and of manually counted "overdense" reflections, overdense reflections longer than 10 seconds and longer than 1 minute, as observed here at Kampenhout (BE) on the frequency of our VVS-beacon (49.99 MHz) during the month of October 2023.

The hourly numbers, for echoes shorter than 1 minute, are weighted averages derived from:

$$N(h) = \frac{n(h-1)}{4} + \frac{n(h)}{2} + \frac{n(h+1)}{4}$$

Local interference and unidentified noise remained moderate to low for most of the month, and solar activity also caused only limited periods of increased noise.

Lightning activity was observed on 2 days.

The Orionids were especially active during the period October 19–28, with a clearly increased number of overdense and long reflections.

Over the entire month, 20 reflections longer than 1 minute were recorded. A small selection of these, along with some other interesting reflections is included (*Figures 5 to 19*). Many more of these are available on request.

In addition to the usual graphs, you will also find the raw counts in cvs-format[14] from which the graphs are derived. The table contains the following columns: day of the month, hour of the day, day + decimals, solar longitude (epoch J2000), counts of "all" reflections, overdense reflections, reflections longer than 10 seconds and reflections longer than 1 minute, the numbers being the observed reflections of the past hour.

[14] https://www.meteornews.net/wp-content/uploads/2023/11/202310_49990_FV_rawcounts.csv

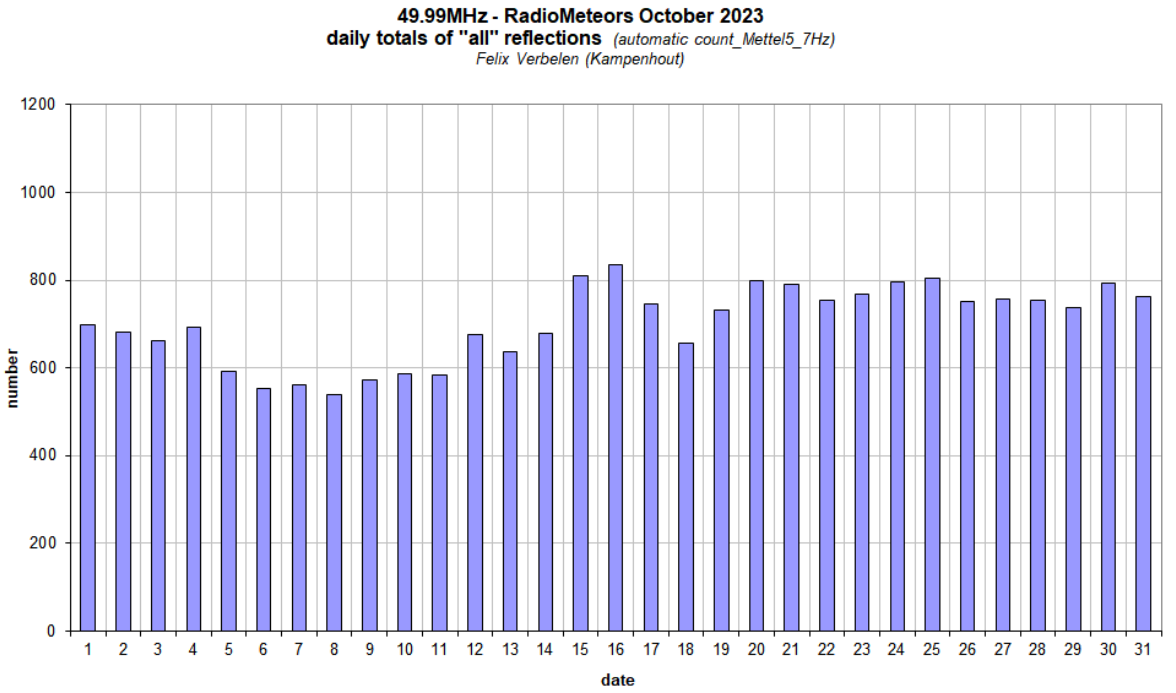

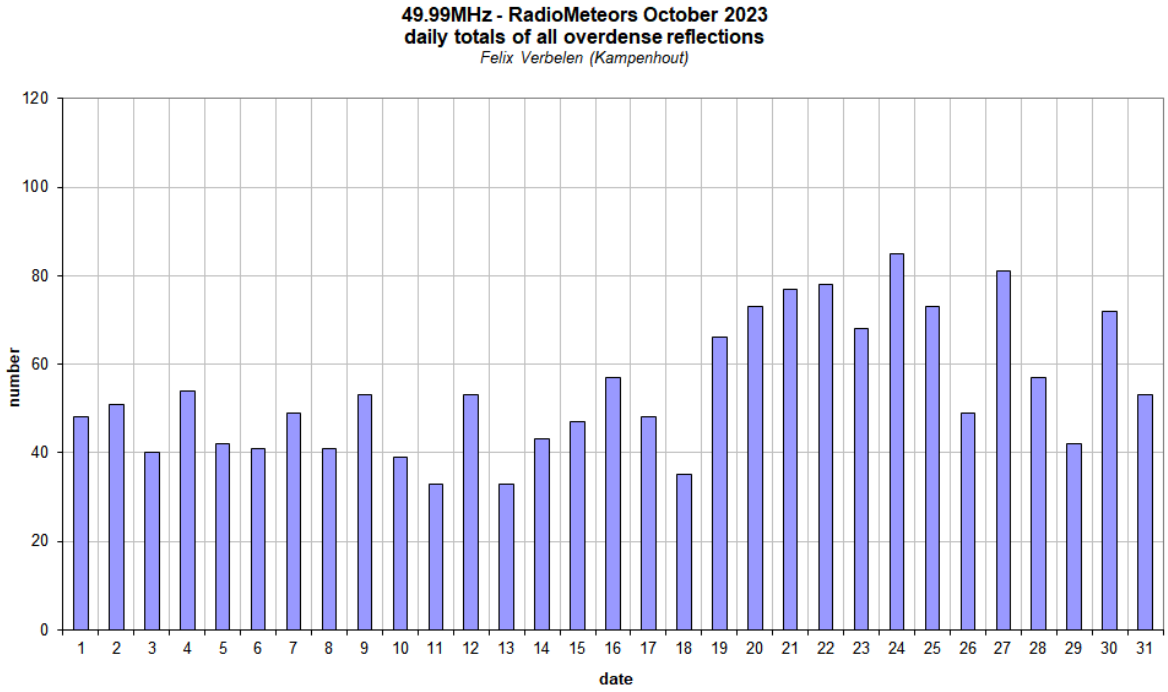

Figure 1 – The daily totals of "all" reflections counted automatically, and of manually counted "overdense" reflections, as observed here at Kampenhout (BE) on the frequency of our VVS-beacon (49.99 MHz) during October 2023.

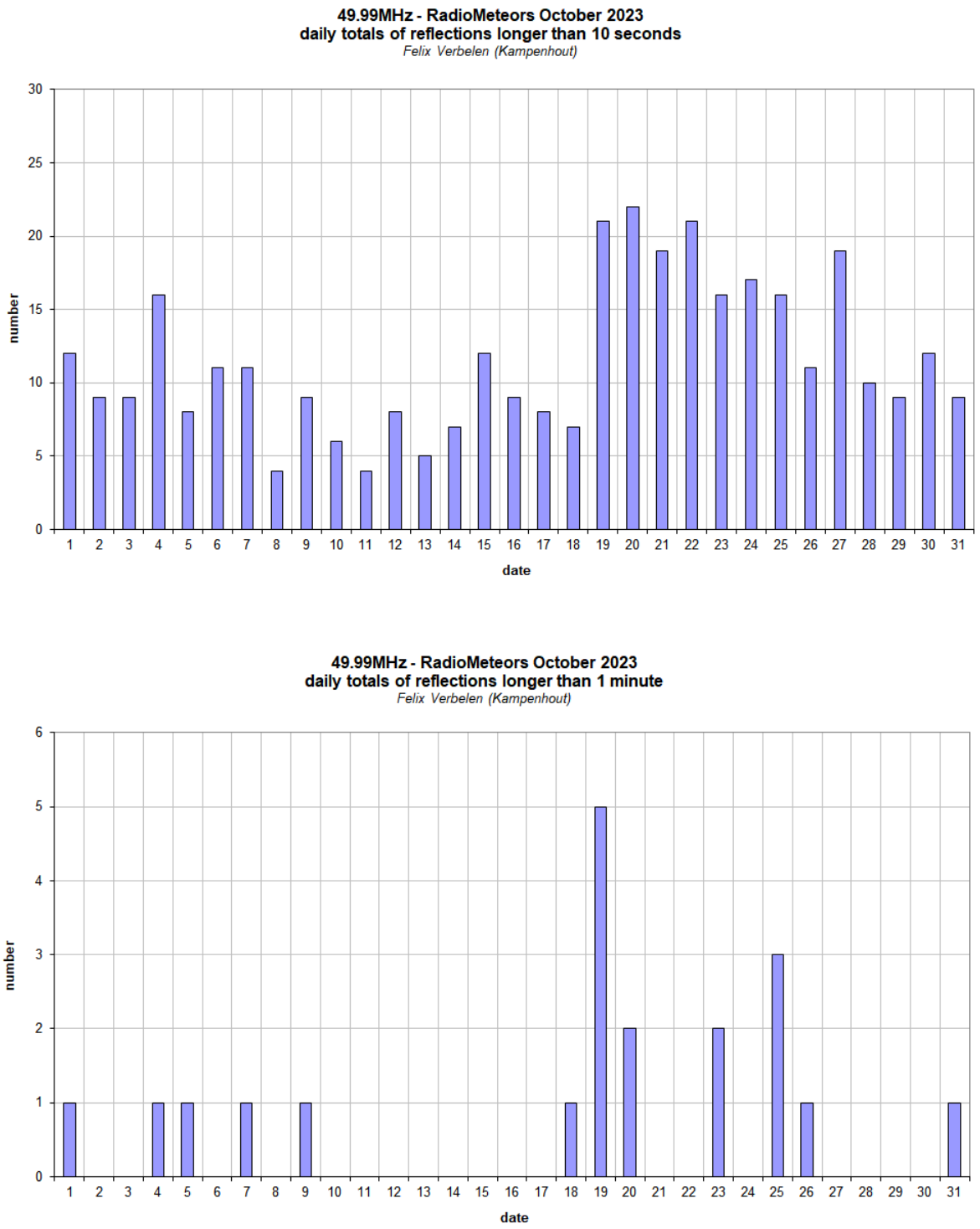

Figure 2 – The daily totals of overdense reflections longer than 10 seconds and longer than 1 minute, as observed here at Kampenhout (BE) on the frequency of our VVS-beacon (49.99 MHz) during October 2023.

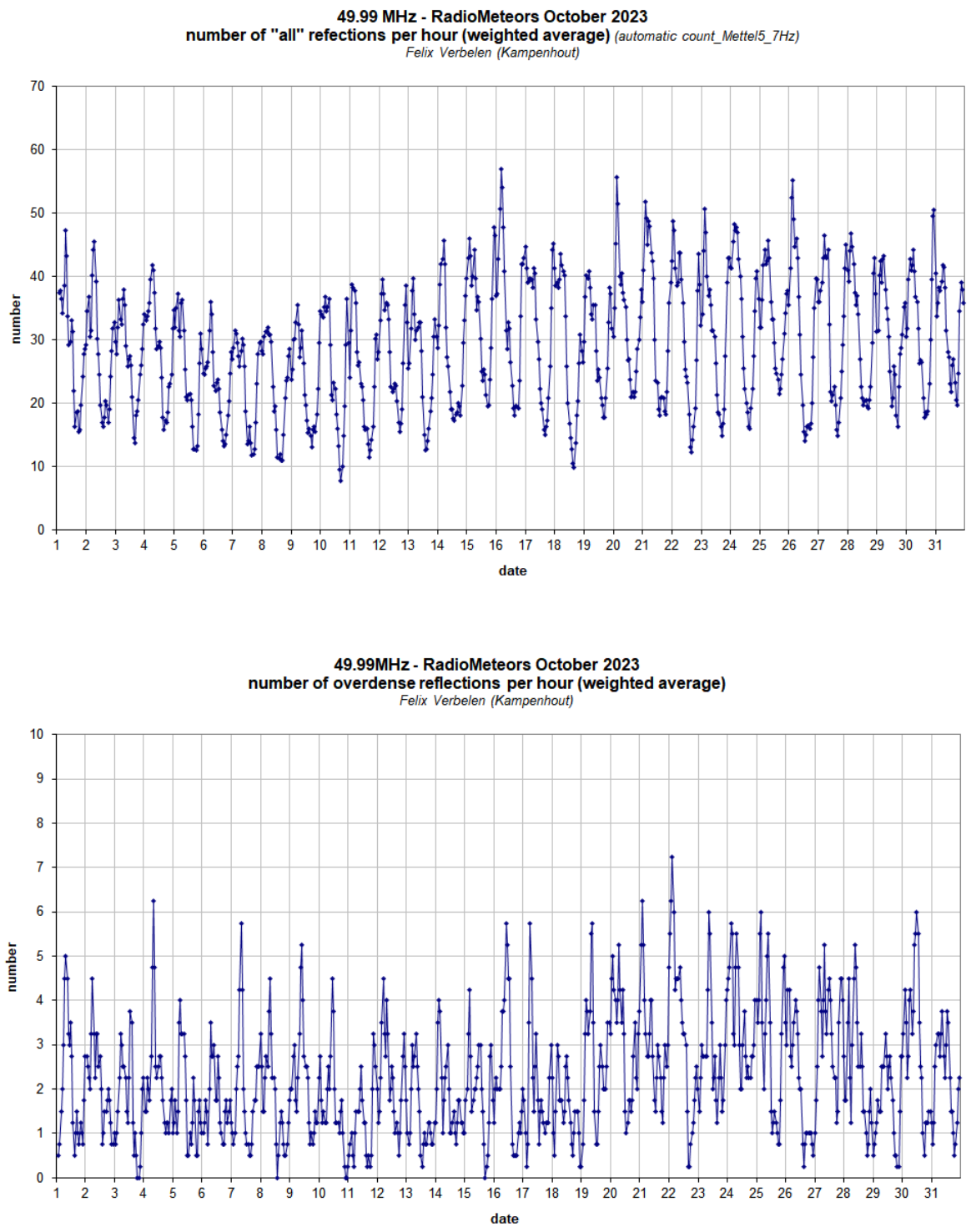

Figure 3 – The hourly numbers of "all" reflections counted automatically, and of manually counted "overdense" reflections, as observed here at Kampenhout (BE) on the frequency of our VVS-beacon (49.99 MHz) during October 2023.

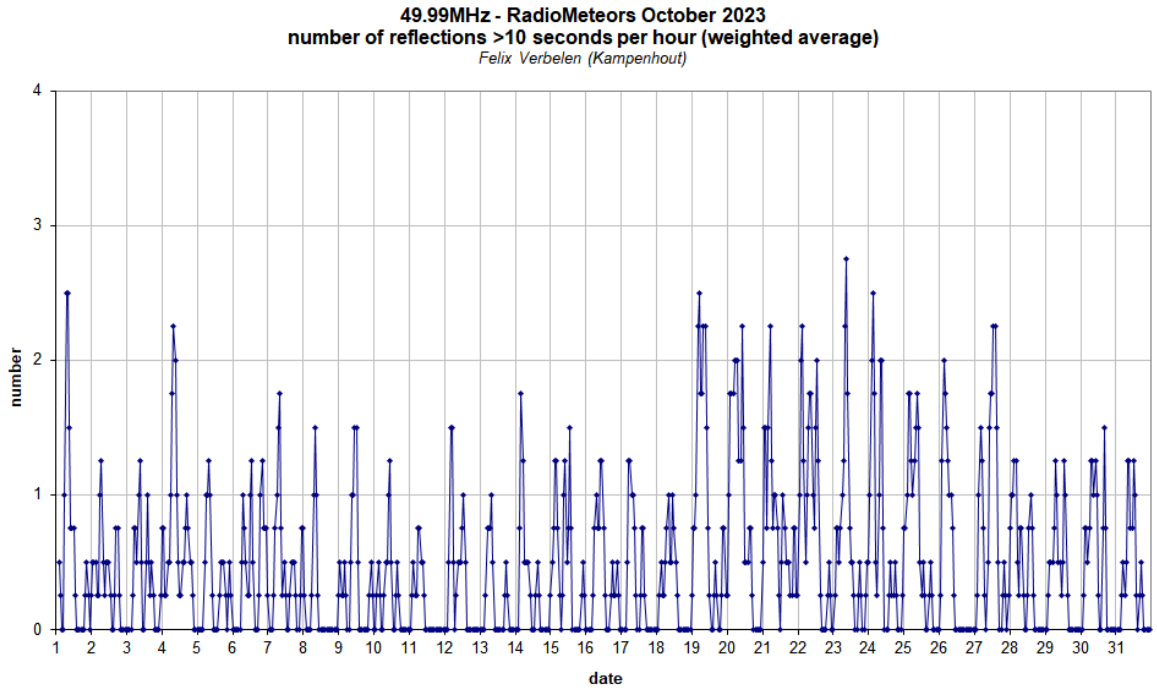

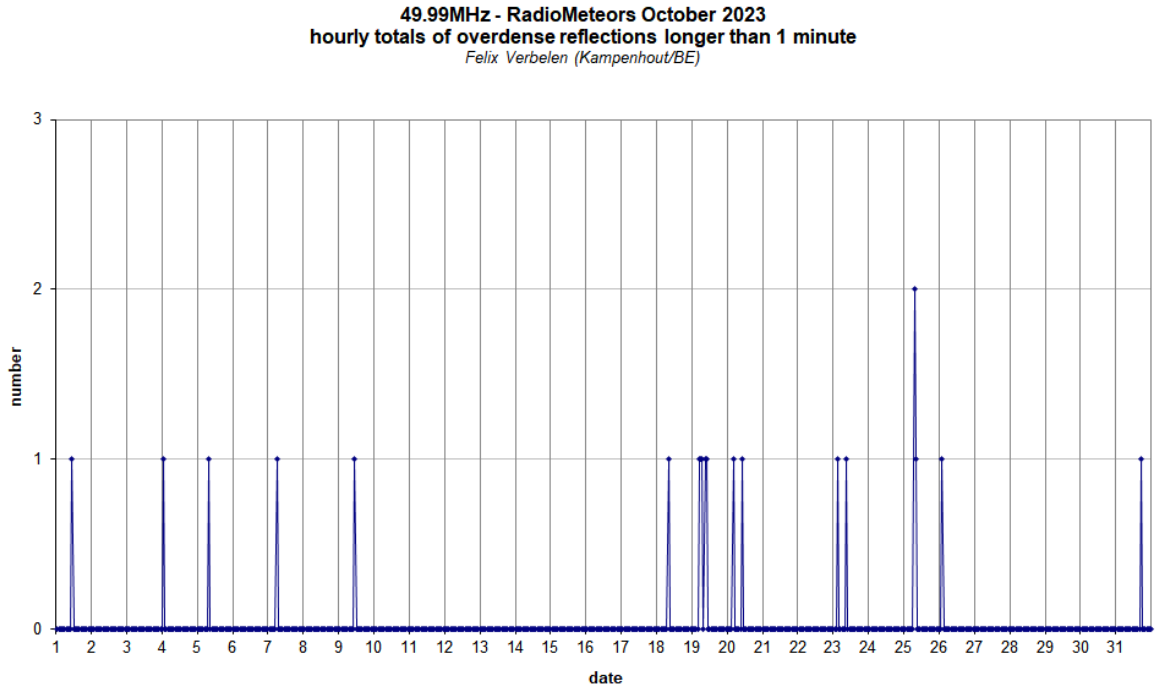

Figure 4 – The hourly numbers of overdense reflections longer than 10 seconds and longer than 1 minute, as observed here at Kampenhout (BE) on the frequency of our VVS-beacon (49.99 MHz) during October 2023.

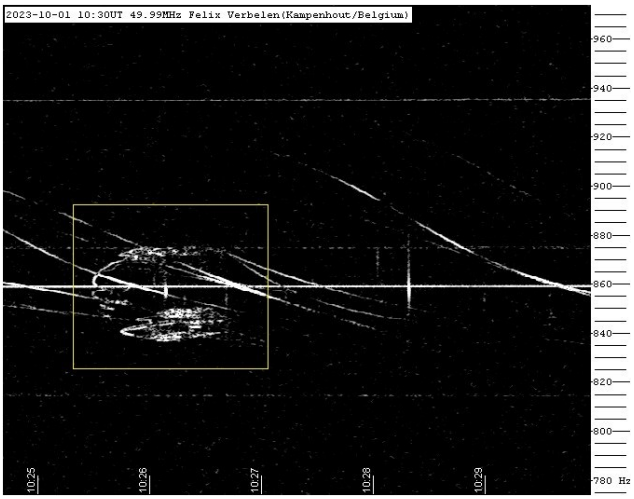

Figure 5 – Meteor echo 1 October 2023, 10^h30^m UT.

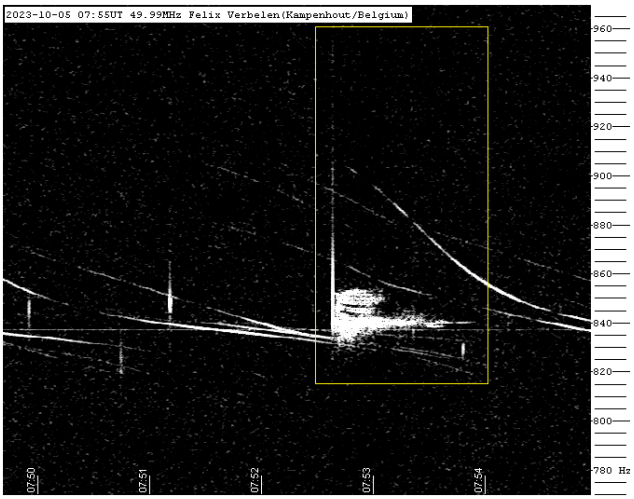

Figure 6 – Meteor echo 5 October 2023, 7^h55^m UT.

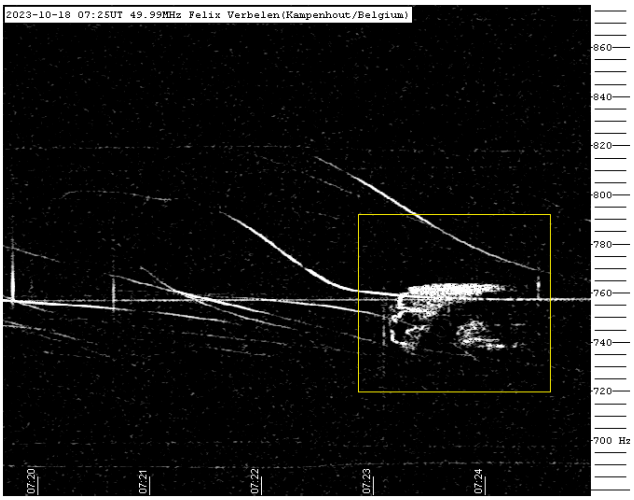

Figure 7 – Meteor echo 18 October 2023, 7^h25^m UT.

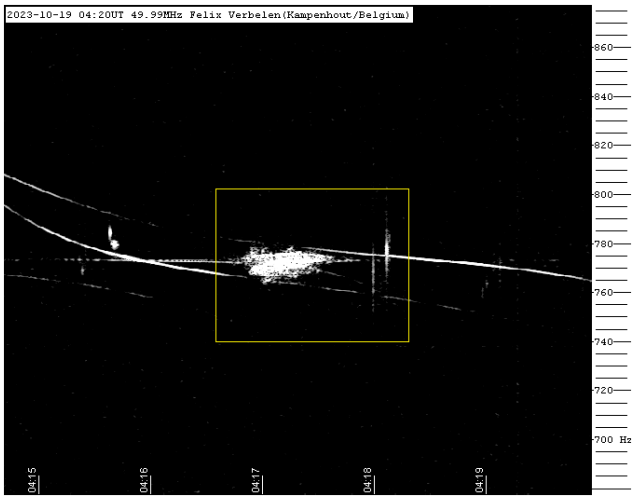

Figure 8 – Meteor echo 19 October 2023, 4^h20^m UT.

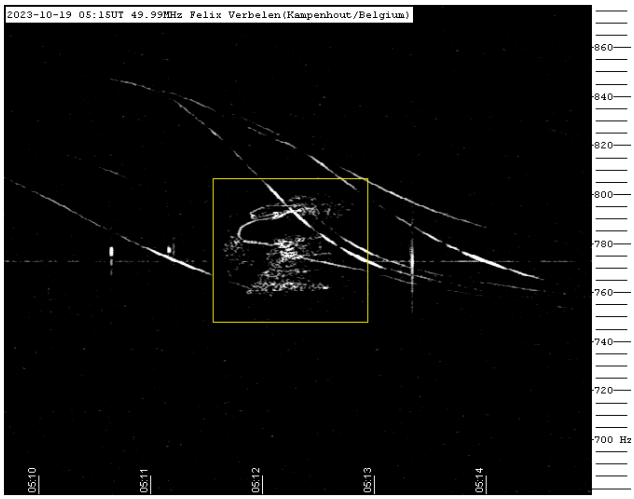

Figure 9 – Meteor echo 19 October 2023, 5^h15^m UT.

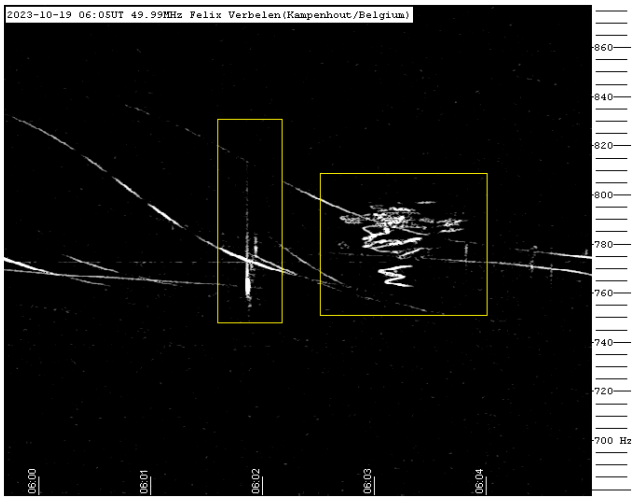

Figure 10 – Meteor echo 19 October 2023, 6^h05^m UT.

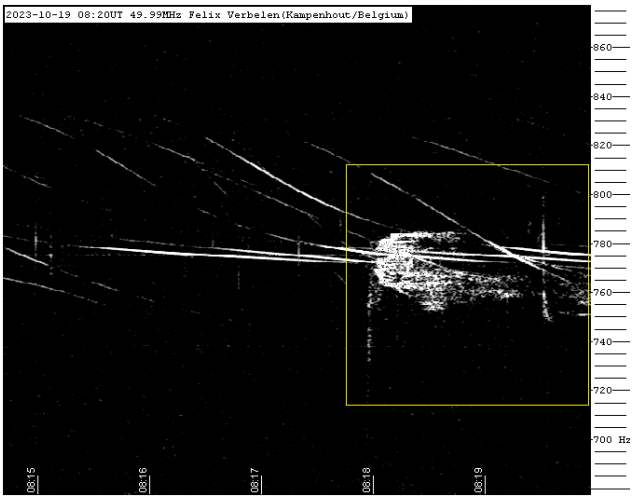

Figure 11 – Meteor echo 19 October 2023, 8^h20^m UT.

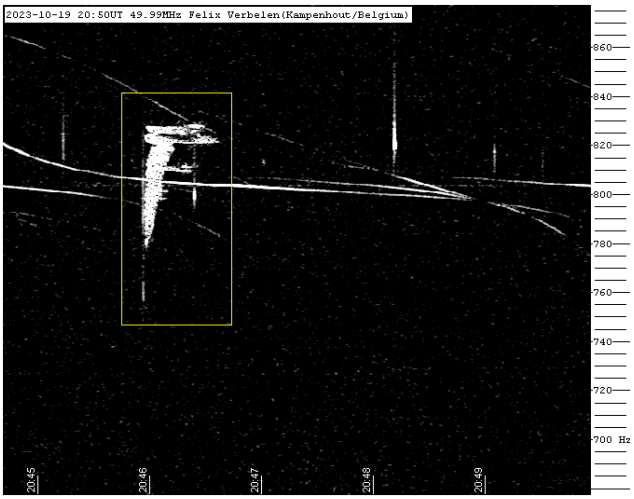

Figure 12 – Meteor echo 19 October 2023, 20^h50^m UT.

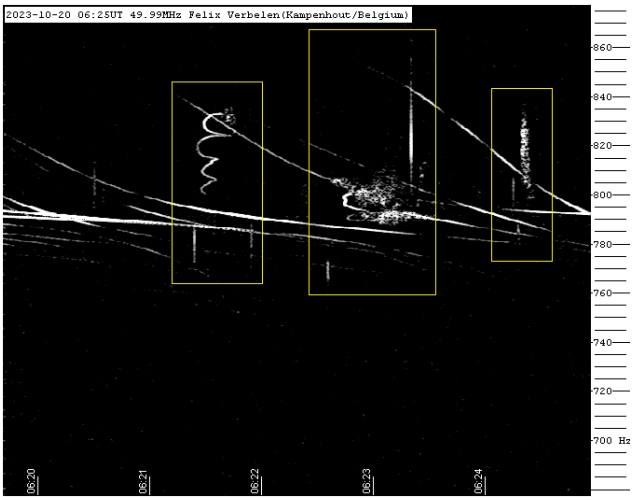

Figure 13 – Meteor echo 20 October 2023, 6^h25^m UT.

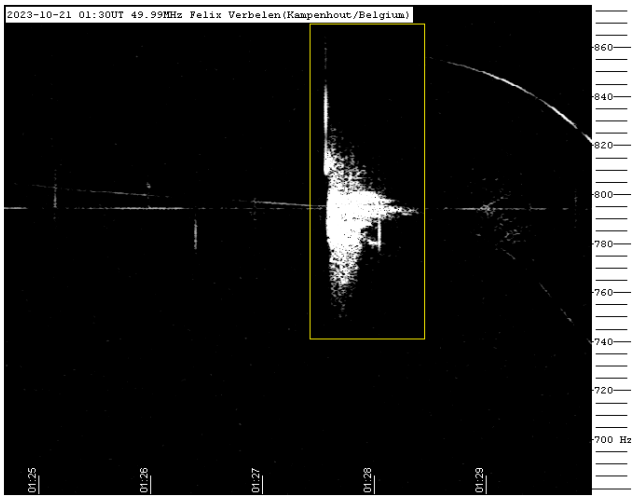

Figure 14 – Meteor echo 21 October 2023, 1^h30^m UT.

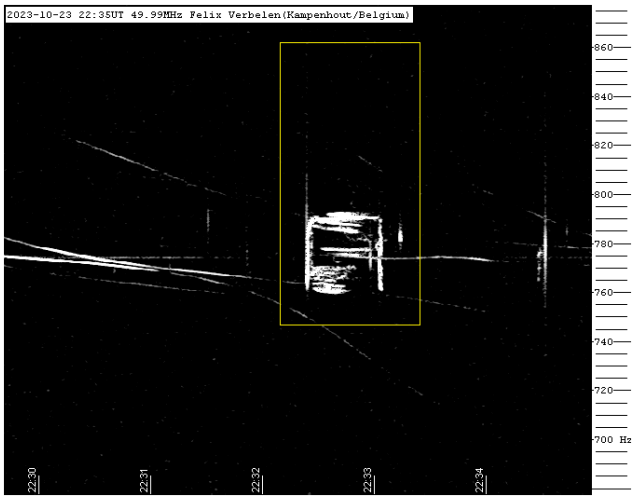

Figure 15 – Meteor echo 23 October 2023, 22^h35^m UT.

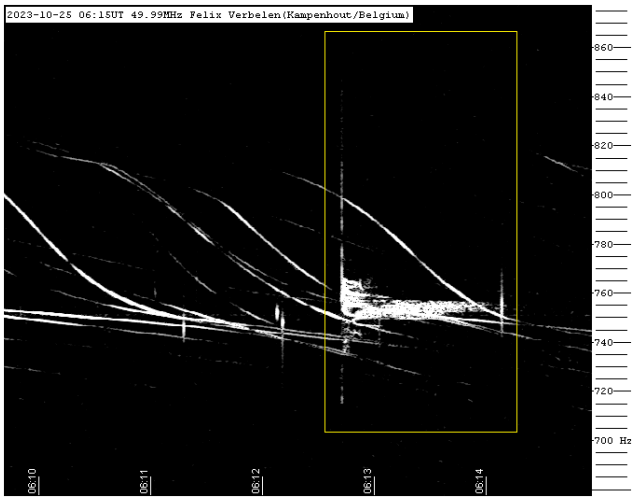

Figure 16 – Meteor echo 25 October 2023, 6^h15^m UT.

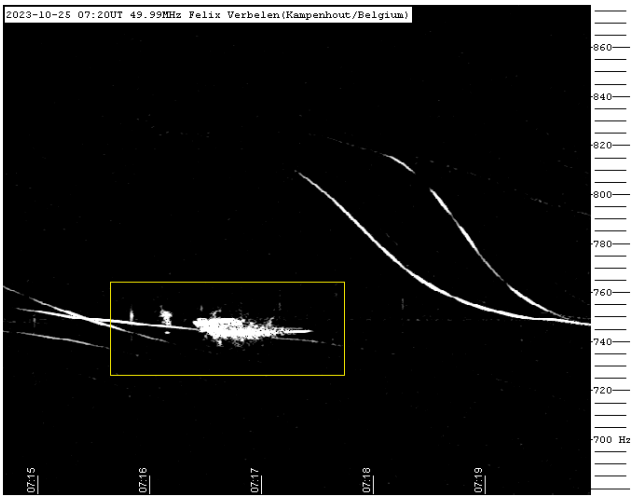

Figure 17 – Meteor echo 25 October 2023, 7^h20^m UT.

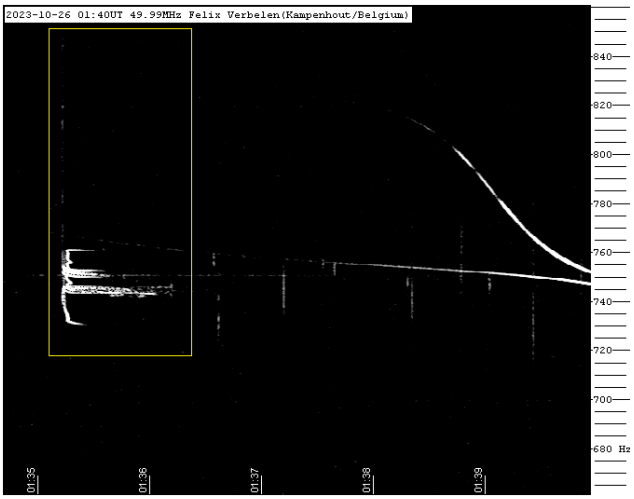

Figure 18 – Meteor echo 26 October 2023, 1^h40^m UT.

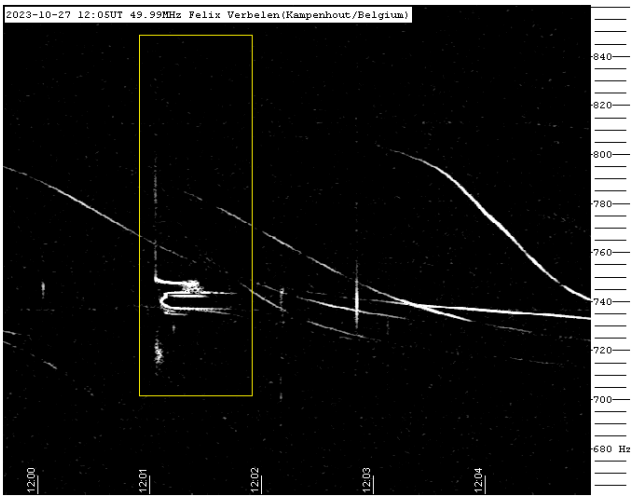

Figure 19 – Meteor echo 27 October 2023, 12^h05^m UT.

Radio meteors November 2023

Felix Verbelen

Vereniging voor Sterrenkunde & Volkssterrenwacht MIRA, Grimbergen, Belgium
felix.verbelen@gmail.com

An overview of the radio observations during November 2023 is given.

1 Introduction

The graphs show both the daily totals (*Figure 1 and 2*) and the hourly numbers (*Figure 3 and 4*) of "all" reflections counted automatically, and of manually counted "overdense" reflections, overdense reflections longer than 10 seconds and longer than 1 minute, as observed here at Kampenhout (BE) on the frequency of our VVS-beacon (49.99 MHz) during the month of November 2023.

However, due to technical problems, the beacon signal was very unstable from the beginning of the month until the 22nd at 09^h27^m UT and therefore the data are given with strict reservations.

The hourly numbers, for echoes shorter than 1 minute, are weighted averages derived from:

$$N(h) = \frac{n(h-1)}{4} + \frac{n(h)}{2} + \frac{n(h+1)}{4}$$

Local interference and unidentified noise remained moderate to low for most of the month, and solar activity also caused only limited periods of increased noise.

Weak lightning activity was observed on 3 days.

Despite the problems with the beacon, 10 reflections longer than 1 minute were recorded.

A selection of these, along with some other interesting reflections is included (*Figures 5 to 16*). More of these are available on request.

In addition to the usual graphs, you will also find the raw counts (subject to strict reservations as previously said) in cvs-format[15] from which the graphs are derived. The table contains the following columns: day of the month, hour of the day, day + decimals, solar longitude (epoch J2000), counts of "all" reflections, overdense reflections, reflections longer than 10 seconds and reflections longer than 1 minute, the numbers being the observed reflections of the past hour.

[15] https://www.meteornews.net/wp-content/uploads/2023/12/202311_49990_FV_rawcounts.csv

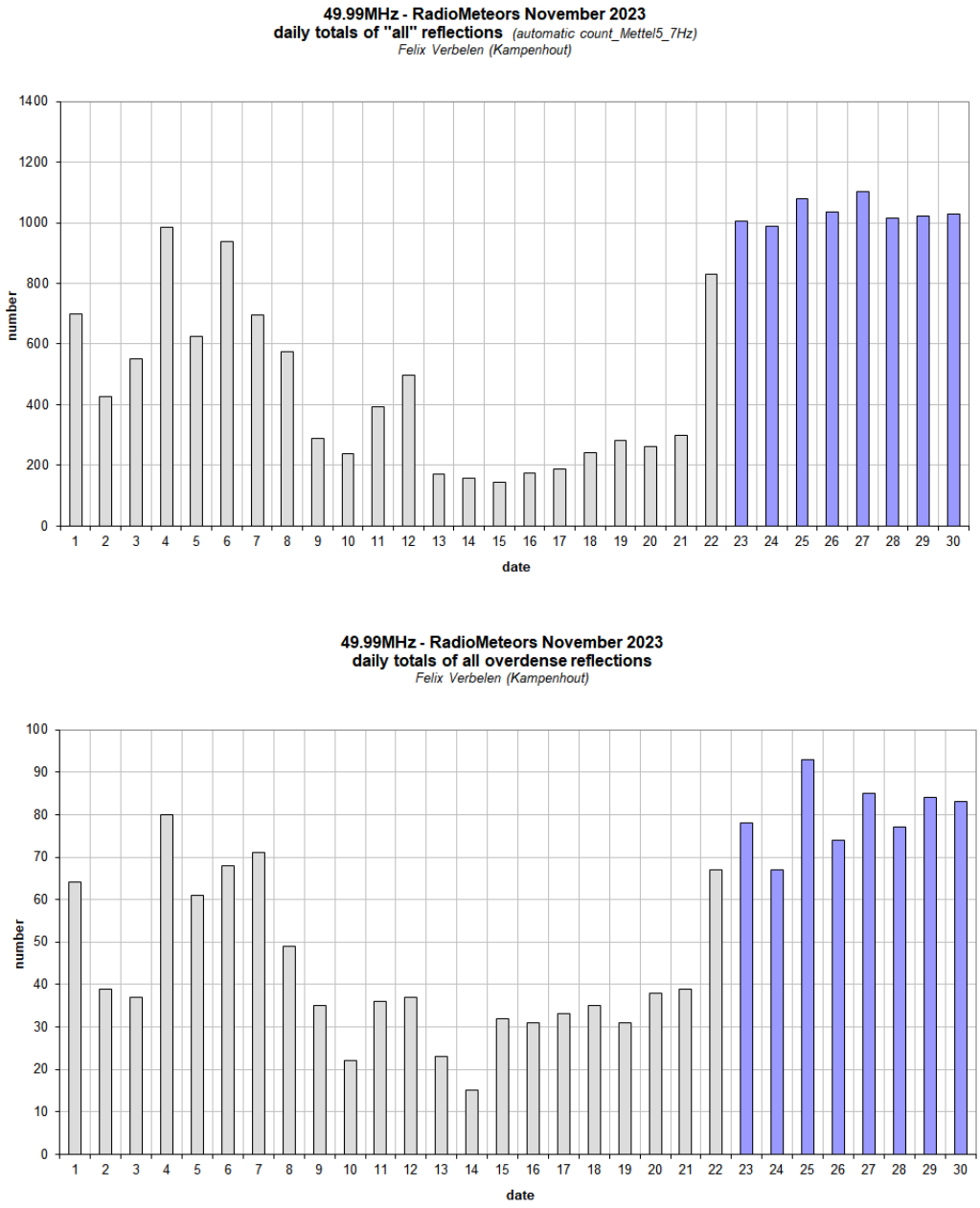

Figure 1 – The daily totals of "all" reflections counted automatically, and of manually counted "overdense" reflections, as observed here at Kampenhout (BE) on the frequency of our VVS-beacon (49.99 MHz) during November 2023.

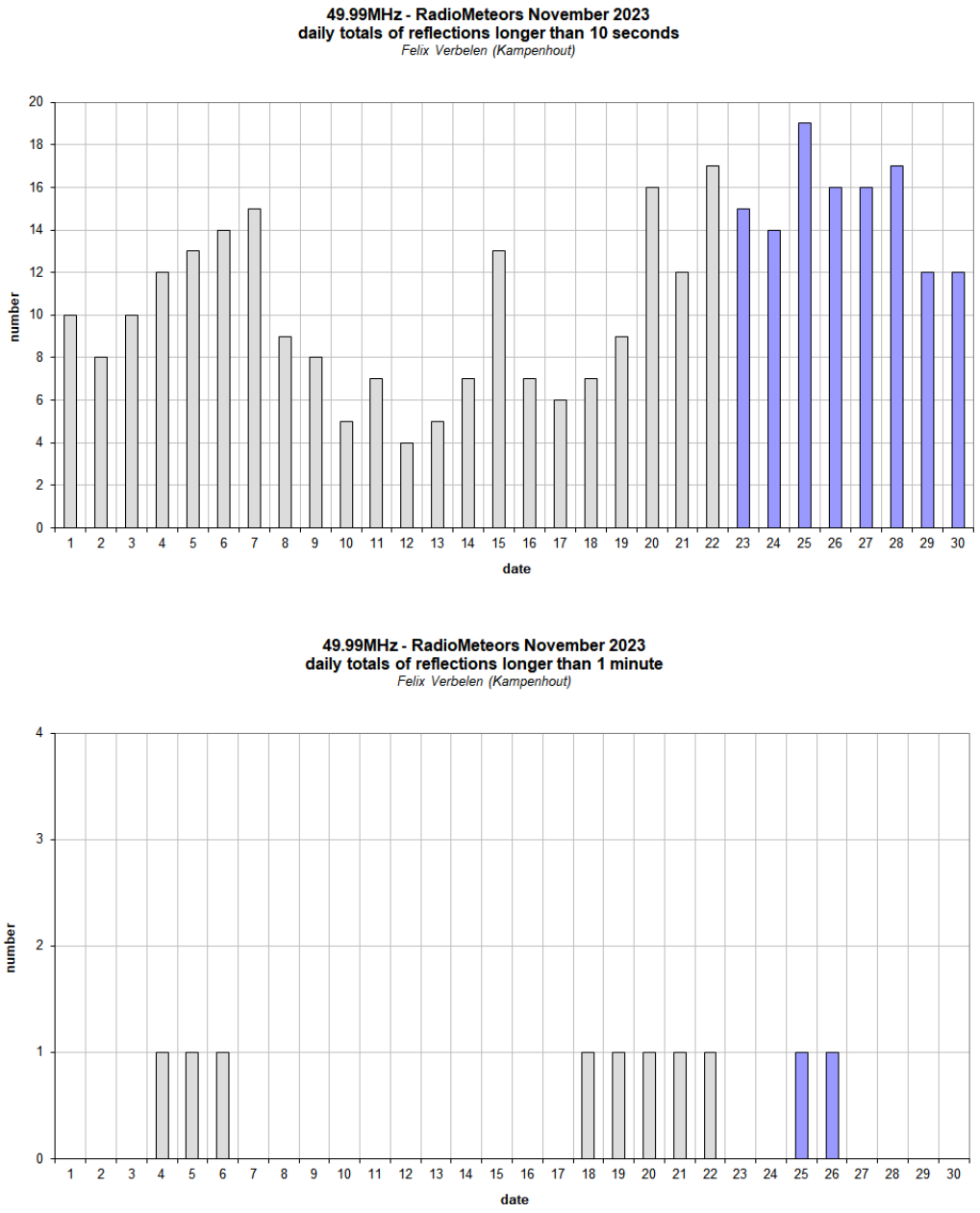

Figure 2 – The daily totals of overdense reflections longer than 10 seconds and longer than 1 minute, as observed here at Kampenhout (BE) on the frequency of our VVS-beacon (49.99 MHz) during November 2023.

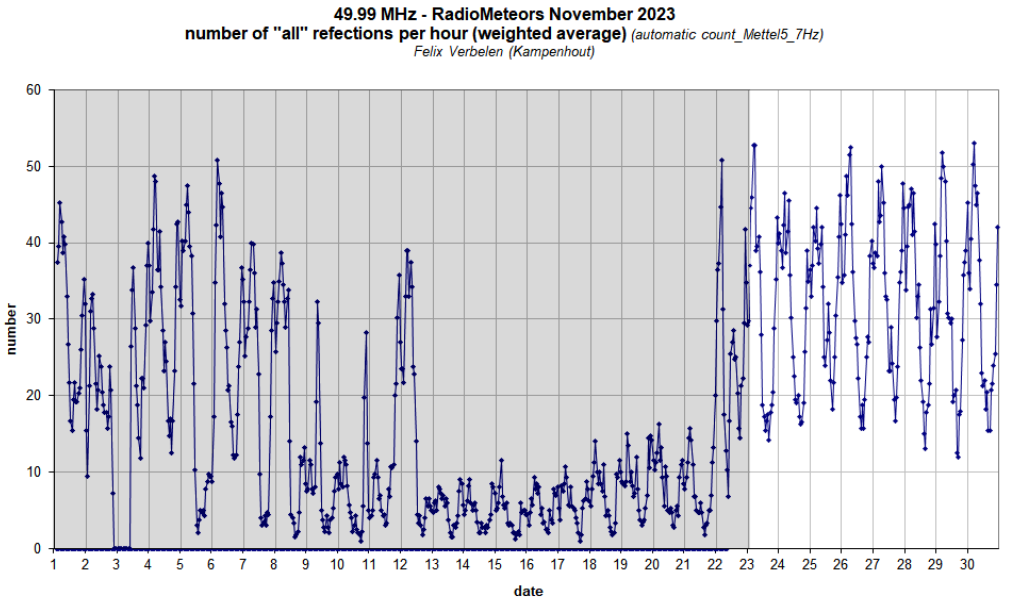

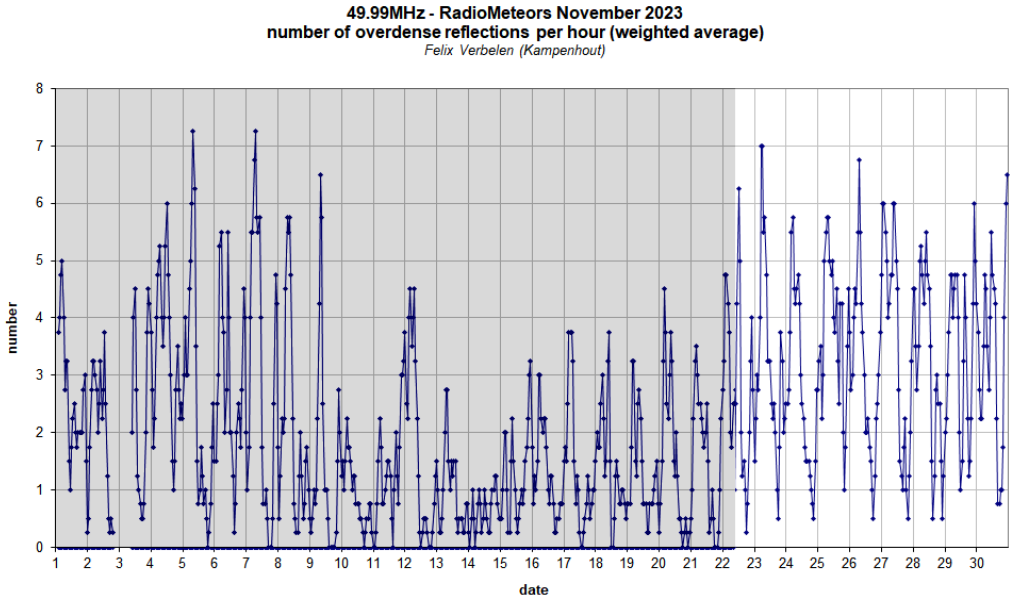

Figure 3 – The hourly numbers of "all" reflections counted automatically, and of manually counted "overdense" reflections, as observed here at Kampenhout (BE) on the frequency of our VVS-beacon (49.99 MHz) during November 2023.

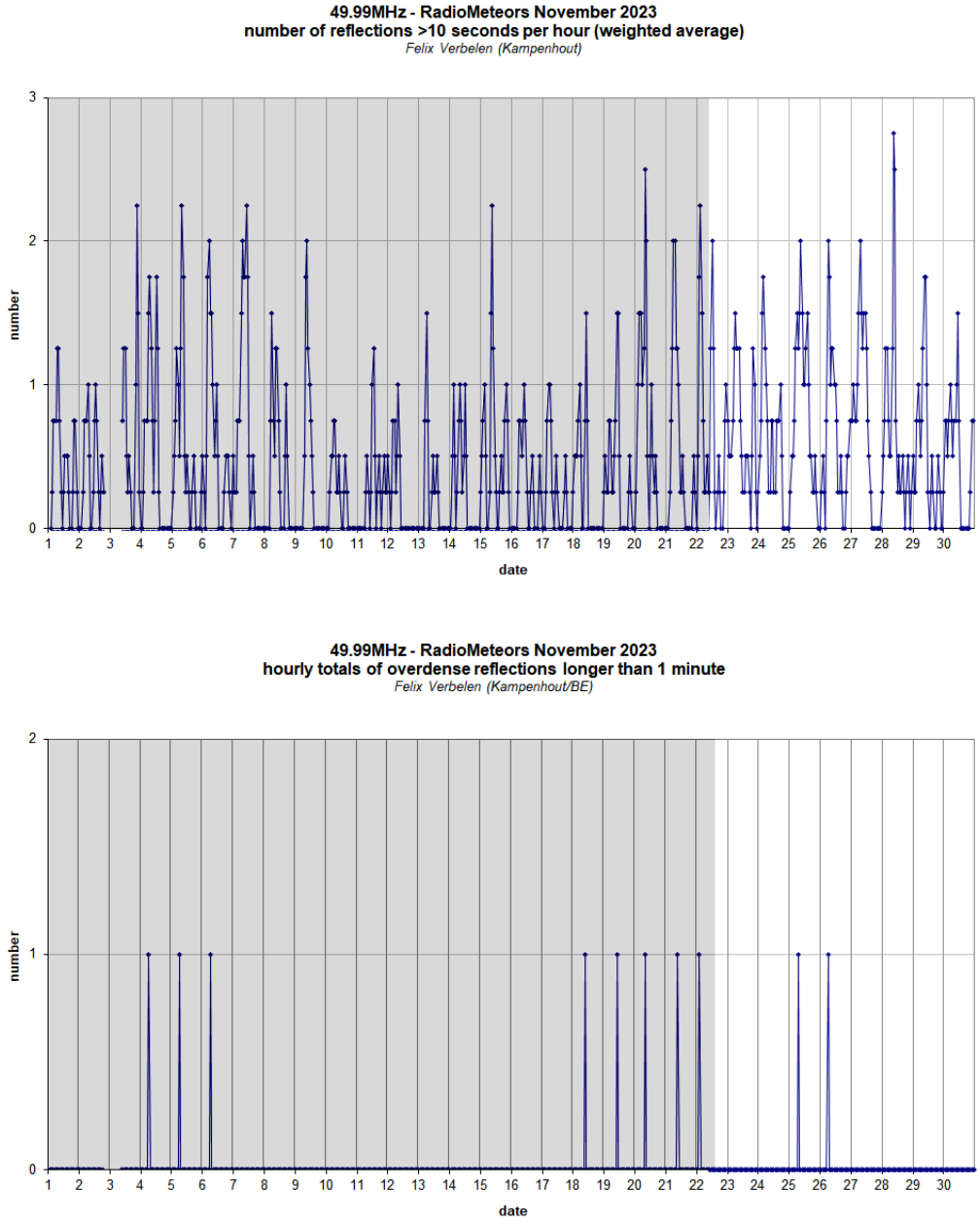

Figure 4 – The hourly numbers of overdense reflections longer than 10 seconds and longer than 1 minute, as observed here at Kampenhout (BE) on the frequency of our VVS-beacon (49.99 MHz) during November 2023.

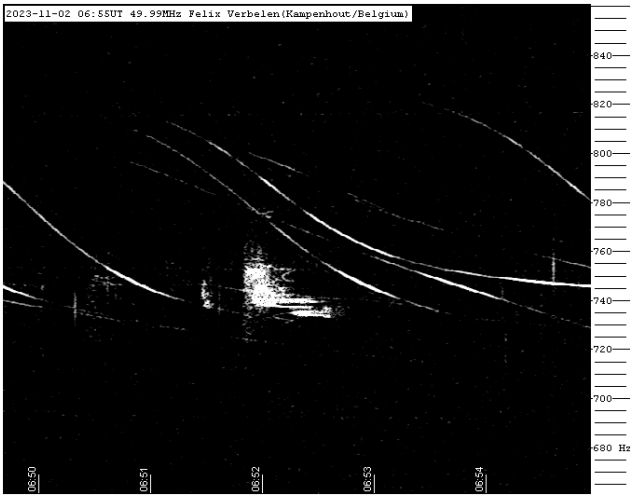

Figure 5 – Meteor echo 2 November 2023, 06^{h}55^{m} UT.

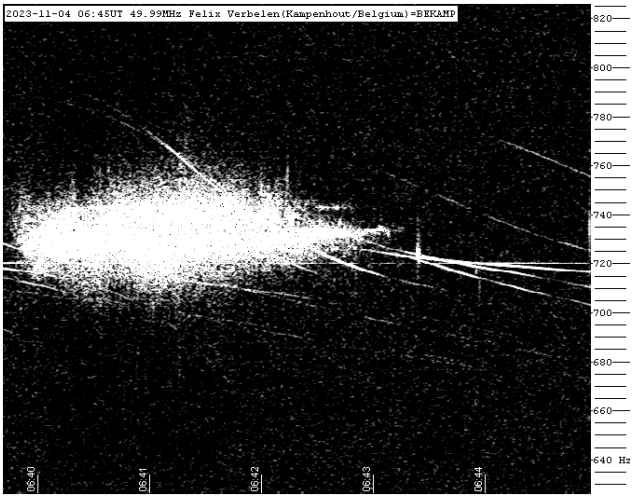

Figure 6 – Meteor echo 4 November 2023, 06^{h}45^{m} UT.

Figure 7 – Meteor echo 5 November 2023, 03^{h}40^{m} UT.

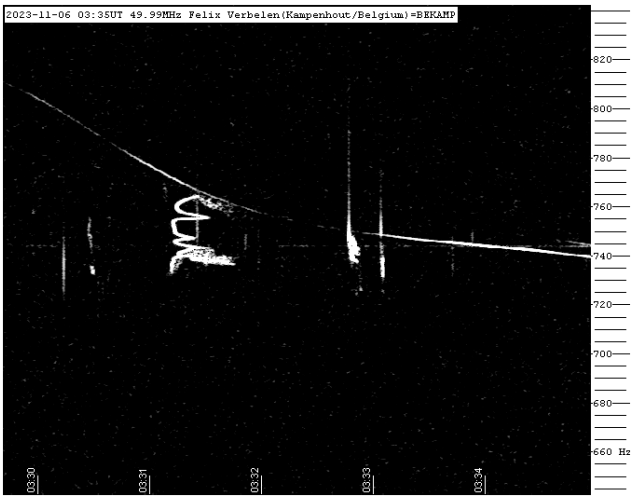

Figure 8 – Meteor echo 6 November 2023, 03^{h}35^{m} UT.

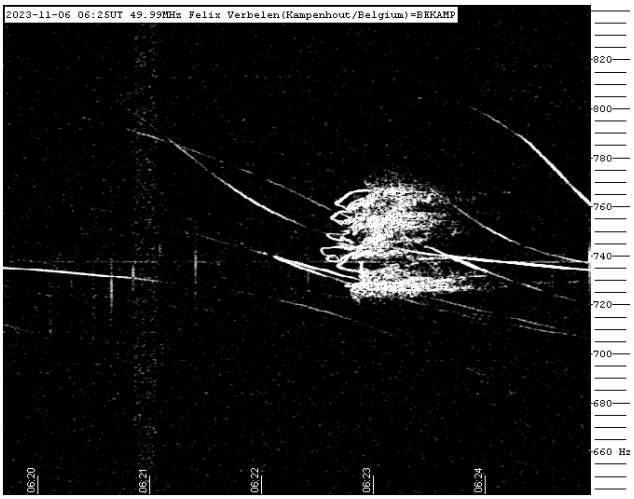

Figure 9 – Meteor echo 6 November 2023, 06^{h}25^{m} UT.

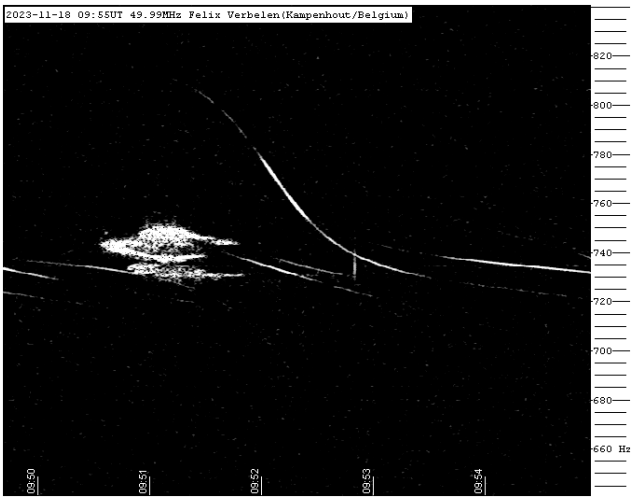

Figure 10 – Meteor echo 18 November 2023, 09^{h}55^{m} UT.

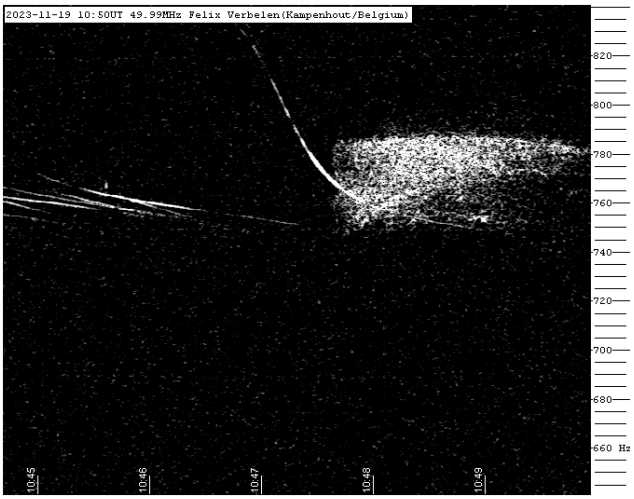

Figure 11 – Meteor echo 19 November 2023, 10^h50^m UT.

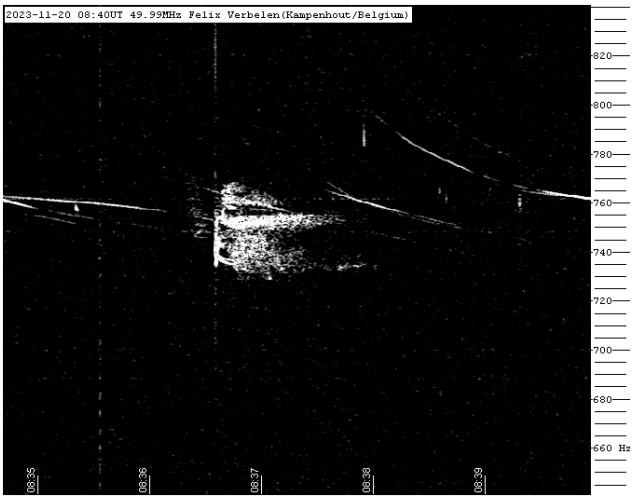

Figure 12 – Meteor echo 20 November 2023, 08^h40^m UT.

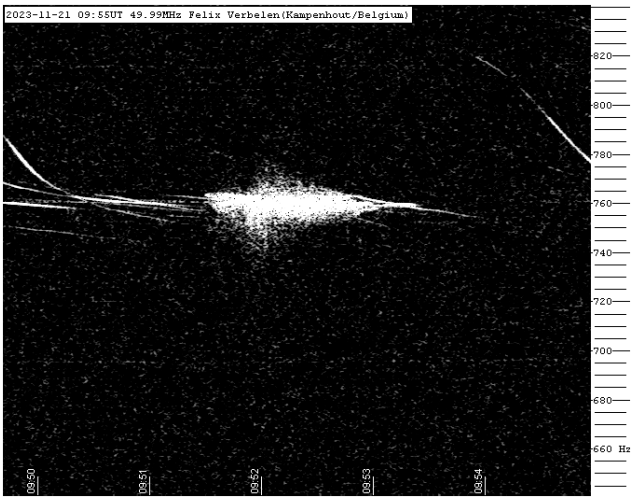

Figure 13 – Meteor echo 21 November 2023, 09^h55^m UT.

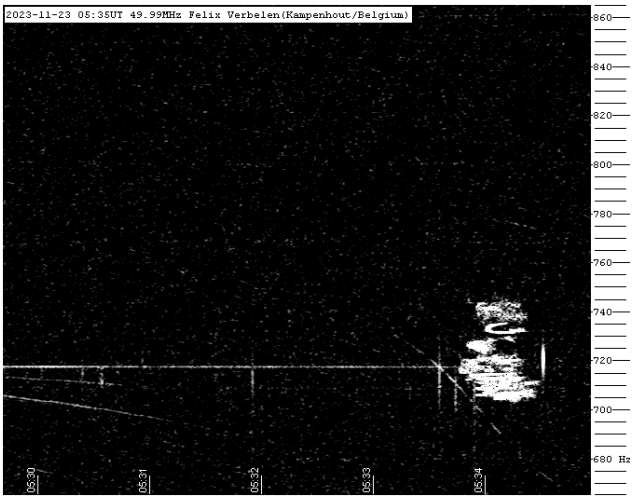

Figure 14 – Meteor echo 23 November 2023, 05^h35^m UT.

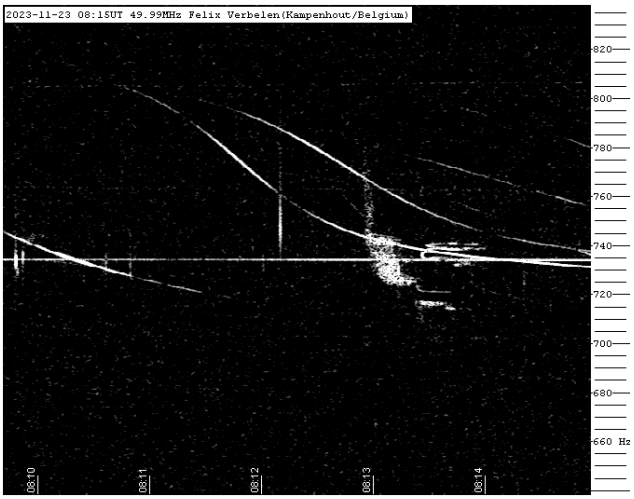

Figure 15 – Meteor echo 21 November 2023, 08^h15^m UT.

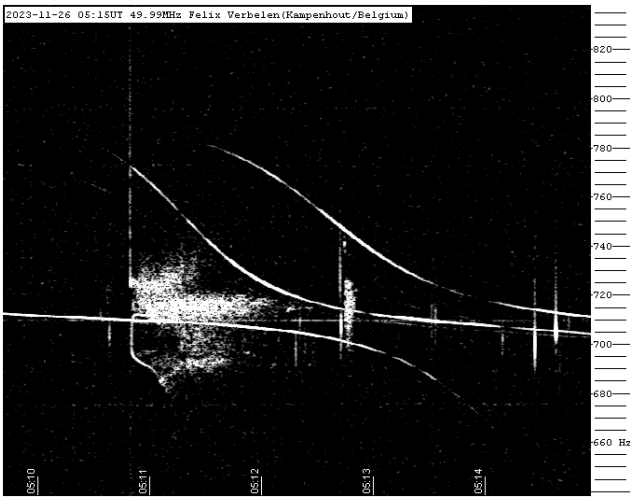

Figure 16 – Meteor echo 26 November 2023, 05^h15^m UT.

The mission of MeteorNews is to offer fast meteor news to a global audience, a swift exchange of information in all fields of active amateur meteor work without editing constraints. MeteorNews is freely available without any fees.

You are welcome to contribute to MeteorNews on a regular or casual basis, if you wish to. Anyone can become an author or editor, send an email to us. For more info read: https://meteornews.net/writing-content-for-emeteornews/

MeteorNews account manager: Jakub Koukal <j.koukal007@gmail.com>.

The running costs for website hosting are covered by a team of sponsors. We want to thank the 2022-2023 sponsors: Anonymous (3x), Mikhail Bidnichenko, Gaetano Brando, TomB, Trevor C, Nigel Cunnington, Richard Glassner, Kevin Heider, Paul Hyde, K. Jamrogowicx, Dave Jones, Richard Kacerek, Richard Lancaster, Joseph Lemaire, Mark McIntyre, Hiroshi Ogawa, Paul Mohan, Stan Nelson, Lubos Neslusan, BillR, Whitham D. Reeve, John Schlin, Ann Schroyens and Denis Vida.

Contributing to this issue:

- Jenniskens P.
- Johannink C.
- Kacerek R.
- Koukal J.
- Lenža L.
- Maslov M.
- Roggemans P.
- Rollinson D.
- Scott J.M.
- Šegon
- Sicking W.
- Srba J.
- Verbelen F.
- Vida D.

ISSN 2570-4745 Online publication https://meteornews.net

Listed and archived with ADS Abstract Service: https://ui.adsabs.harvard.edu/search/q=eMetN

MeteorNews Publisher:

Valašské Meziříčí Observatory, Vsetínská 78, 75701 Valašské Meziříčí, Czech Republic